SISSA – International School for Advanced Studies

Ph.D. course in Statistical Physics

Investigating Localization Transitions with the Forward Approximation

Thesis submitted for the degree of *Doctor Philosophiae*
27 November 2015

Advisor:
Antonello Scardicchio

Candidate:
Francesca Pietracaprina

Academic Year 2014/2015

Abstract

In this Ph.D. thesis we review the Anderson localization problem and its relevance in the current panorama of Physics; we discuss the single- and many-body problem and the features of the localization transition.

We discuss in detail the forward approximation of the locator expansion, showing how it is a powerful tool for inspecting both the single- and the many-body localization transition. We analyze its predictions in the Bethe lattice, in the hypercubic lattice, and in a many-body Heisenberg model. The approximation provides an upper bound for the transition point; this result becomes increasingly accurate as the dimensionality of the system increases. We also find that the forward approximation result can be closely approximated by a single term as long as cancellations in the full series expansion are not relevant (this happens in the single particle Anderson systems but not in the many-body case).

Moreover, we study a system interacting with a mesoscopic bath which shows peculiar localization properties; this is done both analytically through the forward approximation and numerically through exact diagonalization techniques. We find that, as the coupling with the bath increases, the system goes through a crossover between two mechanisms for localization, i.e. from Anderson to Zeno localization. The stability of the localized state is a non-monotonic function of the coupling with the bath, as the increasing hybridization of the bath states allows different particle hopping processes.

Contents

Preface

Motivations

Quantum dynamics in the presence of disorder is a fascinating and challenging problem in statistical mechanics and exhibits a number of surprising features. Arguably, the most striking one is the absence of diffusion and transport, a phenomenon called *Localization* by P. W. Anderson, who predicted it in 1958 [1]. Recently, the topic has gained a lot of attention again due to the work done by Basko, Aleiner and Altshuler [2], which showed the stability of localization in presence of interactions; this phenomenon, named *Many Body Localization*, is characterized by a lot of interesting properties both for fundamental quantum physics (breakdown of thermalization, lack of ergodicity, existence of local integrals of motion) and for the practical applications (protection against decoherence and symmetry breaking). Indeed, localization is observed in cold atoms experiments and could be an important ingredient for building a quantum computer.

One can therefore appreciate how compelling a deeper investigation of this topic is. An attempt of a better understanding of localization in quantum systems is presented in this Ph.D. thesis, whose main aim is both to improve the (mostly numeric) toolset available to physicists for inspecting systems showing localization properties and using these tools to obtain a picture of what happens in non-isolated localized systems.

Thesis outline

This thesis is organized in five chapters. After an introductory first chapter, in which we review the single particle and many-body localization problem and its relevance in the current panorama of Physics, in the second chapter we go into detail in showing how the so-called locator expansion emerges from the analysis of the single particle problem.

In the third chapter, we discuss in detail the forward approximation of the locator expansion, showing how it is a powerful tool in analysing the localization transition. Additionally, in the fourth chapter we study a sys-

tem interacting with a mesoscopic bath, which shows peculiar localization properties; this is done both analytically through the forward approximation and numerically through exact diagonalization techniques.

In the fifth chapter we discuss the many-body interacting disordered systems, proceeding to the analysis of the ergodicity properties and the detection of the transition. Furthermore, we discuss the use of the forward approximation in a many-body system, proposing it as a powerful tool for the inspection of this class of systems.

The original part of this thesis is contained in Chapters 3 [3], 4 [4] and 5 [3, 5].

Acknowledgments

The original work of this thesis and additional works during my Ph.D. have been performed in collaboration with the co-authors of the journal articles: my advisor Antonello Scardicchio, Andrea De Luca, Valentina Ros, Rahul Nandkishore, David Huse, John Goold, Vipin Varma and Alessio Lerose. To them I address my deepest thanks.

I also express my gratitude to my teachers, my fellow students and postdoctoral researchers at SISSA and at ICTP: nobody is born educated, and my Ph.D. at SISSA has been an extraordinary opportunity for learning, both for my Physics education and as a life experience.

Finally, I would like to thank all those who have supported me during these hard but rewarding four years; at the end of the day it is the encouragement and support of the people closer to us which pushes and enables us to achieve the best and most difficult goals we set for ourselves.

Chapter 1

Localization in single particle and many body systems

1.1 From impurities to disorder

The modern theories of solid state physics are based on Bloch's theory of electron states in perfect regular lattices, supplemented by the description of electron and phonon interactions and accounting for imperfections in the lattice when describing the kintetics. The Boltzmann equation and the results of Debye, Born and Brillouin on phonons give a fairly clear idea of what happens in a metal with low concentration of impurities; highly disordered materials, however, are much less understood, but they are nonetheless very interesting both from a purely theoretical point of view and eventually for applications [6–9].

The idea of the absence of diffusion in disordered quantum materials was first formulated by Anderson in his paper published in 1958 [1], which contained many of the fundamental intuitions which have been subsequently developed. This theory was first introduced in order to explain some experimental data of electron conductivity in metals containing impurities [10]. Electrons in a metal behave diffusively, as in a random walk between collision with impurities, such that their probability of being at position r at time t, having started from the origin at the initial time, is

$$P(r,0,t) \simeq \frac{\exp\left(-\frac{r^2}{2Dt}\right)}{(2\pi Dt)^{\frac{d}{2}}}, \qquad D = \frac{\hbar k_F l}{2m}, \tag{1.1}$$

where l is the electron mean free path, and the Drude conductivity arises

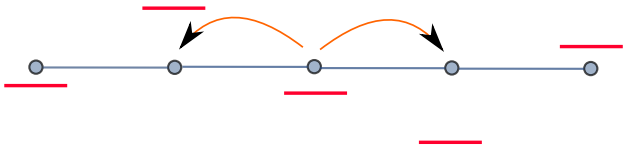

Figure 1.1: A schematic depiction of the Anderson model Hamiltonian (1.3).

from diffusion through the Einstein relation

$$\sigma = \mathrm{e}^2 D\, N(E_f) = \frac{e^2 k_f l}{2\pi\hbar}, \tag{1.2}$$

being proportional to the mean free path. Anderson found that this reasoning breaks down abruptly if the density of impurities is increased above a critical amount, so that the mean free path is of the order of the electron wavelength; then the diffusive scattering stops, the electrons become trapped (localized) and the conductivity becomes zero.

The result by Anderson is understandably fundamental in a complete description of transport in solid state systems. Nonetheless, localization is rich in significance even on a deeper level, including connections with random matrix theory, ergodicity and thermalization.

As we will see in more detail in Chapter 2, the class of models which show the Anderson localization transition are tight binding models where the (noninteracting) particles are able to move, e.g. hop to their neighboring sites, and in which a disordered on-site potential, with values extracted from a probability distribution of a given width, is present. The paradigmatic example is given by the Anderson model

$$H = \sum_i \epsilon_i c_i^\dagger c_i - t \sum_{\langle ij \rangle} c_i^\dagger c_j + h.c. \tag{1.3}$$

where $c^\dagger$ and c are fermionic creation and annihiliation operators and ϵ_i are independent and identically distributed random variables extracted from, e.g., a box distribution:

$$p(\epsilon) = \begin{cases} W^{-1} & \epsilon \in [-W/2, W/2] \\ 0 & \text{else.} \end{cases} \tag{1.4}$$

The localization transition happens between the phase where the hopping is strong enough to sustain conduction and a diffusive behavior and the one where the on-site disorder is strong enough to suppress diffusion, meaning that a particle 'becomes stuck' in the vicinity of a given site and its wavefunction has an exponentially decaying envelope. This seemingly simple model has a very rich phenomenology, which will be outilned in part in this chapter.

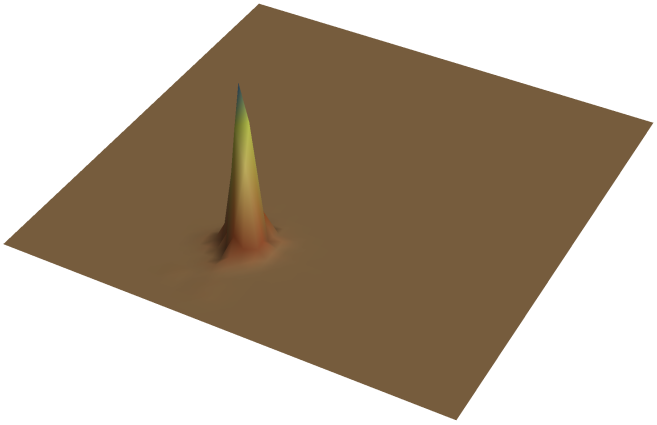

Figure 1.2: A localized state of the Anderson Hamiltonian (1.3) in a two dimensional square lattice.

1.2 Phenomenology of single particle localized and delocalized states

Before going on to understand how localization emerges from the physics of disordered systems, let us describe the properties of single particle localized states and how they are different from extended states [11, 12].

The wavefunction of a particle is a plane wave of definite wavenumber in a perfect periodic system; introducing even a small amount of disorder the picture changes to a superposition of Bloch waves, formed by scattering of the plane waves from the impurities, with degeneracy broken by the disorder. The amplitude will fluctuate through the system and typically will be of order $\psi_E \sim V^{-\frac{1}{2}}$, where V is the size of the system.

The localized wavefunctions have a peak around a center r_0 and an exponentially decreasing envelope

$$|\psi_L(r)| \sim A \exp\left(-\frac{|r - r_0|}{\xi}\right) \tag{1.5}$$

with a characteristic localization length ξ; the amplitude will additionally be modulated by a sinusoidal factor, so that the orthogonality between states is preserved. The oscillating part of the wavefuction amplitudes has a Porter

Thomas distribution,

$$P_{\rm osc}(x) = \frac{{\rm e}^{-x/2}}{\sqrt{2\pi x}}. \tag{1.6}$$

The localization centers r_0 are uniformly distributed if the system is macroscopically homogeneous.

One can discriminate between a localized and an extended wavefunction by means of the moments of the amplitudes distribution:

$$p_q = \sum_i |\psi_i|^{2q} \tag{1.7}$$

where we have assumed that $||\psi|| = 1$. The lowest useful moment is the second one, also called participation ratio; its inverse $I_2 = p_2^{-1}$, unimaginatively called inverse participation ratio, is a quantity which is usually employed to recognize localization. In the ergodic, delocalized phase the typical value of the wavefunction coefficients will be inversely proportional to the square root of the volume:

$$\psi(i) \sim \frac{1}{\sqrt{V}}; \tag{1.8}$$

this reflects the fact that the wavefunction is extended over all the domain. In a localized state, instead, there will be a $\mathrm{O}(1)$ number of coefficients which will be of order one, namely the coefficients corresponding to the sites near the localization center, while all the others will be nearly zero. This features are captured by the inverse participation, so that

$$I_2 \sim \mathrm{O}\left(\sum_{i=1}^{V} \frac{1}{V^2}\right)^{-1} = \mathrm{O}(V) \tag{1.9}$$

for an extended state and

$$I_2 \sim \mathrm{O}(1) \tag{1.10}$$

for a localized state. Note that this picture will have to be modified in the many-body context, but will still be a useful way to inspect the transition.

1.2.1 Connection with random matrix theory

Orthogonal matrices composed of normal distributed random numbers, i.e. random matrices belonging to the GOE ensemble, with distribution

$$P_{\rm GOE}(H) \propto {\rm e}^{-\frac{1}{2}\,{\rm tr}\left[H^2\right]} \tag{1.11}$$

capture the properties of Hamiltonians with extended states (and time-reversal symmetry) [13]. Their spectrum is a set of highly correlated values $\{E_i\}_i$ which exhibits level repulsion, the distribution of level spacing $s_i = |E_{i+1} - E_i|$ being

$$P(s) \approx \frac{\pi s}{2\delta^2} \exp\left(-\frac{\pi s^2}{4\delta^2}\right) \tag{1.12}$$

where $\delta = \langle s \rangle$ (averaging over the ensemble). Hamiltonians associated with localized states instead have exponentially suppressed off-diagonal terms, since typically two energy adjacent states are spatially far away. This means that the spectrum is effectively a set of uncorrelated random numbers, and therefore the level spacings have a Poisson distribution:

$$P_P(s) = \frac{1}{\delta} \exp\left(-\frac{s}{\delta}\right). \tag{1.13}$$

This distribution is observed also in integrable systems [14].

Indeed, for the purpose of discriminating whether a system is in a localized or extended state, a frequently used parameter is one related to the eigenvalues statistic [15–21]: we build, from subsequent energy level spacings s_i, the parameter

$$r_i = \frac{\min(s_{i+1}, s_i)}{\max(s_{i+1}, s_i)} \tag{1.14}$$

and its average over a certain spectrum window $r = \langle r \rangle$. The value of the r parameter is $r_{\mathrm{GOE}} = 0.5307(1)$ for the spectrum of a GOE matrix and of a system in the delocalized phase [22] and $r_{\mathrm{P}} = 2\log 2 - 1 \approx 0.3863$ for a Poisson spectrum, as in a localized system. This is a good way to tell the two phases apart provided that we consider the thermodynamic limit; for finite systems we should rather look at the finite size scaling of r because it will have intermediate values between r_{GOE} and r_{P} in the proximity of the transition.

1.2.2 Connection with ergodicity and quantum chaos

As mentioned in Sec. 1.2.1, there are deep connections between the concept of integrability and Poisson level statistics and chaos and random matrix theory [23]. Indeed, let us consider a quantum billiard [24–27], i.e. a system described by the Schrödinger equation

$$\begin{cases} (\nabla^2 + \frac{2m}{\hbar^2} E_n)\psi_n(\mathbf{x}) = 0 \\ \psi_n(\mathbf{x})|_{\mathbf{x}\in\partial\Omega} = 0 \end{cases} \tag{1.15}$$

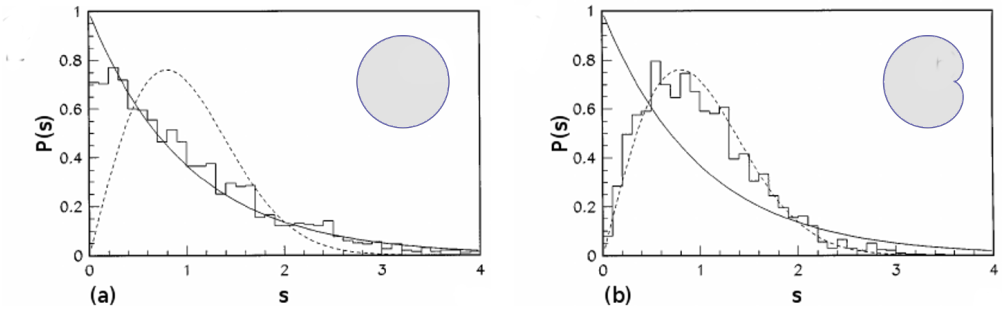

Figure 1.3: Level statistics in two quantum billiards. (a) circular billiard, with a Poisson statistic; (b) cardioid billiard, with a Wigner-Dyson statistic.

where $\Omega \in \mathbb{R}^2$ is an arbitrarily shaped surface that we address as the billiard; the shape of the billiard is solely responsible for the integrability of the system. Let us take as examples the circular and the cardioid billiards. The circular billiard is integrable and can indeed be solved analytically resulting in Bessel functions as its eigenfunctions and zeros of Bessel functions as its spectrum [28]; the cardioid billiard, instead, is not analytically solvable. We can look at the statistic of the level spacings $s_i = |E_{i+1} - E_i|$; it turns out that they follow a Poission statistic for the circular billiard and a Wigner Dyson statistic for the cardioid one.

Indeed, in the works of Berry and Tabor [14] and Bohigas, Giannoni and Schmit [29], two congectures regarding the correspondence between level statistics and integrability are formulated: that generic integrable systems (except in special cases, which are actually counterexamples of this) have Poissonian level spacings and that non-integrable and ergodic or quantum chaotic systems have Wigner Dyson level spacings, establishing a connection with random matrix theory.

1.3 Violation of the Eigenstate Thermalization Hypothesis

The idea of quantum chaos [30] is relevant to our characterization of the localization transition due to the breaking of ergodicity that happens in the localized phase. An important aspect of this is the fact that when there is localization the Eigenstate Thermalization Hypothesis [31–33] (ETH), according to which each eigenstate is representative of the microcanonical ensemble, does not hold; actually, localization is an important counterexample in the scope of validity of this hypothesis.

More precisely, the Eigenstate Thermalization Hypothesis is a statement on the equilibration of local observables. Let us consider an isolated system in a nonstationary state; in such a system, an observable is said to thermalize if it relaxes to the microcanonical value and remains close to it under time evolution. Indeed, consider a time-independent Hamiltonian H with eigenvectors $|m\rangle$ and eigenvalues E_m and an initial state[1] $|\psi_I\rangle$; the time-evolved state is

$$|\psi(t)\rangle = \sum_m C_m \, \mathrm{e}^{iE_m t}|m\rangle, \quad C_m = \langle m|\psi_I\rangle. \tag{1.16}$$

Let us now focus on an observable $\hat{O}$ and its time evolution, which, in the basis of the eigenstates of H (so that $O_{mn} = \langle m|\hat{O}|n\rangle$), can be written as

$$\begin{aligned} \hat{O}(t) \equiv \langle\psi(t)|\hat{O}|\psi(t)\rangle &= \sum_{m,n} C_m^* C_n \, \mathrm{e}^{i(E_m - E_n)t} O_{mn} \\ &= \sum_m |C_m|^2 \, O_{mm} + \sum_{m,n\neq m} C_m^* C_n \, \mathrm{e}^{i(E_m - E_n)t} O_{mn}. \end{aligned} \tag{1.17}$$

Under the previously stated conditions of relaxation to the microcanonical value and small temporal fluctuations, we have that the system thermalizes and the long time average of $\hat{O}$ is in agreement with its expectation value over a single eigenstate (this is von Neumann's quantum ergodic theorem):

$$\lim_{t\to\infty} \langle\psi(t)|\hat{O}|\psi(t)\rangle = \langle\psi_{n,\mathrm{typical}}|\hat{O}|\psi_{n,\mathrm{typical}}\rangle. \tag{1.18}$$

An intuition on how this requirements can be satisfied by a delocalized Hamiltonian can be gained by comparing with what is predicted for a random matrix. In this case, the eigenvectors are random orthogonal unit vectors, and therefore

$$\langle (\psi_i^m)^* \, \psi_j^n \rangle_{RV} = \frac{1}{\mathcal{N}} \delta_{mn} \delta_{ij}, \tag{1.19}$$

where $\mathcal{N}$ is the size of the Hilbert space, the mean is intended over the random vectors and the eigenvectors are in the basis of the eigenvectors of $\hat{O}$, $\hat{O}|i\rangle = O_i|i\rangle$, so that $\psi_i^m = \langle i|m\rangle$. It follows that for the operator $\hat{O}$ we have:

$$\begin{aligned} &\langle O_{mm}\rangle_{RV} = \mathcal{N}^{-1} \sum_i O_i \equiv \bar{O} \\ &\langle O_{mn}\rangle_{RV} = 0 \quad \text{for } m \neq n, \end{aligned} \tag{1.20}$$

[1] For the purpose of this reasoning we consider only pure states; however, everything can be generalized to mixed states.

with a variance $\propto \mathcal{N}^{-1}$. Indeed, this can be rewritten as

$$O_{mn} \approx \bar{O}\delta mn + \sqrt{\mathcal{N}^{-1}\overline{O^2}}R_{mn}, \tag{1.21}$$

where R_{mn} is a random variable (real in the case of a GOE random matrix). This implies that in Eq. (1.17) the second sum is zero and the first sum is independent of the initial state; therefore

$$\hat{O}(t) = \sum_m |C_m|^2 O_{mm} \approx \bar{O} \sum_m |C_m|^2 = \bar{O}, \tag{1.22}$$

that is, the time evolved value becomes equal to the microcanonical result.

This random matrix description is however insufficient to describe observables even in chaotic or delocalized Hamiltonians. Indeed, at least two features are present in real systems which are absent in a random matrix: the dependence of the thermal expectation values of observables on the energy density (i.e., the temperature) of the system and the fact that relaxation times depend on the specific observable. This means that additional information is embedded in the diagonal and off-diagonal matrix elements of observables in 'real systems'. Srednicki provided a generalization of the result in Eq. (1.21), known as the Eigenstate Thermalization Hypothesis [31,34,35]; this can be formulated as an ansatz on the matrix elements of $\hat{O}$:

$$O_{mn} = O(\bar{E})\delta_{mn} + \mathrm{e}^{-\frac{S(\bar{E})}{2}} f_O(\bar{E}, \omega) R_{mn}, \tag{1.23}$$

where $\bar{E} = (E_m + E_n)/2$, $\omega = E_n - E_m$ and $S(E)$ is the entropy at energy E. $O(\bar{E})$ and $f_O(\bar{E}, \omega)$ are smooth functions of $\bar{E}$ and ω, $O(\bar{E})$ is equal to the microcanonical expectation value O_{ME} at energy $\bar{E}$ and R_{mn} is a random variable with zero mean and unit variance. Moreover, by taking the Hermitian conjugate of Eq. (1.23), we obtain that the relations

$$\begin{aligned} R^*_{nm} &= R_{mn} \\ f^*_O(\bar{E}, -\omega) &= f_O(\bar{E}, \omega) \end{aligned} \tag{1.24}$$

must be satisfied.

The difference between the random matrix result of Eq. (1.21) and the one in Eq. (1.23) lies on the fact that the diagonal matrix elements are no longer the same in all eigenstates but, rather, they are smooth functions of the energy of the eigenstates; moreover, the off-diagonal matrix elements have an envelope f_O which depends on the mean energy and the energy difference of the involved eigenstates. It is worthwile to note that the ansatz (1.23) reduces

to Eq. (1.21) in a very small energy window where f_O can be considered constant; the scale of this window is given by the Thouless energy

$$E_T = \frac{\hbar D}{L^2}, \tag{1.25}$$

where D is the diffusion coefficient and L is the linear size of the system.

Going back to the localized states of a disordered Hamiltonian, the failure of the Eigenstate Thermalization Hypothesis can be intuitively understood noting that equilibration should depend on the time scales of the system dynamics. We can identify two time scales in a system with not so many degrees of freedom: one is diffusion, which governs long time relaxation, and the other is the mean level spacing, which is related to the fast decay dynamics. In order to be able to apply the Eigenstate Thermalization Hypothesis, diffusive relaxation must indeed be much slower than the fast decays, that is

$$s \ll \frac{\hbar}{\tau_{\text{diffusion}}} \tag{1.26}$$

which is the condition that is violated in the localized phase, where there is high probability of small energy gaps [36–38].

1.4 From one particle to many body

Anderson's results have influenced our fundamental understanding of disordered systems and a whole class of metals and insulators. A crucial question, however, is whether the picture we have so far about localization survives once interaction between the particles is added, which could make this mechanism robust. This problem has remained unsolved for fifty years; the first treatments focused on coupling the localized Anderson model to a phonon bath, which results in the restoring of the conductivity at low finite temperature, in an enhanced way with respect to the contribution of only a thermal activation of the mobility edge (this is called variable range hopping [39]). It was not until the work of Basko, Aleiner and Altshuler [2] in 2005 that the original question was answered comprehensively, showing that, as the interactions act in a nonperturbative way, a localized state can still exist and there is a transition, named Many Body Localization transition, governing the dynamical properties of the system. This development has sparked a renewed interest in the topic of Anderson localization and has become the most robust mechanism for ergodicity breaking in interacting systems [40–44].

The idea of localization in interacting systems is twofold. One can characterize the localization properties based on the dynamics of the system and

on the response to a small perturbation; in this way of thinking, a state is localized as soon as a perturbation is no longer able to travel to macroscopic distances. However, one can also picture the phenomenon as a localization happening in the Fock space, meaning that a many-body localized state is similar to a Slater determinant of single particle states. This suggests a close analogy between the properties of single particle and many-body localized states. This is actually true only up to a point; some properties, for example the entanglement spreading, show a different behavior in the noninteracting and in the interacting case.

The interest in this class of models which has unfolded in the recent years has been both theoretical and experimental, including a regard to technological applications due to the unique features of the localized phase. Nonetheless, this topic has proven to be a difficult one to attack both analytically and numerically. The main result of this thesis is showing that the *forward* approximation is a method which can be used proficiently in the analysis of both single particle and many-body systems, for both analytic and numerical calculations; this result will be presented in detail in Chapter 5, toghether with a discussion on the ergodicity properties of many-body localized and delocalized states. Let us now proceed instead to review some fundamental phenomenology of the many-body localization transition.

1.5 The many body model and definition of localization

As a reference, let us introduce the tight binding Hamiltonian

$$\begin{aligned} H &= \sum_i \epsilon_i c_i^\dagger c_i - t \sum_{\langle ij \rangle} c_i^\dagger c_j - \Delta \sum_{\langle ij \rangle} c_i^\dagger c_i c_j^\dagger c_j + h.c. \\ &\equiv H_0 + T + H_{\text{int}}, \end{aligned} \tag{1.27}$$

i.e. with respect to Anderson's Hamiltonian (1.3) we are turning on a nearest-neighbour interaction term H_{int}. c and $c^\dagger$ are fermionic annihiliation and creation operators. This is equivalent to consider an XXZ spin-1/2 chain, since a Jordan Wigner transformation maps the two Hamiltonians one into the other. The full many-body Fock space has size 2^L, where L is the size of the system (i.e. the number of spins). We note that the symmetry of this Hamiltonian partitions the full space into sectors of fixed number of particles N, or fixed total magnetization in spin language; it is common to restrict ourselves to the biggest of this sectors, i.e. the half filling sector, which has dimension $\binom{L}{N} = \binom{L}{L/2}$.

This class of Hamiltonian is realizable experimentally [45–48]. Indeed, one is able to create an optical lattice which reproduces the desired lattice; then, there are two main ways to introduce on-site disorder, that is a speckle potential, where a laser light is scattered over all the lattice resulting in a random but correlated contribution to the on-site potential, and a quasidisordered potential. In the latter case, one uses interfering lasers to generate a standing wave whose period is incommensurable with that of the optical lattice; this is actually the implementation of the Aubry–André model, i.e. where the on-site quasidisorder is given by

$$\epsilon_i = \cos(2\pi\phi^{-1} i + \delta), \tag{1.28}$$

where we denoted with ϕ the golden ratio, and δ is an arbitrary phase. Note that neither case implements true randomness in the on-site potential.

We can define localization in a many-body system in multiple ways. One is, analogously to Anderson's statement, the absence of dynamics in the many-body localized system. More precisely, Basko, Aleiner and Altshuler define localization based on the properties of the correlators of local observables. Indeed, it is a consequence of single-particle localized wavefunctions (i.e. with an exponentially decaying envelope) that, taking the matrix elements of a local operator $A(r)$ (e.g. the mass density or current density operator)

$$A_{ab}(r) = \int \mathrm{d}r' \psi_a(r')^* A(r) \psi_b(r'), \tag{1.29}$$

then its correlator satisfies

$$\mathcal{L}^A_{ab}(r) = \int \mathrm{d}r' A_{ab}(r') A_{ba}(r'+r) \propto \begin{cases} \leq \mathrm{e}^{-|r|/\xi} & \text{localized} \\ f\left(\frac{|r|}{L_\omega(a,b)}\right) & \text{extended,} \end{cases} \tag{1.30}$$

where L_ω is a length scale controlled by $\omega(a,b) = E_a - E_b$, the difference in energy between the levels a and b. This statement implies that in the localized region there is no diffusion, by means of the Kubo formula; in other words, an excitation caused by a local external perturbation can not propagate. This line of reasoning can be extended to the many-body case, by considering a local additive one-particle observable

$$\mathcal{A}(r) = \sum_{ab} A_{ab}(r) c^\dagger_a c_b, \tag{1.31}$$

whose matrix elements between many-body eigenstates $|\Psi\rangle$ are $\mathcal{A}_{kk'}(r) = \langle \Psi_k | \mathcal{A}(r) | \Psi_{k'} \rangle$; then localization is defined by:

$$\mathcal{L}_{kk'}(r) = \int \mathrm{d}r' A_{kk'}(r') A_{k'k}(r'+r) \propto \begin{cases} \leq \mathrm{e}^{-\frac{|r|}{\xi_k}} & \text{localized} \\ f\left(\frac{|r|}{L_\omega}\right) & \text{extended.} \end{cases} \tag{1.32}$$

As in the single particle case, this definition implies that the Kubo linear response function gives a zero conductivity or diffusion coefficient.

States which are completely characterized by a set of occupation numbers have correlators of proper local observables that follow the localization definition in (1.32). Indeed, another way to picture it is localization in the Fock space of configurations: a localized state is similar to a Slater determinant of a few (but still exponentially many), near elements of the configurations basis. We can use a properly normalized participation ratio in order to spot this property; denoting with $\Psi_i^{(k)}$ the many-body wavefunction amplitude over the configurations basis, the normalized participation ratio is defined as:

$$\mathrm{NPR}_2 = \left\langle \frac{1}{\mathcal{N} \sum_i \left|\Psi_i^{(k)}\right|^4} \right\rangle, \tag{1.33}$$

where $\mathcal{N} \propto 2^L$ is the size of the Fock space, with $\mathcal{N} \to \infty$ in the thermodynamic limit, and the average is intended over disorder realizations. In the ergodic regime the wavefunction is spread across all the volume $\mathcal{N}$ of the configurations space, therefore the sum in the denominator is of the form $\sum_i |\Psi_i|^4 \sim \mathcal{N} \cdot \mathcal{N}^{-2}$, and thus $\mathrm{NPR}_2 \propto O(1)$. Instead, in the localized regime, only few of the coefficients are of $O(1)$ and will contribute to the sum; however, they are still exponentially many in the system size L, behaving as 2^{aL} with $a < 1$. Therefore, the sum in the denominator becomes $\sum_i |\Psi_i|^4 \sim 2^{aL} \cdot O(1)$, and thus $\mathrm{NPR}_2 \propto 2^{-(1+a)L} \to 0$ as $L \to \infty$.

1.5.1 The many body localization transition

The idea expressed so far is that the question of many-body localization is related to the thermalization of an Hamiltonian such as (1.27) for an arbitrary initial condition. In order to inspect a system for its localization properties, one can make use of an extension of Anderson's reasoning to the many-body problem.

The first step towards a microscopic analytic understanding of many-body localization is approximating an interacting, zero-dimensional, infinite system with a single particle problem on a Bethe lattice [49]. Extending this result, Basko, Aleiner and Altshuler investigated the microscopic mechanism for localization in interacting systems, definitively obtaining that localization is stable with respect to interactions and there is a localization/delocalization transition up to a finite temperature. Indeed, they started from a system whose Hamiltonian, written in the basis of the exact single particle wave-

functions, is

$$H = \sum_{\alpha} \zeta_\alpha c_\alpha^\dagger c_\alpha + \sum_{\alpha\beta\gamma\delta} V_{\alpha\beta\gamma\delta} c_\alpha^\dagger c_\beta^\dagger c_\gamma c_\delta \tag{1.34}$$

with the interaction term $V_{\alpha\beta\gamma\delta} = \frac{1}{2}\int V(\mathbf{r},\mathbf{r}')\rho_{\alpha\delta}(\mathbf{r})\rho_{\beta\gamma}(\mathbf{r}')\,\mathrm{d}^d\mathbf{r}\,\mathrm{d}^d\mathbf{r}'$, where $\rho_{\alpha\delta}(\mathbf{r}) = \phi_\alpha^*(\mathbf{r})\phi_\delta(\mathbf{r})$, restricted both in space and to states closer in energy than the single-particle level spacing. The basis of single particle states is composed of the eigenvectors $\phi_\alpha(\mathbf{r})$ given by

$$\left[-\frac{\nabla^2}{2m} + U(\mathbf{r})\right]\phi_\alpha(\mathbf{r}) = \zeta_\alpha \phi_\alpha(\mathbf{r}) \tag{1.35}$$

where ζ_α are the corresponding eigenvalues; $U(\mathbf{r})$ is the on-site disorder potential. By discretizing the Hamiltonian (1.34) and rewriting it in the basis of states localized in one site (or localization cell), we obtain a form, slightly more general than (1.27) (because of the more general form of the interaction $V_{l_1 l_2 l_3 l_4}$):

$$H = \sum_{l} \zeta_l c_l^\dagger c_l - t\sum_{\langle lm\rangle} c_l^\dagger c_m - \sum_{\langle l_1 l_2 l_3 l_4\rangle} V_{l_1 l_2 l_3 l_4}\, c_{l_1}^\dagger c_{l_2} c_{l_3}^\dagger c_{l_4} + h.c. \tag{1.36}$$

Taking a finite size system, one can then consider an excitation on top of an eigenstate and study the perturbative expansion of the imaginary part of the self energy, using the Keldysh formalism. This pertubative series, once the thermodynamic limit is carefully taken, is then found to converge, implying, as in Anderson's calculation, a many-body localized phase.

Besides the detection of a many-body localized phase using this suitable version of the locator expansion, an additional claim of their work is the persistence of localization up to a finite, extensive energies in systems where not all many-body states are localized. One therefore obtains the behavior of the conductivity pictured in Fig. 1.4, where the critical temperature is a function of said extensive energy. The conductivity vanishes in the localized phase, meaning that a memory of the local initial conditions is preserved for arbitrarily long times. Note that the reverse is not true, i.e. there exist models with zero conductivity in which thermal states appear (e.g. Floquet systems).

As a final note, it is worth pointing out that many-body localized states can exists, besides in models with true randomness, also in systems with quasiperiodic disorder such as the Aubry–André model; this is of great importance for experimental works.

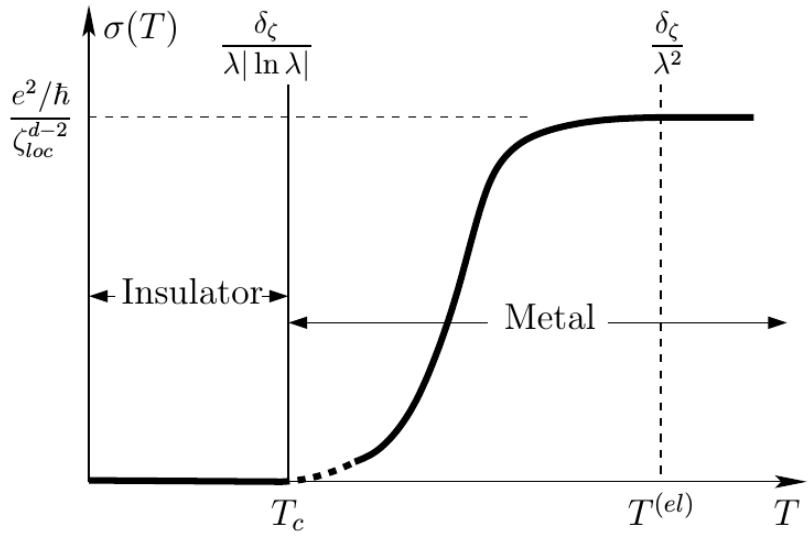

Figure 1.4: Qualitative plot of the conductivity $\sigma(T)$ as a function of temperature in a system showing a many-body localization transition. Figure taken from Ref. [2].

1.5.2 Phenomenology of many body localized and delocalized state

It is interesting to compare the properties of a many-body localized state to a delocalized state and spot the differences with respect to the single particle case. In Table 1.1 (taken from Ref. [42]) we list the most relevant ones; besides the already discussed phenomenology of transport (causing, e.g., zero conductivity in a localized phase, both for single particle and for many-body) and the violation of the Eigenstate Thermalization Hypothesis (ETH), one can see the consequences of localization also in the spectral properties, with the distribution of the level gaps going from a Wigner Dyson distribution to a Poisson distribution in the localized phase. This is in analogy with the single particle case, and the r parameter defined in Eq. (1.14) can also be used in the many-body context to discriminate between localized and delocalized states.

Localized states are peculiar also with regards to entanglement. First, let us note that the entanglement entropy must be well-behaved in a thermalizing state, i.e. it is extensive in the volume of the Hilbert space for an eigenstate, at finite temperature. This is not the case for the localized phase, where one can approximate the state with the product state of the contributions of the single lattice sites (for the single particle case), or with a Slater determinant of localized single particle states (for the many-body

	Delocalized	Single particle Localized	Many Body Localized
Memory of initial conditions	in global observables	yes, in local observables	yes, in local observables
ETH	holds	does not hold	does not hold
DC conductivity	can be nonzero	zero	zero
Local spectrum	continuous	discrete	discrete
Eigenstate entanglement	volume-law	area-law	area-law
Spreading of entanglement	power-law	no spreading	logarithmic
Dephasing and dissipation	yes	no	dephasing but no dissipation

Table 1.1: Comparison of some of the properties of delocalized, single particle localized and many-body localized states. Table taken from Ref. [42].

case). Therefore, the entanglement entropy will be subextensive, following an area law [50]. Moreover, in the delocalized phase, one expects that interactions generate entanglement; indeed, it is understood that, as an initial, unentangled state thermalizes, entanglement grows due to the range of interactions with a speed which can be up to ballistic, or sub-ballistic (i.e. power law in time) in presence of weaker propagation. Since the single particle state does not involve interactions of any kind, if we start from a non entangled state, the initial state will not thermalize and there will be no creation of entanglement. The picture changes in the many-body case: here, the interactions due to the nature of the system will create entanglement even if there is no thermalization; however, the interaction will act only directly and on a range which is exponentially suppressed within the localization length, and its growth will be slower than any kind of subdiffusion, meaning that the entanglement spreads logarithmically in time [19]. The latter case is related to the dephasing of an initial state; indeed one can understand that in the many-body case, contrary to the single particle one, there must be some dephasing, which is however unaccompanied by the dissipation which is a clear consequence of a thermal state.

Finally, additional support to the idea that a localized state preserves a memory of the initial state is given by the fact that in the localized phase there exist a full set of integrals of motion (which can be explicitly constructed) which are local and encode this information. One can still construct such kind of operators in the delocalized phase; however, it turns out that they are not local, thus diluting, or hiding, this memory [51–53].

Chapter 2

Localization in the Anderson model

2.1 Introduction

As the problem of diffusion in strongly disordered materials was tackled and solved by Anderson, the investigation of this class of models has flourished, resulting in the understanding of many peculiarities about the localized states. Sixty years after, this topic is still on the cutting edge of research. This chapter is a recollection of results that have been obtained for the (noninteracting) disordered tight binding model commonly referred to as the Anderson model, starting from the main result by Anderson [1], who showed that for sufficiently strong disorder a transition to localized and nondiffusive states occur. A full analytical solution has been obtained in the Bethe lattice [54], where one can make use of helpful simplifications. The setup that will be presented in this chapter will be useful once we discuss the *forward* approximation in Chapter 3.

2.2 The localization transition

In his original paper [1] Anderson introduced a tight binding model of a particle subject to nearest neighbour hopping and on-site interaction; the disorder enters through the latter and its strength is taken randomly from a uniform distribution of width W. This is the simplest model which exhibits a localization phenomenology. In this section we will review the main results of Ref. [1].

More precisely, let us consider a system whose Hamiltonian is

$$H = \sum_i \epsilon_i c_i^\dagger c_i - V \sum_{\langle ij \rangle} c_i^\dagger c_j + h.c. \equiv H_0 + T \tag{2.1}$$

where $c^\dagger$ and c are fermionic creation and annihiliation operators. In the first term we introduce the diagonal random on-site energies ϵ_i, independently extracted from the distribution

$$p(\epsilon) = \begin{cases} W^{-1} & \epsilon \in [-\frac{W}{2}, \frac{W}{2}] \\ 0 & \text{otherwise,} \end{cases} \tag{2.2}$$

while the second term is the nearest neighbour hopping with strength V. Our aim is to understand under which conditions a perturbation in a small region of the lattice does not propagate and wash out over the whole system as time evolves.

Anderson's idea was to build a perturbative expansion in the hopping starting from a localized state; the signal of localization is the convergence of such expansion. Instead, if one tries to start from the freely hopping system without disorder, one cannot extract the qualitative features of the localized state and the transition is not visible. We call this series the *locator expansion*, since it involves the inverse of the on-site energies $(E - \epsilon_i)^{-1}$ for each site.

2.2.1 The perturbative expansion

Let us start by considering the resolvent operator for the Hamiltonian H at energy E, defined as the Fourier transform

$$G(E) \equiv (E - H)^{-1} = F^{-1}\left[-\imath\theta(t)\, \mathrm{e}^{-\imath H t}\right] \tag{2.3}$$

and, analogously, the one for just the on-site disorder term, $G^0 = (E - H_0)^{-1}$. In the lattice, its matrix elements are

$$G_{ij}(E) = \langle i | \, (E - H)^{-1} \, | j \rangle, \tag{2.4}$$

where the vectors $|a\rangle$ make up a basis of states associated to a single lattice site. We can build a perturbative expansion using Dyson's equation

$$G = G^0 + G^0 T G; \tag{2.5}$$

in terms of the matrix elements we obtain:

$$G_{ij}(E) = \frac{\delta_{ij}}{E - \epsilon_i} + V \sum_k \frac{1}{E - \epsilon_i} G_{kj}. \tag{2.6}$$

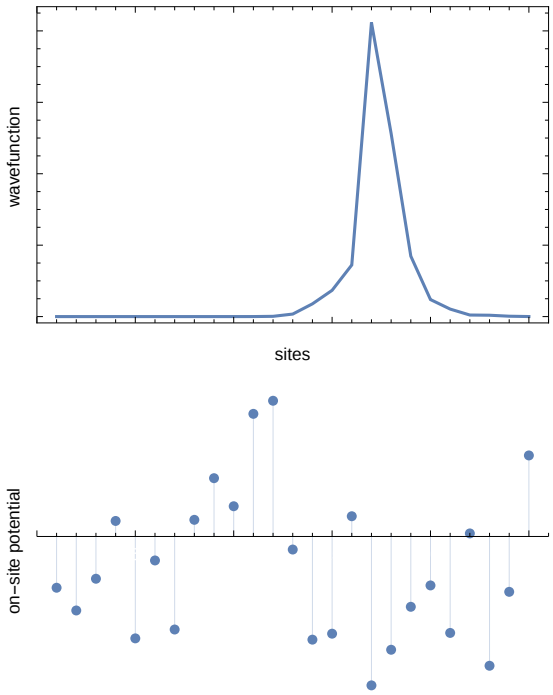

Figure 2.1: A realization of a one dimensional Anderson model. Bottom: value of the disorder on each site; top: a (localized) wavefunction at low energy.

We can iterate Dyson's equation and obtain a perturbative expansion in the hopping V; let us rewrite

$$\begin{aligned} G_{ij}(E) =& \frac{\delta_{ij}}{E-\epsilon_i} + V\sum_k \frac{1}{E-\epsilon_i} G_{kj} \\ =& \frac{\delta_{ij}}{E-\epsilon_i} + \frac{V}{E-\epsilon_i} G_{jj} + V\sum_{k\neq j} \frac{1}{E-\epsilon_i} G_{kj}; \end{aligned} \tag{2.7}$$

then, iterating, we obtain:

$$\begin{aligned} G_{ij}(E) =& \frac{\delta_{ij}}{E-\epsilon_i} + \left(\frac{V}{E-\epsilon_i} + V^2 \sum_{k\neq j} \frac{1}{E-\epsilon_i}\frac{1}{E-\epsilon_k} \right) G_{jj} \\ &+ V^2 \sum_{k\neq j,\, l\neq j} \frac{1}{E-\epsilon_i}\frac{1}{E-\epsilon_k} G_{lj} \\ =& \cdots = \frac{\delta_{ij}}{E-\epsilon_i} + \sigma_{ij} G_{jj}, \end{aligned} \tag{2.8}$$

where

$$\sigma_{ij} = \frac{V}{E-\epsilon_i} + V^2 \sum_k \frac{1}{E-\epsilon_i}\frac{1}{E-\epsilon_k} + \dots . \tag{2.9}$$

Let us now consider the resolvent which connects to the same lattice site, G_{ii}:

$$\begin{aligned} G_{ii} &= \frac{1}{E-\epsilon_i} + \frac{V}{E-\epsilon_i} \sum_k G_{ki} \\ &= \frac{1}{E-\epsilon_i} + \frac{V}{E-\epsilon_i} \sum_k \sigma_{ki} G_{ii}. \end{aligned} \tag{2.10}$$

Introducing the self-energy

$$\begin{aligned} \Sigma_i(E) =& V\sum_k \sigma_{ki} \\ =& V^2 \sum_{k\neq i} \frac{1}{E-\epsilon_k} + V^3 \sum_{k,l\neq i} \frac{1}{E-\epsilon_k}\frac{1}{E-\epsilon_l} + \dots , \end{aligned} \tag{2.11}$$

we can rewrite the expansion for G_{ii} in a compact way:

$$\begin{aligned} G_{ii}(E) &= \frac{1}{E-\epsilon_i} \left(1 + V\sum_k \sigma_{ki} G_{ii} \right) \\ &= \frac{1}{E-\epsilon_i} \left(1 - \frac{V}{E-\epsilon_i} \sum_k \sigma_{ki} \right)^{-1} \\ &= [E - \epsilon_i - \Sigma_i(E)]^{-1}. \end{aligned} \tag{2.12}$$

This is the locator expansion for the Green's function and the starting point to determine whether there is localization, in Anderson's work [1] as well as in the one presented in Chapter 3. Indeed, the Fourier transform of the resolvent

$$G_{ii}(t) = \langle i|G(t)|i\rangle = -\imath\theta(t)\langle i|\,\mathrm{e}^{-\imath Ht}|i\rangle \tag{2.13}$$

corresponds to the probability that a particle is in the site i at time t; therefore, if the initial state is fully localized in i, i.e.

$$\psi_j = \delta_{ij}, \tag{2.14}$$

by looking at

$$\begin{aligned} G_{ii}(t) &= F^{-1}\left[G_{ii}(E)\right] = F^{-1}\left[\frac{1}{E-\epsilon_i-E_i+\imath\Delta_i}\right] \\ &= -\imath\,\mathrm{e}^{\imath t(\epsilon_i+E_i)-\Delta_i t}\theta(t), \end{aligned} \tag{2.15}$$

where $E_i = \Re(\Sigma_i)$ and $\Delta_i = -\Im(\Sigma_i)$, we are able to spot whether at long times there will be a nonzero amplitude in site i. A nonzero imaginary part in the self energy means that there is an exponential decay in time and the probability of the perturbation returning to the site i is vanishing; inversely, if the imaginary part is zero, there is localization. Therefore we should look at the imaginary contribution or, more precisely, at its mean (which however may very well be ill defined in the localized region) or, rather, at its most probable value, in order to check whether it vanishes, since we are dealing with random variables. It turns out that the probability distribution for Δ_i is well behaved, with a finite mean, at any finite perturbative order; one has indeed to take into account the whole series in order to obtain a vanishing most probable value (and an ill defined mean value).

There is still a problem with the perturbation series of the self energy written as in (2.11). This series can be seen as the sum over all the paths of all lengths that come back to the initial point only once. If in these paths happen to bounce back repeatedly between few sites, due to having energies close to E, then the result is a product of many small denominators which can cause a divergence which is unrelated to the localization properties of the state, and is instead related to the clonesess and crossings of energy levels. In order to understand the reason why this can happen, let us take a trivial example: let us consider a system with two sites, which has Hamiltonian

$$H = \begin{pmatrix} e_1 & t \\ t & e_2 \end{pmatrix} = \Lambda \begin{pmatrix} e_- & 0 \\ 0 & e_+ \end{pmatrix} \Lambda^\dagger, \tag{2.16}$$

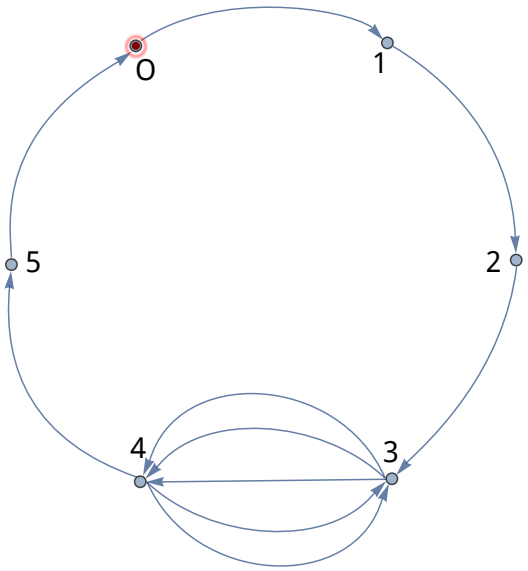

Figure 2.2: Resonating loops in a given path contributing to the locator expansion. These kind of loops are the ones whose contribution can be resummed by reordering the terms of the series, as in Eq. (2.24).

with its spectrum given by

$$e_\pm = \bar{e} \pm \frac{1}{2}\sqrt{\Delta e + 4t^2} \tag{2.17}$$

and its eigenfunctions by

$$\psi_\pm = \left(\frac{\Delta e}{2t} \pm \frac{1}{2t}\sqrt{\Delta e^2 + 4t^2},\ 1 \right), \tag{2.18}$$

where

$$\bar{e} = \frac{e_1 + e_2}{2}, \quad \Delta e = e_1 - e_2. \tag{2.19}$$

It can be noted that the square root in the eigenfunctions amplitudes can be expanded perturbatively in the hopping t up to the radius of convergence $t \leq \frac{\Delta e}{2}$, which is proportional to the spacing of the random on-site energies. For n random variables the typical minimum spacing decreases with the power law n^{-2}; therefore, increasing the size of the system the radius of convergence vanishes.

We can remove the uninteresting divergences caused by energy levels that are close to each other in the thermodynamic limit by restricting the series only to non-repeating, renormalized paths. We can rearrange the terms in

Eq. (2.10) so that the series is defined over a set of indices with no repetitions while at the same time we sum over the loops corresponding to index repetitions for each of the indices step by step. Thus in Eq. (2.10) we can rewrite

$$\begin{aligned} G_{ii} &= \frac{1}{E-\epsilon_i} + \frac{V}{E-\epsilon_i}\sum_k G_{ki} \\ &= \frac{1}{E-\epsilon_i} + \frac{V^2}{E-\epsilon_i} G_{l_1 l_n}, \end{aligned} \tag{2.20}$$

where

$$G_{l_1 l_n}(E) = \sum_n \sum_{\{l_i\}\in \mathrm{paths}_n(l_1,l_n)} \frac{V^{n-1}}{(E-\epsilon_{l_1})\cdots(E-\epsilon_{l_n})} \tag{2.21}$$

contains all the contributions from the (repeating) paths between the intermediate sites between l_1 and l_n (see Fig. 2.2), as

$$G_{l_1 l_n}(E) = \frac{V}{E-\epsilon-\Sigma_{l_1}} \sum_{l'\neq l_1} G^{(\neq l_1)}_{l' l_n}, \tag{2.22}$$

where in $G^{(\neq l_1)}_{l' l_n}$ only paths which do not visit site l_1 appear. Respectively, $G^{(\neq l_1)}_{l' l_n}$ is given by

$$G^{(\neq l_1)}_{l' l_n}(E) = \frac{V}{E-\epsilon_{l'}-\Sigma^{(\neq l_1)}_{l'}} \sum_{l''\neq l'} G^{(\neq l_1, l')}_{l'' l_n} \tag{2.23}$$

and an analogous form holds for the self energy, which now has to be computed self-consistently:

$$\Sigma_j(E) = \sum_n \sum_{l_1,\ldots,l_n\neq j} \frac{V^{n+1}}{(E-\epsilon_{l_1}-\Sigma^{(\neq j)}_{l_1})\ldots(E-\epsilon_{l_n}-\Sigma^{(\neq j)}_{l_n})}. \tag{2.24}$$

There is a case (the Bethe lattice) in which these equations can be solved exactly; in the other cases, we can obtain at least an estimation of the transition point by neglecting the self energies in the denominators, which has the effect of making the terms of the series larger and provide an overestimation of the critical value of W/V of the convergence of this expansion.

In Chapter 3 we will resume this discussion by presenting the forward approximation, i.e. we will neglect the self energy and we will take into account only the contributions coming from the paths of minimum length.

2.2.2 Upper bound to the critical disorder for localization

Let us now attempt to identify the transition by inspecting the convergence of the locator expansion. Let us start from the expansion of the self energy over the non-repeating paths, Eq. (2.24):

$$\Sigma_j(E) = \sum_n \sum_{i \in \text{paths}} T_n^{(i)} \tag{2.25}$$

where T_n are the individual terms at order n; they will be a sum of elements of the form

$$T_n = V^n \prod_{i=1}^{n} \frac{1}{e_{l_i}}, \quad e_l = E - \epsilon_l - \Sigma_l^{(\neq \dots)}, \tag{2.26}$$

where the indices l_i are non-repeating because ot the rearranging of the expansion. The transition can be determined by studying their probability distribution in order to determine under which condition the series for the self energy is convergent.

We make the approximation of neglecting the self energies $\Sigma_i^{(\neq \dots)}$ in the denominators, which means that (2.26) is a product of independent random variables. This, as explained before, results in an overestimation of the terms of the series and therefore in an upper bound of the transition value.

Moreover, the number of non-repeating paths returning to the starting point after n steps is $\mathrm{O}(K^n)$, where K is the connectivity of the lattice; we assume that each of such paths gives a contribution which is statistically independent from the others. This is clearly not the case, since the paths can have sites in common; however, using this approximation we can obtain a result which is again an upper bound to the transition, making the two approximations compatible.

Let's proceed by calculating the probability distribution of T_n. The random variables e_l in the denominators of (2.26) will have, under our approximations, the same distribution as the on-site energies:

$$p(e_l) = \begin{cases} W^{-1} & e_l \in [-W/2, W/2] \\ 0 & \text{otherwise} \end{cases}. \tag{2.27}$$

Let us now define a set of auxiliary variables:

$$\begin{aligned} y_i &= -\log \left| \frac{2e_{l_i}}{W} \right| \\ Y &= \sum_i y_i \\ w_n &= \mathrm{e}^Y; \end{aligned} \tag{2.28}$$

then

$$|T_n| = \left(\frac{2V}{W}\right)^n w_n. \tag{2.29}$$

Using the standard method of the Laplace transform we can calculate the distributions of y_i and Y:

$$\begin{aligned} P_y(y) &= \mathcal{L}^{-1}\left[\int_{-\infty}^{\infty} p_\epsilon(\epsilon)\,\mathrm{e}^{-sy}\,\mathrm{d}\epsilon\right] \\ &= \mathcal{L}^{-1}\left[\int_{-\frac{W}{2}}^{\frac{W}{2}} \frac{1}{W}\left(\frac{2\,|\epsilon|}{W}\right)^s \mathrm{d}\epsilon\right] \\ &= \mathcal{L}^{-1}\left[\frac{1}{s+1}\right] \\ &= \mathrm{e}^{-y}\,\theta(y) \end{aligned} \tag{2.30}$$

and

$$\begin{aligned} P_Y(Y) &= \mathcal{L}^{-1}\left[\prod_{i=1}^{n} \mathcal{L}\left[P_y(y)\right](s)\right] \\ &= \mathcal{L}^{-1}\left[\frac{1}{(s+1)^n}\right] \\ &= \frac{Y^{n-1}\,\mathrm{e}^{-Y}}{(n-1)!}\theta(Y) \end{aligned} \tag{2.31}$$

and therefore, substituting $w_n = \mathrm{e}^Y$:

$$\begin{aligned} \mathrm{Prob}(Y,\,\mathrm{d}Y) = \frac{Y^{n-1}\,\mathrm{e}^{-Y}}{(n-1)!}\,\mathrm{d}Y = \\ = \frac{(\log w_n)^{n-1}}{(n-1)!\,w_n^2}\,\mathrm{d}w_n = \mathrm{Prob}(w_n,\,\mathrm{d}w_n), \end{aligned} \tag{2.32}$$

we obtain

$$P_{w_n} = \frac{(\log w_n)^{n-1}}{(n-1)!\,w_n^2}. \tag{2.33}$$

Recall that the term of order n is the sum over the K^n non-repeating paths

$$\sum_{i\in\mathrm{paths}} T_n^{(i)} \equiv \left(\frac{2V}{W}\right)^n O_n \tag{2.34}$$

in which we assume that its terms are statistically independent. Note that the probability distribution of w_L has a long tail, in that its first and second moment are not finite. The sum of such long tailed distributed random variables is dominated by the maximum term and we can limit ourselves to consider only the probability distribution of this maximum instead of the full distribution. Therefore, we can write

$$\begin{aligned}\text{Prob}(|O_n| < O) \approx &\text{Prob}\left(\max\left\{w_n^{(1)} \dots w^{(K^n)}\right\} < O\right) \\ &= \left(1 - \int_O^\infty P_{w_n}(w_n)\,\mathrm{d}w_n\right)^{K^n}\end{aligned} \tag{2.35}$$

and, differentiating in order to obtain the probability density, we get for the tail of large O:

$$\begin{aligned}P_{O_n}(O_n) &= K^n\, P_{w_n}(O)\left(1 - \int_O^\infty P_{w_n}(w_n)\,\mathrm{d}w_n\right)^{K^n-1} \\ &\approx K^n P_{w_n}(O).\end{aligned} \tag{2.36}$$

The last step consist of making sure that the full series

$$\Sigma = \sum_n \left(\frac{2V}{W}\right)^n O_n \tag{2.37}$$

converges; this can be done by showing that it is bounded by a convergent geometric series with high probability, that is, term by term the condition

$$\left(\frac{2V}{W}\right)^{\tilde{n}} O_{\tilde{n}} \leq x^{\tilde{n}} \tag{2.38}$$

has to be verified for an $x < 1$ and from a $\tilde{n}$ onwards. Indeed, let us compute the probability that the terms of the geometric series will be greater than O_n asimptotically, that is:

$$p = \text{Prob}\left(\exists N, x < 1 : \forall n > \tilde{n}\ |O_L| < \left(\frac{Wx}{2V}\right)^n\right); \tag{2.39}$$

then

$$p = \lim_{x\to 1}\lim_{N\to\infty}\prod_{n=\tilde{n}}^{\infty}\int_0^{\left(\frac{W}{2V}x\right)^n} P_{O_n}(O_n)\,\mathrm{d}O_n, \tag{2.40}$$

which can be worked out as

$$\begin{aligned}\int_0^{\left(\frac{W}{2V}x\right)^n} P_{O_n}(O_n)\,\mathrm{d}O_n &= 1-\int_{\left(\frac{W}{2V}x\right)^n}^{\infty} P_{O_n}(O_n)\,\mathrm{d}O_n \\ &= 1-K^n\int_{\left(\frac{W}{2V}x\right)^n}^{\infty} P_{w_n}(O_n)\,\mathrm{d}O_n \\ &\approx \left(\frac{2VeK\log\frac{Wx}{2V}}{Wx}\right)^n \mathrm{O}\left(n^{-1/2}\right),\end{aligned} \tag{2.41}$$

having used Stirling's approximation

$$\int_a^{\infty}\frac{(\log x)^{n-1}}{(n-1)!\,x^2}\,\mathrm{d}x \approx \left(\frac{e}{a}\log a\right)^n \mathrm{O}\left(n^{-\frac{1}{2}}\right). \tag{2.42}$$

Therefore we obtain

$$p=\lim_{x\to 1}\lim_{N\to\infty}\prod_{n=N}^{\infty}\left[1-\left(\frac{2VeK\log\frac{Wx}{2V}}{Wx}\right)^n \mathrm{O}\left(n^{-1/2}\right)\right] \tag{2.43}$$

and this probability goes to 1 if the geometric series is convergent, that is

$$\frac{2VeK}{W}\log\frac{W}{2V}<1, \tag{2.44}$$

which means that the series is almost surely convergent and therefore the state is localized; in the opposite regime analogously the series will diverge almost surely.

We stress again that an important factor in the reasoning is that in the term of order n in the pertubation theory of the self energy, of the K^n terms that contribute to it, it is the largest weight that dominates; this means that the main contribution to the decay of the localized state comes from a single path. Indeed, if we were to assume that the paths with typical weights are the relevant ones to the purpose of the convergence of the series, we would obtain that

$$T_n\sim\left(\frac{KV}{\tilde{\epsilon}}\right)^n \tag{2.45}$$

with $\tilde{\epsilon}$ a typical value of the denominator (we assume $E=0$ or the center of the band); a typical value for it is

$$\int_{-\frac{W}{2}}^{\frac{W}{2}}|\epsilon|\,P_\epsilon(\epsilon)\,\mathrm{d}\epsilon=\frac{W}{4} \tag{2.46}$$

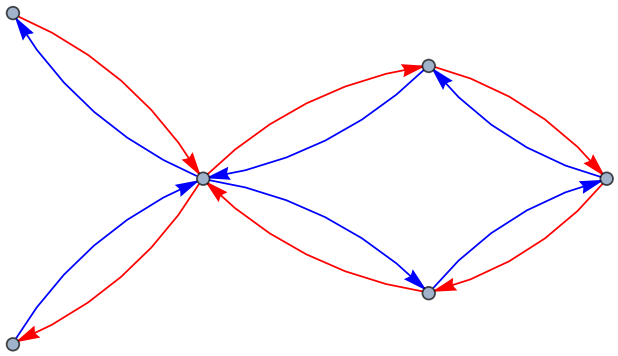

Figure 2.3: Example of resonance caused by self-crossing paths which enhance constructive interference and therefore localization in low dimensions.

and that leads to the convergence condition

$$\frac{4KV}{W} < 1 \tag{2.47}$$

which is a larger condition than (2.44), which means that the localized states are actually much less stable than what would result by considering only typical paths, and it is the particularly favorable paths that are key to destroying localization.

2.2.3 The role of dimensionality and temperature

Up to now, we have disregarded any discussion on the lattice on which the Anderson model is set up. However, it turns out that dimensionality plays a strong role in the localization properties.

Scaling theory arguments [55] show that in one and two dimensions the conductivity vanishes for arbitrarily small disorder; this means that, as soon as we turn on an infinitesimal disorder, the system becomes localized. This is independent of the convergence of the locator expansion, which has a finite radius of convergence even in one and two dimensions. The localization, in this cases, is due to new effects which are specific to the low dimensionality, namely the presence of ehnanced resonances.

An intuitive argument to understand this involves the semiclassical return probability of a particle in a lattice [12]. Let us consider the amplitude of a quantum particle which starts in the origin and which returns to it; this is given by a sum over Feynman paths,

$$a_{0\to 0} = \sum_i a_i \, \mathrm{e}^{\imath S_i}, \tag{2.48}$$

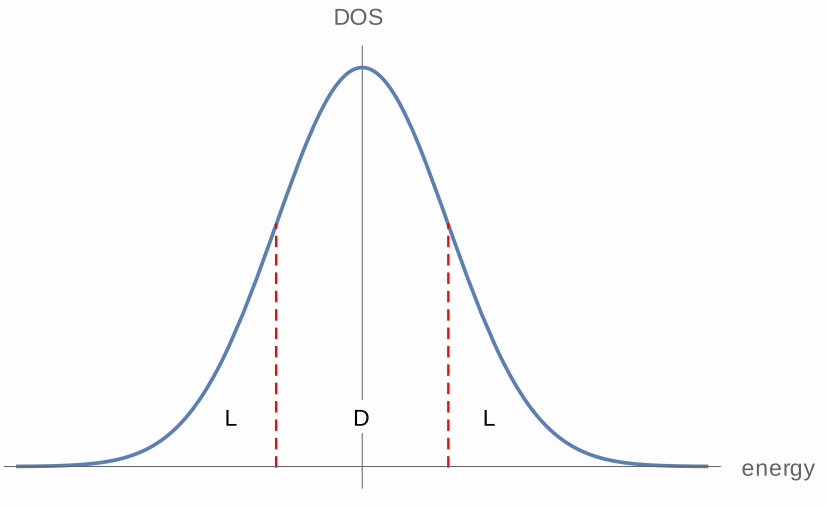

Figure 2.4: Typical mobility edge in the density of states.

where s_i is the action of the i-th path and a_i are amplitude coefficients. Then the return probability is given by the modulus square of $a_{0\to 0}$:

$$P_0 = |a_{0\to 0}|^1 = \sum_i |a_i|^2 + \sum_{i\neq j} a_i a_j^* \, \mathrm{e}^{\imath(S_i - S_j)}. \tag{2.49}$$

The second term in Eq. (2.49) is the result of quantum interference. Transmission over the lattice is reduced and the return probability is enhanced with respect to the classical one if there are a large number of contributions from paths that don't cancel each other out, as it happens if there is a time reversal symmetry so that certain loops in the paths can be followed in both directions. The probability of finding a self-crossing path is higher in low dimensionality systems; it turns out that this effect is prevalent in one and two dimensions and it does succeed in inhibiting delocalization.

Outside the radius of convergence of the locator expansion there is weak localization in the sense that the localization length is significantly larger than the lattice spacing, but still much smaller than the system size, therefore disallowing equilibration.

Another fine point that has to be addressed is the dependence on temperature; we can however reformulate the question in simpler terms if instead of temperature we discuss energy windows in the spectrum band. Not all of the spectrum localizes at once for the same critical parameters of disorder and hopping strength; instead, it is the bottom and top regions of the spectrum that localizes more easily, i. e. at lower values of the disorder strength. These localized regions are referred to as Lifshits tails; note that the density

of states is usually much lower at the edges of the band in Anderson-like systems. The middle of the band is the part in which extended states are most robust, and the value of the energy which separates localized and extended states is called the mobility edge [56].

2.3 On the Bethe lattice

An important exact result on localization has been obtained in 1973 by Abou-Chacra, Anderson and Thouless in Ref. [54] (of which we will give an overview in this section) when they solved the self energy equation self-consistently on a Bethe lattice. This kind of analysis, in addition of its relevance on its own in the framework of single particle localization, is the foundation of many-body localization as formulated by Basko, Aleiner and Altshuler (as it will be explained in Sec. 5.1).

In Anderson's estimation two key approximations are made, which weaken his reasoning. The first is neglecting the energy shifts caused by the self energies in the renormalized locator expansion; the second is treating the K^L terms, each coming from a non-repeating path, as independent random variables. Working in the Bethe lattice helps to address both these weak points while at the same time allowing to recover Anderson's values for the transition point, allowing a better understanding and control of the approximations. The feature that allows this is the peculiar structure of the Bethe lattice, which is the same at every point in the lattice, making it possible to exaclty apply self-consistent techniques, and, additionally, has no loops, allowing us to truncate the series to the second order.

The Bethe lattice is defined as an infinite graph without loops in which each node has connectivity z; it is the infinite limit of a Cayley tree, in which each node has $K = z - 1$ children, or equivalently of a regular random graph. Its main property for our purposes is the fact that it has no loops: this means that the series expansion for the self energy can be greatly simplified. Indeed, there is only one path connecting the origin and any given site, and in order to come back to the origin we must retrace our steps; namely, the paths in the self energy expansion are of the form

$$O \to i_1 \to \cdots \to i_{N-1} \to i_N \to i_{N-1} \to \cdots \to i_1 \to O \tag{2.50}$$

where the paths involved are exclusively non-repeating: the bouncing paths as, for example, $i_j \to i_{j+1} \to i_j \to i_{j+1}$ are not considered since they are absorbed into the resummed self energy. Because the only possible paths are

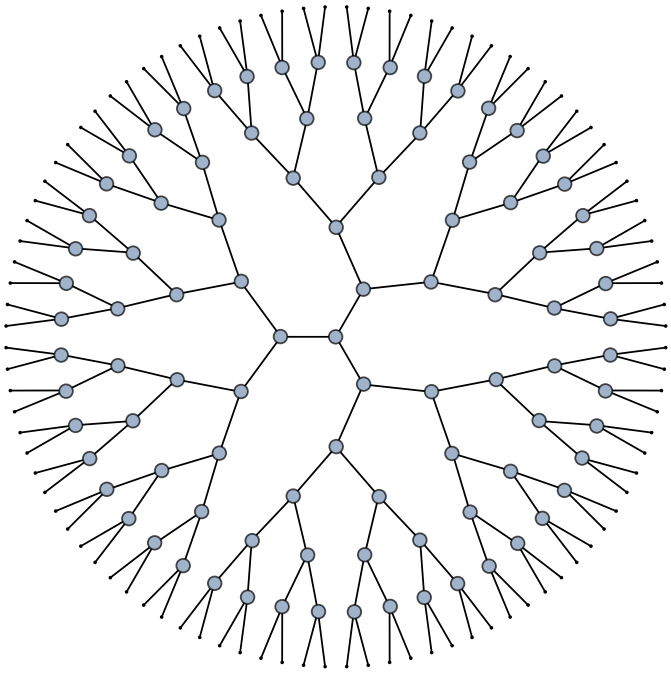

Figure 2.5: The Bethe lattice (with coordination $z = 3$).

of form (2.50), the series is reduced to just the second order term, namely

$$\begin{aligned}\Sigma_i(E) &= \sum_{j\neq i} \frac{|V_{ij}|^2}{E-\epsilon_j-\Sigma_j^{(\neq i)}} \\ \Sigma_i^{(\neq i)}(E) &= \sum_{k\neq i,j} \frac{|V_{jk}|^2}{E-\epsilon_k-\Sigma_k^{(\neq i,j)}} \\ &\ldots,\end{aligned} \tag{2.51}$$

all higher order terms being zero. The self energy Σ on both the right and the left hand side of Eq. (2.51) have the same probability density function (PDF), regardless of the excluded sites. Imposing this condition we obtain a self-consistent equation for the PDF; forgetting about the exclusion of some sites, let us consider the random variable $S_i(E)$, whose self-consistent equation is then:

$$S_i(E) = \sum_j \frac{|V_{ij}|^2}{E-\epsilon_j-S_j(E)}. \tag{2.52}$$

Let us separate real and imaginary part:

$$E = R + \imath\eta, \qquad S_i(E) = E_i - \imath\Delta_i. \tag{2.53}$$

Then the expression for the self energy is

$$\begin{aligned}S(R+\imath\eta) &= E_i - \imath\Delta_i \\ &= \sum_j \frac{|V_{ij}|^2}{E-\epsilon_j-E_j+\imath\Delta_j}\end{aligned} \tag{2.54}$$

and therefore

$$\begin{aligned}E_i &= \sum_j \frac{|V_{ij}|^2\,(R-\epsilon_j-E_j)}{(R-\epsilon_j-E_j)^2+(\eta+\Delta_j)^2} \equiv \sum_{j=1}^{K} X_j \\ \Delta_i &= \sum_j \frac{|V_{ij}|^2\,(\eta+\Delta_j)}{(R-\epsilon_j-E_j)^2+(\eta+\Delta_j)^2} \equiv \sum_{j=1}^{K} Y_j,\end{aligned} \tag{2.55}$$

where K is the connectivity. Exactly solving these equations is quite involved; therefore, one can resort to approximations.

2.3.1 Recovering the upper bound

An upper bound for the transition point can be obtained by neglecting the real part of the self energy E_j in the denominators and looking for the value of the parameters at which the self-consistent equation no longer has a solution. This is the same approximation used by Anderson in his original reasoning which was explained in Sec. 2.2.2; here we show that we can recover the same result. Under this assumption the equation for the imaginary part Δ_i becomes independent of the real part:

$$\Delta_i = \sum_j \frac{|V|^2 (\eta + \Delta_j)}{(R - \epsilon_j)^2}. \tag{2.56}$$

Let us write once again the self-consistent equation for the distribution f; doing a Laplace transform we obtain

$$\mathcal{L}[f](s) = \left[\int \mathrm{d}x p(R-x) \mathcal{L}[f] \left(\frac{s - V^2}{x^2} \right) \mathrm{e}^{-\frac{sV^2\eta}{x^2}} \right]^K \tag{2.57}$$

Note that in the localized regime $\mathcal{L}[f](0) = 1$ and we expect $\mathcal{L}[f](s)$ to become smaller for $s > 0$; moreover f should have fat tails, that is $f(x) \sim x^{-\alpha}$ with $\alpha < \frac{3}{2}$ which translates in $\mathcal{L}[f](s) \sim s^\beta$ with $0 < \beta < \frac{1}{2}$. Therefore, we make the ansatz

$$\mathcal{L}[f](s) = 1 - As^\beta + \dots \tag{2.58}$$

for the solution. Inserting it into Eq. (2.57) we obtain

$$\begin{aligned} \mathcal{L}[f](s) &= \left[1 - A \int p(R-x) \frac{V^{2\beta} s^\beta}{x^{2\beta}} \, \mathrm{d}x + \dots \right]^K \\ &= 1 - As^\beta K V^{2\beta} \int \frac{p(R-x)}{x^{2\beta}} \, \mathrm{d}x + \mathrm{O}(s) \end{aligned} \tag{2.59}$$

and, comparing it with the ansatz (2.58), we obtain

$$KV^{2\beta} \int \frac{p(R-x)}{x^{2\beta}} \, \mathrm{d}x = 1, \tag{2.60}$$

which is an implicit equation for $V = V(\beta)$. This equation has a solution up to a critical value of $V(\beta)$. The failure of the solution signals that above the critical value of β the reasoning that we followed is no longer valid, i.e. the assumptions from which we started no longer hold; this means that the

regime is not of localized states. Let us then find the maximum of $V(\beta)$; differentiating we obtain

$$\log V_c = \frac{\int p(R-x)\,|x|^{-2\beta_c} \log x \,\mathrm{d}x}{\int p(R-x)\,|x|^{-2\beta_c}\,\mathrm{d}x}. \tag{2.61}$$

Taking the box distribution (2.2) and the center of the band (so that $R = 0$), from Eq. (2.60) we obtain

$$\begin{aligned} K V_c^{2\beta_c} \int_{-W/2}^{W/2} \frac{1}{x^{2\beta} W}\,\mathrm{d}x &= 1 \\ \frac{K}{1-2\beta_c}\left(\frac{2V_c}{W}\right)^{2\beta_c} &= 1 \end{aligned} \tag{2.62}$$

and from Eq. (2.61)

$$\begin{aligned} \log V_c &= \frac{\int_{-W/2}^{W/2} \frac{1}{W}\,|x|^{-2\beta_c} \log x \,\mathrm{d}x}{\int_{-W/2}^{W/2} \frac{1}{W}\,|x|^{-2\beta_c}\,\mathrm{d}x} \\ \log V_c &= \log \frac{W}{2} - \frac{1}{1-2\beta_c} \end{aligned} \tag{2.63}$$

and therefore the critical value of V_c is given by the condition

$$\frac{2KeV_c}{W} \log \frac{W}{2V_c} = 1, \tag{2.64}$$

which is the same expression found by Anderson using a very different calculation (Eq. (2.44)) and the same result as the one given by looking at the probability of resonances at a far away distance in the forward approximation (see Eq. 3.38 in Chapter 3). The approximations used in Sec. 2.2.2 can then be understood in view of the reasoning followed here, that is they actually correspond to considering a lattice in which loops are rare. Note also that the forward approximation which will be discussed in Chapter 3 is equivalent to take into account only the imaginary part of the self-energy, as has been done here.

2.4 The current impact of fifty years old results

In this chapter we have discussed the fundamental features of both single particle localization, including the locator expansion. A legitimate question

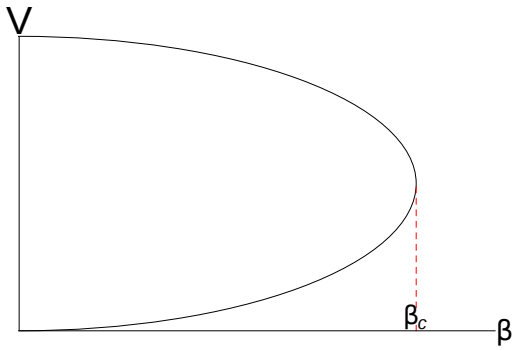

Figure 2.6: Qualitative plot of $V(\beta)$ in Eq. (2.60), showing a maximum for $\beta = \beta_c$ and no solution for $\beta > \beta_c$.

that could be asked is the relevance of this kind of reasoning more than fifty years after the original publication of Anderson's results.

Here we are interested in the details of the original Anderson's reasoning because its method of analysis has a deeper potential and can actually be very useful when inspecting both single particle and many-body localized systems. Indeed, this work of thesis focuses on the locator expansion and its approximations as a tool to perform a controlled analysis of localization properties. We will explore this topic in detail in the following Chapter 3.

Chapter 3

Locator expansion and forward approximation

3.1 Introduction

In Chapter 2 Anderson's reasoning for the presence of localization was explained in detail, particularly regarding the way to extract information from the locator expansion in the hopping strength of the Green's function. However, for a generic system, it turns out that using the full, exact series is a daunting task even in simple setups; being able to truncate the infinite series to the second order term in the Bethe lattice indeed plays a big role in the ability to exaclty solve the question of localization, resulting in the only exact solution known for Anderson localization.

A rather crude, but ultimately effective, approximation of the locator expansion is the *forward approximation*, which is obtained by neglecting to renormalize the on-site energies with the self energy; this results in an overestimation of the delocalizing mechanisms. We already used this approximation in Sec. 2.2.2 to calculate the upper bound to the localization transition. Indeed, the idea behind it is simple and dates back to Anderson's original article, but nonetheless is a technique which can be used to its full potential in Anderson-like disordered models and proficiently extended to interacting many-body problems.

In this and in the next chapter the main original work of this Ph.D. thesis is presented: it consists in a detailed analysis of the forward approximation in single particle and many-body systems (in Sec. 5.3). This will show that the forward approximation is a powerful tool in exploring the properties of both types of systems, e.g. allowing to determine transition values, localization lengths and their scaling, and properties of the wavefunction coefficients

distribution [3]. Two kind of improvements are proposed, namely the further approximation of considering only the dominating term of the full expression (which works extremely well in the single particle models due to the absence of correlations in the disorder) and a way to reintroduce a self-energy correction in a perturbative way.

3.2 The forward approximation

In Chapter 2 the expression for the Anderson's locator expansion has been stated for the Hamiltonian

$$H = \sum_{i=1}^{N} \epsilon_i c_i^\dagger c_i - t \sum_{\langle ij \rangle} \left(c_i^\dagger c_j + \text{h.c.} \right), \tag{3.1}$$

where ϵ_i are independent random variables uniformly distributed in $[-\frac{W}{2}, \frac{W}{2}]$, one for each of the N sites in the lattice. The edges $\langle i, j \rangle$ define the lattice topology, and the distance between two arbitrary sites of the lattice is the number of edges in a shortest path connecting them, and we refer to it as 'lattice distance' in the following. Indeed, the resolvent operator between two sites a and b at energy E has been derived in Sec. 2.2.1 as

$$\begin{aligned} G_{ba}(E) &= \langle b | \frac{1}{E - H} | a \rangle \\ &= \frac{1}{E - \epsilon_a} \sum_{p \in \text{paths}(a,b)} \prod_{i \in p} \frac{t}{E - \epsilon_i}, \end{aligned} \tag{3.2}$$

where the sum is over all the paths p in the lattice connecting i to j, and i labels the sites visited by the path p (site a excluded). We also considered the renormalized perturbation theory in which the closed paths are resummed in order to treat the local, uninteresting divergences (which occur also in the localized phase and do not imply delocalization), and the locators take on a dependence on the specific path via a self-energy. The full series is recast into a sum, finite in a finite-size lattice, over the *non-repeating paths* $\text{nrpaths}(a, b)$ connecting the sites a and b:

$$G_{ba}(E) = \frac{1}{E - \epsilon_a - \Sigma_a(E)} \sum_{p \in \text{nrpaths}(a,b)} \prod_{i \in p} \frac{t}{E - \epsilon_i - \Sigma_i^{(p)}(E)}, \tag{3.3}$$

which we obtained through a proper resummation of (3.2) in order to exclude those paths which contain repeated visits to the same sites. The latter expression diverges if hybridizations are not just local rearrangements and

occur at all length scales, which signals delocalization; instead, it converges if there are at most local hybridizations and resonances do not proliferate at asymptotically large distances in space, implying localization. $\Sigma_a(E)$ is the local self-energy at the site a, defined through the identity

$$G_{aa}(E) \equiv \frac{1}{E - \epsilon_a - \Sigma_a(E)}; \tag{3.4}$$

it is equal to the sum of the amplitudes of all the closed paths in which site a appears only as starting and ending point, i.e., to lowest order in t:

$$\Sigma_a(E) = \sum_{j \in \partial a} \frac{t^2}{E - \epsilon_j} + O(t^3), \tag{3.5}$$

where ∂a is the set of nearest neighboring sites of a. The path-dependent term $\Sigma_i^{(p)}(E)$ is a modified self-energy, which re-sums the loops around site i, with the requirement that it never crosses the site i again along the path, nor any of the sites $(a, 1, \cdots, i-1)$ already visited by the non-repeating path p.

The forward approximation of Eq. (3.3), as introduced in Anderson's original paper [1], consists in neglecting the self energy corrections Σ in the denominators, i. e. in not renormalizing the on-site energies (while still considering self avoiding paths). The resulting effect is to weaken the role of resonances and overestimate the effect of small denominators; the latter would be mostly cancelled out by the correction in the self energy. Indeed, suppose there is a self avoiding loop $i \to l_1 \to l_2 \to \cdots \to i$ and that site l_2 is resonant with energy E, so that $\frac{V}{E-\epsilon_{l_2}} \gg 1$ for $E - \epsilon_{l_2} \to 0$. The locator corresponding to its previous site l_1 is then

$$\Sigma_{l_1}^{\neq i}(E) = t \, \frac{1}{E - \epsilon_{l_2}} \, t + \ldots, \tag{3.6}$$

that is, it contains a big factor and brings a big correction. Therefore the weight of the given self avoiding loop contains the term

$$t \, \frac{1}{E - \epsilon_{l_1} - \frac{t^2}{E-\epsilon_{l_2}} + \ldots} \, t \, \frac{1}{E - \epsilon_{l_2} - \ldots}, \tag{3.7}$$

that is, the divergence in the second locator is compensated by the divergence of the self energy in the first locator. This mechanism is clearly not present if we neglect the self energy corrections; this may cause the eventual divergence in the full series even though the system is localized.

In the following we will frequently calculate the wavefunction amplitude in the forward approximation. The expression for the eigenfunction can be obtained by considering, for any exact eigenvalue E_α of the full system Hamiltonian, the spectral decomposition

$$\lim_{E\to E_\alpha}(E-E_\alpha)G_{ij}(E)=\psi_\alpha^*(j)\psi_\alpha(i). \tag{3.8}$$

Note that G_{ij} has a pole at every eigenvalue, since $E_\alpha-\epsilon_i-\Sigma_i(E_\alpha)=0$ by definition, and for $E=E_\alpha$ it is cancelled in Eq. (3.8) by the factor $(E-E_\alpha)$ in front. Then we obtain:

$$\psi_\alpha(b)=\psi_\alpha^{-1}(a)\sum_{p\in\mathrm{nrpaths}(a,b)}\prod_{i\in p}\frac{t}{E_\alpha-\epsilon_i-\Sigma_i^{(p)}(E_\alpha)}, \tag{3.9}$$

Let us now assume that, at sufficiently low hopping t so that generic eigenstates are localized around a single site (without hybridization of near sites), ψ_α is the state localized around site a. To zeroth order perturbation theory, then, $E_\alpha=\epsilon_a$ and $\psi_\alpha(a)=1$. Thus, we can write the forward approximation for the wavefunction as an infinite sum over the self avoiding paths of any length by neglecting the self energies as:

$$\psi_\alpha(b)\approx\sum_{p\in\mathrm{nrpaths}(a,b)}\prod_{i\in p}\frac{t}{\epsilon_a-\epsilon_i}. \tag{3.10}$$

The lowest order forward approximation is obtained restricting to the set $\mathrm{spaths}(a,b)$ of self avoiding paths of shortest length from a to b:

$$\psi_\alpha(b)\approx\sum_{p\in\mathrm{spaths}(a,b)}\prod_{i\in p}\frac{t}{\epsilon_a-\epsilon_i}. \tag{3.11}$$

Note that there is no difference between these two sets of paths on the Bethe lattice. In other lattices, for example the $d-$dimensional hypercube, this translates in setting an orientation in the dimensional axes and taking only paths that never travel in the opposite direction.

As a last remark, note that the loops contributing to the self energy corrections, which are neglected in (3.10) and (3.11), become less relevant when the dimensionality (or connectivity) of the lattice is increased. Thus, the forward approximation is expected to give better and better results the higher the dimension is.

3.2.1 Localization criterion

The way to detect a localized state, as explained in Chapter 2, is to look at the convergence of the locator expansion. The forward approximation, even

though it can result in an overestimation of the delocalizing features in the state, can be used to this effect if the wavefunction amplitudes are bounded by a geometric distribution; when using this technique near the transition point, however, this can result in its overestimation. Note that this is the same reasoning used in Sec. 2.2.2.

In more precise terms, let us denote with L the length scale setting the size of the lattice (thus for a cubic lattice in dimension d the diameter is $L = N^{1/d}$ and for a Bethe lattice or regular random graph it is

$$L = \log \frac{\left[\frac{(N-1)(K-1)}{(K+1)+1}\right]}{\log K} \approx \frac{\log N}{\log K}, \tag{3.12}$$

where $K+1$ is the connectivity of the lattice). For a single particle problem, one defines an eigenstate ψ_α of a system of size L to be localized if, with probability 1 over the disorder realizations, the probability of finding a particle at a distance $O(L)$ from the localization center of the state goes to zero in the limit of large L. More precisely, we ask that there exists a ξ such that, for *any* site b at distance $r = O(L)$ from the localization center a, it holds that

$$P\left(\log |\psi_\alpha(b)|^2 \leq -r/\xi\right) \to 1 \text{ for } r \to \infty. \tag{3.13}$$

Namely, the requirement is that we can enclose the random numbers $|\psi_\alpha(b)|^2$ in an "exponential envelope" for b sufficiently far from the localization center of the state. It can be shown that this condition on the eigenstates implies the vanishing of the DC conductivity by means of the Kubo formula.

The localization length of ψ_α is the minimum value of ξ for which ((3.13)) is true. In general, it depends on the state that is being considered, although it is supposed to depend smoothly on the energy E_α in the thermodynamic limit. A mobility edge exists whenever there is band of energies for which such minimum is not finite.

The critical value of the disorder W_c is determined by considering (3.13) with $\xi = \infty$; indeed, it is the smallest value of disorder W for which:

$$P\left(\log \max_\alpha |\psi_\alpha(a+r)|^2 < 0\right) \xrightarrow[r\to\infty]{} 1, \tag{3.14}$$

where $\max_\alpha |\psi_\alpha(a+r)|$ denotes the maximal among the amplitudes on sites at distance r from the localization center a. The above limit is approached for any $W > W_c$, whereas for $W < W_c$ one finds

$$P\left(\log \max_\alpha |\psi_\alpha(a+r)|^2 < 0\right) \xrightarrow[r\to\infty]{} 0. \tag{3.15}$$

Probability of resonances

As we just saw, the localization/delocalization transition can be detected analyzing the statistics of the wavefunction amplitudes as a function of distance, which can be obtained in the lowest order forward approximation. In this case, it is worth noting that, within this approximation, an amplitude of $O(1)$ at a site b at distance r from a corresponds to the site being resonant with the localization center a. Indeed, the $a-b$ problem can be considered as a two-level system with reduced Hamiltonian

$$h = \begin{pmatrix} 0 & h_r \\ h_r & \Delta \end{pmatrix}, \tag{3.16}$$

where $\Delta = \epsilon_a - \epsilon_b$, and

$$h_r = t \sum_{p \in \text{paths}(a,b)} \prod_{i \in p} \frac{t}{\epsilon_a - \epsilon_i} = t \sum_{p \in \text{nrpaths}(a,b)} \prod_{i \in p} \frac{t}{\epsilon_a - \epsilon_i - \Sigma_i^{(p)}(\epsilon_a)}, \tag{3.17}$$

where the products are taken over all sites in the path, excluding a and b. The sites are resonant when the energy difference $\epsilon_a - \epsilon_b$ is small, i.e., more precisely, $|\Delta| < h_r$. Considering h_r to lowest order in t, one finds that this is equivalent to $|\psi(r)| > 1$, with the wavefunction $\psi(r)$ computed in the lowest order forward approximation. Thus, with (3.14) we are probing the statistics of resonances, and requiring that the probability to find resonant sites at a large distance from the localization center decays to zero in the localized phase.

3.2.2 Numerical calculation with the transfer matrix method

The lowest order of the forward approximation (3.11) can be easily computed by rewriting it as a series of transfer matrix multiplications through which we encode only propagations of paths along a "forward" direction.

To be more precise, let us take a $d-$dimensional hypercube of side L, composed of $N = L^d$ sites. We construct its sub-lattice which has the sites a and b at the opposite corners; assume that their Manhattan distance[1] is

[1] In the case of the hybercube the lattice distance coincides with the Manhattan distance, which is defined as

$$d_1(\mathbf{x}, \mathbf{y}) = \sum_{i=1}^{d} |x_i - y_i| .$$

$d_1(a,b) = n$. Additionally, let us consider $t = 1$. Denoting with ϵ_i the on-site potential on site i, the wavefunction amplitude is given by Eq. (3.11) in terms of sum of individual path weights as:

$$\psi_\alpha(b) = \sum_{p \in \text{spaths}(a,b)} w_p, \qquad w_p = \prod_{i \in p} \frac{1}{\epsilon_a - \epsilon_i}. \tag{3.18}$$

For this system we construct the transfer matrix. First, we build a forward adjacency matrix A_f, which can be seen as the adjacency matrix of the directed graph where all the links follow the positive orientation defined by the ones coming out of the initial site a. It can be easily constructed by means of the forward adjacency matrix in one dimension,

$$T_f = (\{l+1, l\} \to 1)_{l,m=1..L}\,, \tag{3.19}$$

so that:

$$A_f = \left(\underbrace{T_f \otimes \mathbb{1} \otimes \cdots \otimes \mathbb{1}}_{d} + \cdots + \mathbb{1} \otimes \cdots \otimes \mathbb{1} \otimes T_f \right). \tag{3.20}$$

Then, the forward transfer matrix is

$$\mathcal{T} = W A_f, \tag{3.21}$$

where W is the diagonal matrix of the on-site locators,

$$W = \text{diag}\left(\frac{1}{\epsilon_a - \epsilon_k} \right)_{k=1..N}. \tag{3.22}$$

Then, starting from the vector $|\psi_I\rangle = |a\rangle \to (1\ 0\ \ldots\ 0)^T$, that is a state localized in the first site, we iteratively multiply it to the transfer matrix $\mathcal{T}$, feeding back the result of the multiplication. Note that after a single iteration we obtain

$$|\psi_1\rangle = \mathcal{T}|\psi_I\rangle = \frac{-t}{\epsilon_a - \epsilon_{l_1}}|l_1\rangle + \frac{-t}{\epsilon_a - \epsilon_{l_2}}|l_2\rangle + \ldots, \tag{3.23}$$

where $l_1, \ldots, l_n$ are the forward neighbors of site a. After n iterations, equal to the lattice distance between a and b, we take value of the vector

$$\psi_F = \prod_{n^*=1}^{n} \mathcal{T}\psi_I \tag{3.24}$$

at the component corresponding to site b, $\langle b|\psi_F\rangle$, which is equal to (3.11), all other elements in the vector being equal to zero. Note that repeating this operation for all sublattices we can build the wavefunction on the whole lattice[2].

3.2.3 Results on the Bethe lattice

The simplest setting for the application of the forward approximation is a Bethe lattice: in this case, given two sites a and b, there is only one non-repeating path connecting them, along which all the energies are independent and identically distributed random variables. In Chapter 2 some analytic exact results have been shown [54, 57]; here, we are interested in presenting the results obtained in the forward approximation for the transition point, the localization length and its critical exponent [49]. In the following calculations we will heavily reference Sec. 2.2.2; although those results, obtained in the forward approximation, refer to a general lattice, the spirit of the reasoning is the same.

Let a be the root of the tree, and K the branching number (the connectivity being $K+1$). Within the forward approximation we get that the wavefunction at one particular point at distance L from the root is given by

$$\psi_L = \prod_{i=1}^{L} \frac{t}{\epsilon_a - \epsilon_i}. \tag{3.25}$$

This random variable has a power-law tail distribution for any distribution of ϵ_i having a support S such that $\epsilon_a \in S$, as one can see from the divergence of the first moment of the absolute value of ψ_L. It is convenient to consider the distribution of the logarithm of ψ_L, whose moments are all finite. Recall that we choose ϵ_i uniformly distributed in $[-W/2, W/2]$, and in this calculation for simplicity we set $\epsilon_a = 0$. Then, starting from the logarithm of the wavefunction amplitude,

$$x_L = \log|\psi_L|^2 = -2\sum_i \log\frac{|\epsilon_i|}{t}, \tag{3.26}$$

let us calculate its average value. Using the notation of Sec. 2.2.2 we find

[2]Note that it is not necessary to explicitly select the sub-lattice and compute the transfer matrix each time for the specific case of the hypercube. Each step of the transfer matrix multiplication only explores the forward nearest neighbors of the sites explored at the previous step; therefore, by recovering the information from the vectors at each step we obtain the full wavefunction on the lattice.

that

$$\begin{aligned} x_L &= 2\sum_i \left(y_i + \log \frac{2t}{W} \right) \\ &= 2Y + 2L \log \frac{2t}{W}, \end{aligned} \tag{3.27}$$

where $y_i = -\log \frac{2|\epsilon_i|}{W}$ and $Y = \sum_i y_i$. Recall that in Sec. 2.2.2 we found that

$$P_Y(Y) = \frac{Y^{L-1}\ \mathrm{e}^{-Y}}{(L-1)!}\theta(Y), \tag{3.28}$$

and therefore

$$\langle Y \rangle = \frac{1}{(L-1)!}\int_{-\infty}^{\infty} Y^L\, \mathrm{e}^{-y}\theta(y) = \frac{L!}{(L-1)!} = L; \tag{3.29}$$

we obtain then, finally:

$$\begin{aligned} \langle x_L \rangle &= 2\langle Y \rangle + 2L \log \frac{2t}{W} \\ &= 2L \log(2\,\mathrm{e}t/W). \end{aligned} \tag{3.30}$$

The ratio $\langle x_L \rangle / L$ is the typical decay of wavefunction amplitudes from the center of localization,

$$\xi_{\mathrm{typ}}^{-1} = 2\log(2et/W). \tag{3.31}$$

Note that this is different than the localization length ξ as defined in (3.13). Indeed, the latter is a uniform bound over the $\sim K^L$ points at distance L from the localization center, determined by the decay rate of the maximal amplitude over sites in each shell at distance L. The typical decay ξ_{typ} is a point-to-set correlation function decay, which is familiar in the study of disordered systems on the Bethe lattice; on a regular lattice instead of a point-to-set we have a point-to-point correlation function, but with exponentially many shortest paths leading to the final point.

Note that, the typical value of the maximal amplitude x_L^* among K^L samplings is instead the largest solution of

$$x_L^* : \quad K^L P(x_L^*) \simeq 1, \tag{3.32}$$

where $P(x)$ is the distribution of x_L, and the K^L paths are treated as independent. We are interested, asymptotically in L, in the big values of x_L, i.e. in the right tail of the distribution $P(x)$. Rescaling x_L to

$$z = \frac{x_L}{2L} + \log \frac{W}{2t}, \tag{3.33}$$

then, for large z, we obtain:

$$P(z) \simeq \exp\left(-L(z - 1 - \log z)\right). \tag{3.34}$$

The probability distribution of z can be found inverting its Laplace transform (note that z is a sum of independent and identically distributed variables). The maximum z^* over K^L samplings of z is the solution of

$$0 = -z^* + 1 + \log z^* + \log K = \log(z^* e K e^{-z^*}), \tag{3.35}$$

and $x_L^* \simeq -2L \log \frac{W}{2t} + 2Lz^*$. There is localization if the condition $x_L^*/L < 0$ is satisfied; the critical condition can then be written as

$$\log(Kez^* e^{-z^*}) = 0 \tag{3.36}$$

$$z^* - \log \frac{W_c}{2t} = 0, \tag{3.37}$$

and eliminating z^* we recover the familiar equation [54]

$$W_c = 2teK \log \frac{W_c}{2t}, \tag{3.38}$$

which is also the same result as Eq. (2.44) of Sec. 2.2.2, which referred to the lowest order forward approximation.

Moreover, we can obtain a result involving the "true" localization length. Indeed, since z^* is given in terms of W_c from Eq. (3.37) as

$$z^* = \log \frac{W_c}{2t}, \tag{3.39}$$

we can write the localization length as

$$\xi^{-1} = -\frac{x_L^*}{L} = 2 \log \frac{W}{W_c}. \tag{3.40}$$

This gives a mean-field exponent for the divergence of the localization length at the transition:

$$\xi \simeq \frac{2W_c}{|W - W_c|}. \tag{3.41}$$

Note that $\xi_{typ} < \xi$; this is irrespective of the value of the disorder.The difference between ξ_{typ} and ξ is due to the exponential sampling of the probability distribution, and it extends both to the finite-dimensional cube and to the many-body case.

3.3 The forward approximation on the d-dimensional hypercube

Let us now go on to study the Anderson model in a hypercubic lattice in d dimensions, with d varying from 3 to 7; recall that for $d \geq 3$ the non-convergence of the locator expansion implies delocalization. By looking at the wavefunction amplitudes distribution we can obtain results for the transition point in the forward approximation. Moreover, we can estimate the (mean field) critical exponent of the localization length.

An interesting point comes out by comparing the forward approximation of the wavefunction to the partition function of directed polymers [58]. Indeed, let us consider a directed polymer in a random potential, i.e. a polymer whose components are each placed in a site which has random energy h_i; then, its partition function is

$$\begin{aligned} Z &= \sum_{\Gamma} \mathrm{e}^{-\beta \sum_{i\in\Gamma} h_i} \\ &= \sum_{\Gamma} \prod_{i\in\Gamma} \mathrm{e}^{-\beta h_i}, \end{aligned} \tag{3.42}$$

where β is the inverse of the temperature, $T = (k\beta)^{-1}$; the sum is running over all the possible configurations Γ of the directed polymer. In two dimensions, a correspondence between the forward approximation (3.11) and this free energy distribution can be made by mapping βh_i to $\log(\epsilon_a - \epsilon_i)$, where i are the indices of sites belonging to a given path; each path is therefore mapped to a configuration of the polymer. However, note that, for Anderson-like models, there are no restrictions on the argument of the exponential to be real, since $\epsilon_a - \epsilon_i$ can have any sign.

This mapping can not be made explicit for higher dimensions; however, we will see that we can compare many results coming from the analysis of the wavefunction distribution (in particular its higher moments) to the ones corresponding to this kind of directed polymer systems (see Sec. 3.3.4).

3.3.1 The model

Consider the case of a d-dimensional hypercubic lattice of side L, and let a be the site at one corner of the cube, which we take as the origin. In this lattice the number of sites at lattice distance r from the origin increases as $\binom{r+1}{d-1}$, and thus grows at most polynomially in r and slower than $\sim r^d$, each site being reached by a number of path of minimum length equal to r and scaling exponentially with r, that is $r![(r/d)!]^{-d} \sim d^r$. The wavefunction

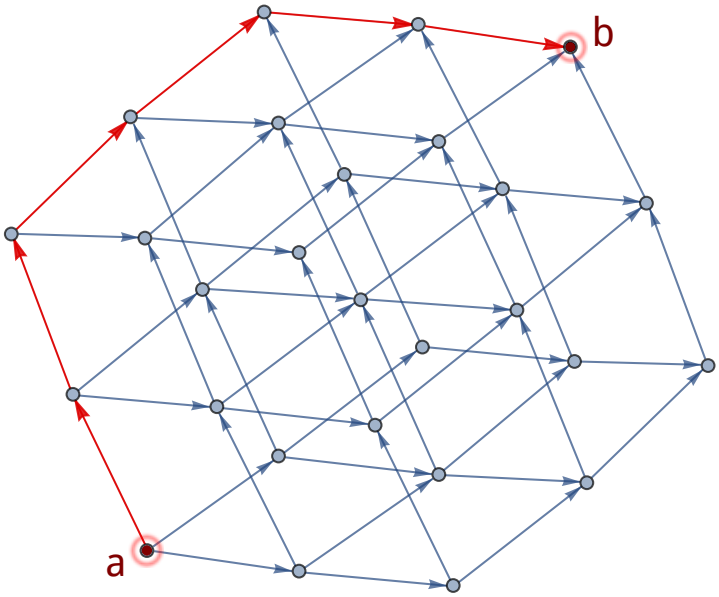

Figure 3.1: Cubic lattice in $d = 3$ of side $L = 3$ used in the forward approximation setup. Starting from a corner of the cube (site a), one of the non-repeating paths connecting it to the opposite corner (site b) is highlighted in red, along with the visited configurations; it has length $r = d(L-1) = 6$. The transfer matrix simultaneously explores all the exponential number of paths connecting the starting and ending point, while the optimal directed path detailed in Sec. 3.4 is the result of a graph search among them.

amplitude at a given site b in the forward approximation is therefore a sum over exponentially many correlated terms, i.e.

$$\psi_\alpha(b) = \sum_{p \in \text{spaths}(a,b)} \prod_{i=1}^{r} \frac{t}{\epsilon_a - \epsilon_i} = \left(\frac{t}{W}\right)^r \psi'_\alpha(b), \tag{3.43}$$

where

$$\psi'_\alpha(b) = \sum_{p \in \text{spaths}(a,b)} \prod_{i=1}^{r} \frac{1}{\epsilon'_a - \epsilon'_i} \tag{3.44}$$

and the random variables ϵ'_i are uniformly distributed in $[-1/2, 1/2]$. Fig. 3.1 shows a schematic representation of this setup in $d = 3$, highlighting a sample shortest path between the sites a and b on opposite corners of the cube.

With respect to the Bethe lattice results of Sec. 3.2.3, in this case it is harder to determine the probability distribution of the wavefunction amplitudes at a given site, due to the correlation between the different paths.

Such correlations can however be easily taken into account as we numerically compute the sum (3.44) using the transfer matrix technique explained in Sec. 3.2.2, which takes polynomial time in r.

A similar treatment was done by Medina and Kardar [59] for the NSS model [60–62], a type of directed polymer with partition function (3.42) with random sign weights and binary disorder, i.e. $h_i \propto \log \epsilon_i$ where $\epsilon_i = \pm W$ with probability p or $1-p$. Note that the present calculation does not reduce to the one for the NSS case, since a major difference between the two models is in the statistics of energy denominators (i.e. the binary disorder). This does not allow for resonances due to a single site; rather, the resonances arise from contributions of different paths. This led to a body of work, following Ref. [59], on the presence of a "sign transition", where effects from different paths accumulate in order to break the sign symmetry. In the forward approximation for the Anderson model, instead, the energy denominators can be arbitrarily small with finite probability, generating path weights that are fat-tailed distributed; the fat tail of this distribution is crucial for the considerations that we are able to make. For instance, a consequence of this is that the main contribution to the transfer matrix result comes from only one of the exponentially many paths in (3.43). The existence of a dominating path resembles the phenomenon of condensation occurring in directed polymer problems [63–65].

The analogies with the polymer problem, the algorithm to determine the best path and its structure will be discussed in Sec. 3.4.2. As it will be shown, the results obtained with the transfer matrix technique are faithfully reproduced by analyzing the statistics of the optimal path alone. Since the algorithm for the best path is computationally more efficient, this method allows to access to much bigger system sizes with respect to the transfer matrix technique. Some of the results presented in this section (i.e. for the higher dimensions) are obtained with this procedure.

The numerical computation is performed as in Sec. 3.2.2, fixing $\epsilon'_a = 0$ and computing the rescaled amplitude (3.44) for all the points b on a shell at the same lattice distance equal to $r = r_{max} - \delta$, $\delta \sim O(1)$, from the origin of a hypercube of side L. We then determine the maximal among the wavefunction amplitudes on those sites; we call this value ψ'_r. We repeat the procedure for hypercubes of different sizes and for many disorder realizations, taking $O(10^5)$ realization for most system sizes, decreasing up to $O(10^3)$ realizations only for the biggest system sizes that we consider. For example, in $d = 3$ we take system sizes $r = 10$ through 292, with $1.5 \cdot 10^5$ disorder realizations each up to $r = 202$ and $2.5 \cdot 10^3$ realizations up to $r = 292$. The hypercube shell, and therefore δ, is fixed so as to have about 20 points per each size of the hypercube.

3.3.2 Fluctuations of the wavefunction amplitudes

We start the analysis by looking at the distribution of the variable

$$Z_r \equiv \frac{\log |\psi_r'|^2}{2r} \tag{3.45}$$

for different values of r; indeed, the probability of resonances for arbitrary values of t and W is easily recovered from the cumulative distribution function of Z_r as

$$P\left(\log |\psi_r|^2 > 0\right) = P\left(Z_r > \log\left(\frac{W}{t}\right)\right) = 1 - P\left(Z_r < \log\left(\frac{W}{t}\right)\right). \tag{3.46}$$

The probability density of Z_r for different values of r has a peak whose position moves as r increases, while the width of the distribution shrinks, as shown in Fig. 3.2 for $d = 3$. This is in agreement with the conditions (3.14) and (3.15), from which it follows that the density of Z_r becomes asymptotically peaked at $\log(W_c/t)$ for $r \to \infty$, with a width going to zero with r. Thus, the critical value of disorder can be estimated inspecting the scaling with r of the density of Z_r.

Plotting, as in Fig. 3.3, the r-dependence of the variance $\sigma^2_{Z_r}$ of (3.45) in a log-log scale, one can spot a clearly linear behavior. This indicates that the fluctuations of Z_r decay to zero as a power law in r, with a coefficient that depends on the dimensionality. The higher cumulants of the distribution exhibit a similar linear behavior in log-log scale. Moreover, we find that for fixed d, the probability densities of the variable

$$\tilde{Z}_r = \frac{Z_r - \langle Z_r \rangle}{\sigma_{Z_r}} \tag{3.47}$$

collapse to a limiting curve for increasing r. Such plots of the density of $\tilde{Z}_r$ are given in Fig. 3.4 for $d = 3$. In Fig. 3.5, instead, the density of $\tilde{Z}_r$ is plotted for fixed $r = 52$ and different dimension d: the curves corresponding to different dimensions are not significantly different, except for a weak d-dependence of the tails.

These numerical observations indicate that for large r the scaling form

$$rZ_r \underset{r\to\infty}{\sim} r \log\left(\frac{W_c}{t}\right) + r^{\omega(d)} u \tag{3.48}$$

holds for Z_r, where u is a random variable of $O(1)$ with a distribution which depends weakly on the dimensionality. According to (3.48), for large r the fluctuations $\sigma^2_{Z_r}$ decay to zero with the power $r^{2(\omega(d)-1)}$. From the linear fit of

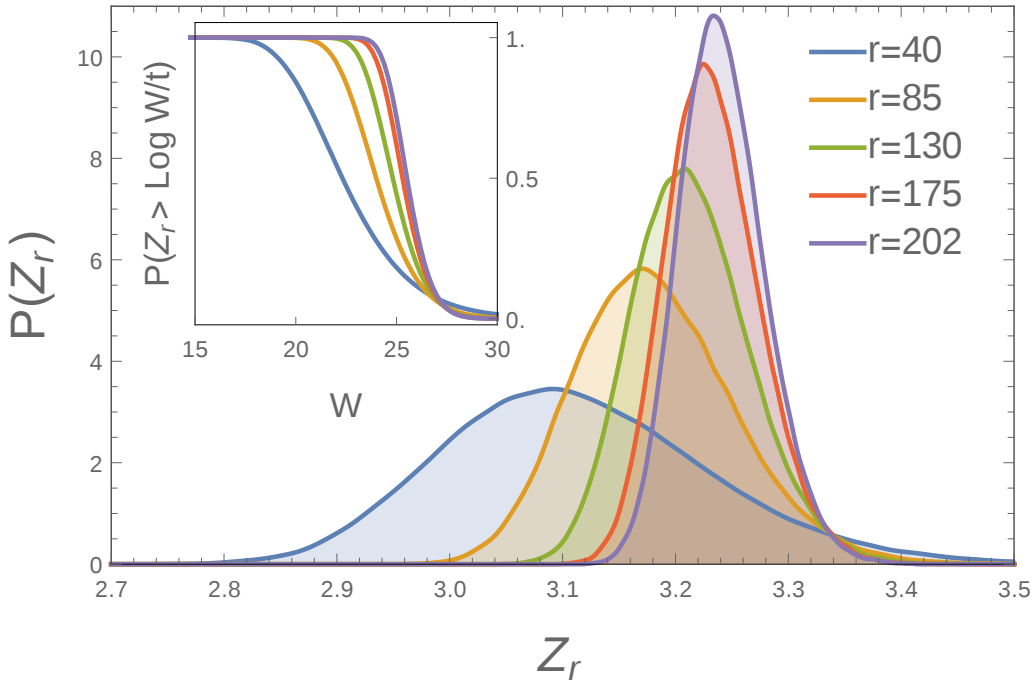

Figure 3.2: Probability density of Z_r for different r in $d = 3$. For $r \to \infty$ the curves become peaked around the critical value W_c/t. Inset: cumulative distribution function. Each curve is obtained with $1.5 \cdot 10^5$ disorder realizations. Very similar results are obtained for higher dimensionality.

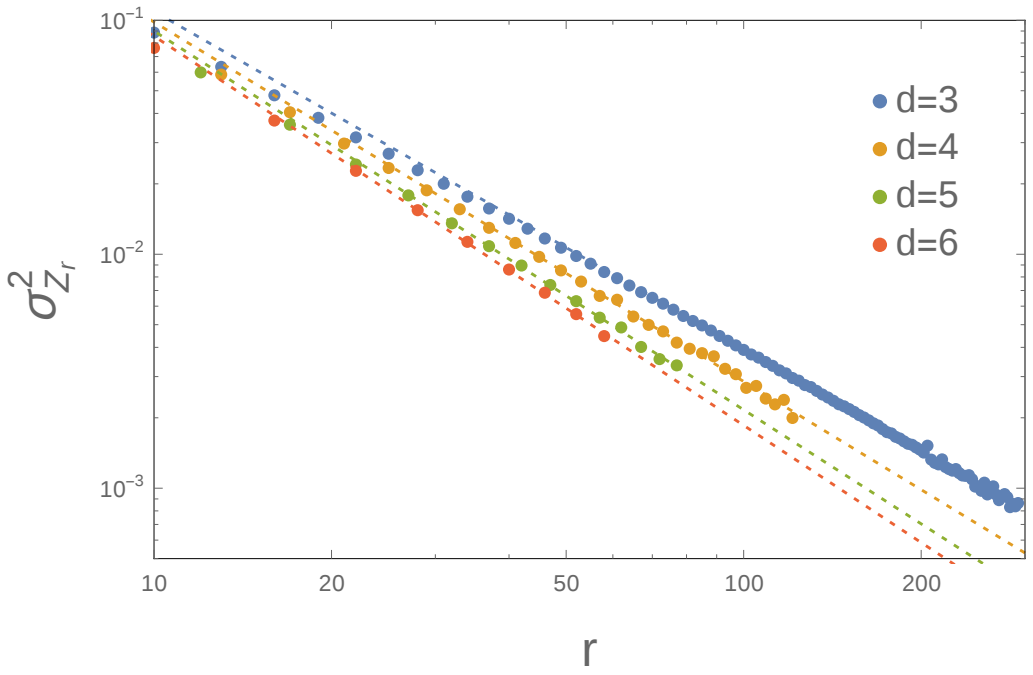

Figure 3.3: Variance $\sigma^2_{Z_r}$ of Z_r, as a function of r. The plot is in log-log scale. The points corresponding to larger r are fitted linearly, and the values of the exponents $\omega_{FA}(d)$ reported in Table 3.1 are extracted from the coefficient of the linear term in the fit. The number of realizations is $1.5 \cdot 10^5$ for r smaller than 202, 53, 52, 40 for $d = 3$, 4, 5, and 6, respectively, and $2 \cdot 10^3$ for larger values of r.

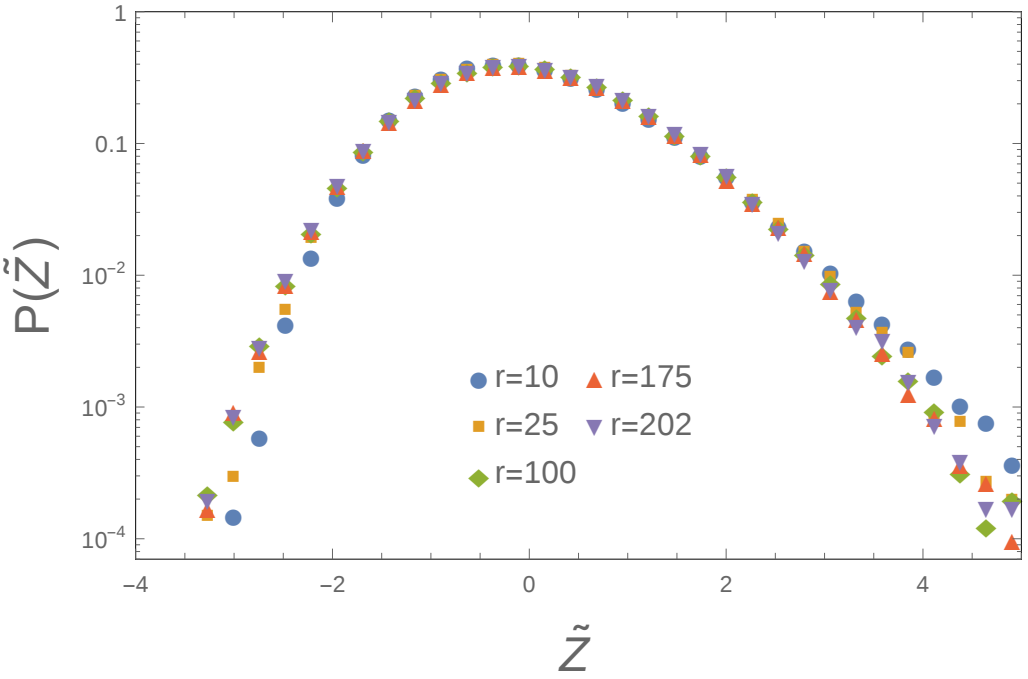

Figure 3.4: Probability density $P(\tilde{Z})$ of the variable $\tilde{Z}_r = (Z_r - \langle Z_r \rangle)/\sigma_{Z_r}$ for different r and $d = 3$. Each curve is obtained with $1.5 \cdot 10^5$ realizations. The curves seem to converge to a unique limiting distribution with increasing r.

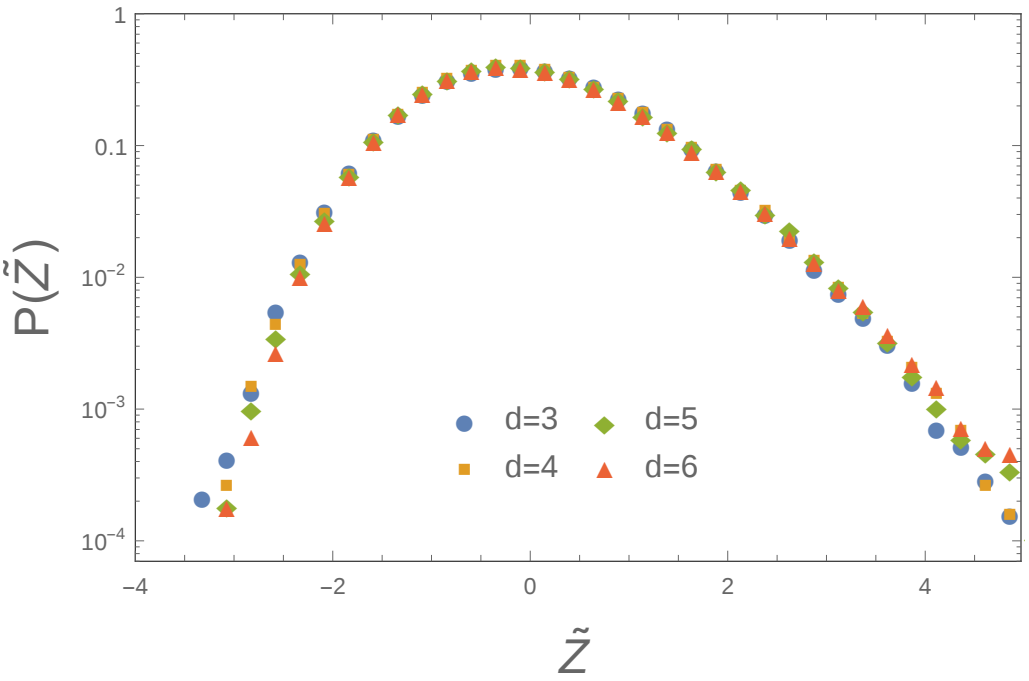

Figure 3.5: Probability density $P(\tilde{Z})$ for fixed $r = 52$ and different system dimensionalities. Each curve is obtained with $1.5 \cdot 10^5$ realizations.

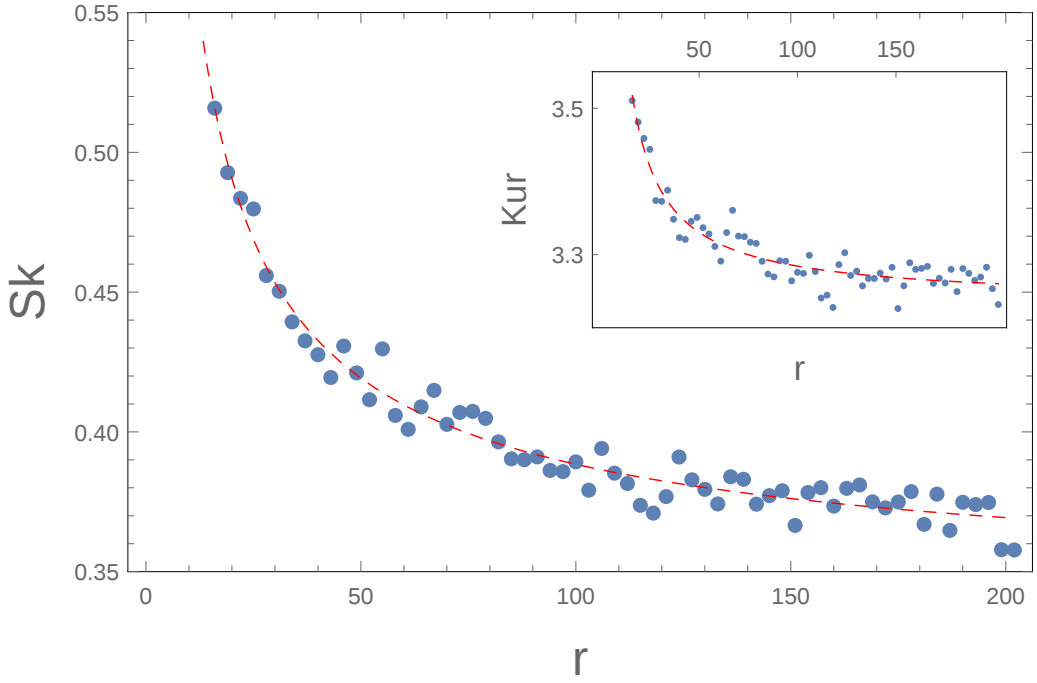

Figure 3.6: Skewness Sk of the distribution of $\tilde{Z}_r$ for $d = 3$, as a function of r. The red dashed line is a fit of the form $\alpha + \beta r^{\gamma}$, with α, β, γ free parameters. The coefficient α is the estimate of the asymptotic value of the skewness, and it equals $\mathrm{Sk} = 0.34 \pm 0.02$. *Inset.* Kurtosis Kur of the distribution of $\tilde{Z}_r$ for $d = 3$, as a function of r. The fitting procedure is analogous to the one for the skewness, and results in an asymptotic value $\mathrm{Kur} = 3.24 \pm 0.04$.

$\log\left(\sigma^2_{Z_r}\right)$ we extract the numerical estimate of the exponent in (3.48), which we denote with $\omega_{FA}(d)$. The results are reported in Table 3.1.

To characterize the limiting distribution in Fig. 3.4, we compute the skewness $\mathrm{Sk} = \kappa_3/\kappa_2^{3/2}$ and the kurtosis $\mathrm{Kur} = \kappa_4/\kappa_2^2$ of the density of $\tilde{Z}_r$ (we denote with κ_i the i-th cumulant of the distribution). From (3.48) it follows that these parameters approach the ones corresponding to the variable u in the limit of large r. We restrict to $d = 3$, value for which the largest statistics is available. Plots of the r-dependence of Sk and Kur are given in Fig. 3.6; the asymptotic values are estimated to be $\mathrm{Sk} = 0.34 \pm 0.02$ and $\mathrm{Kur} = 3.24 \pm 0.04$ (see the caption of Fig. 3.6 for details).

Table 3.1: Values of the exponent $\omega_{FA}(d)$ governing the decay of the fluctuations of Z_r with r (see Eq. (3.48)).

d	$\omega_{FA}(d)$
3	0.278 ± 0.005
4	0.23 ± 0.01
5	0.191 ± 0.007
6	0.168 ± 0.006
7	0.19 ± 0.03

3.3.3 Estimate of the transition point

The transition value W_c for the d-dimensional system can be obtained extrapolating the asymptotic limit of the typical value of Z_r, or equivalently (since the distribution of the variable Z_r is not fat-tailed) of the averages of Z_r. We make use of the values of $\omega_{FA}(d)$ in Table 3.1 to perform the finite size scaling. Let us define:

$$\langle Z_\infty \rangle \equiv \lim_{r\to\infty} \langle Z_r \rangle = \log\left(\frac{W_c}{t}\right). \tag{3.49}$$

Plotting the scaling with r of $r\langle Z_r\rangle$ (see Fig. 3.7), one sees that the mean grows linearly in r as expected; fitting it with the form

$$\langle r Z_r \rangle = c_1 + \log(W_c)\, r + c_2\, r^{\omega(d)}, \tag{3.50}$$

using the numerical values $\omega(d) = \omega_{FA}(d)$ reported in Table 3.1, one is able to read out the value of W_c for $t = 1$ from the coefficient of the linear term. The resulting estimates of the critical disorder in dimensions 3 through 7, which we denote with W_c^{FA}, are displayed in Table 3.2. For the smallest dimensions, up to $d = 5$, a comparison is made with the critical values $W_c^{\rm num}$ in Ref.s [66, 67], which have been determined by means of a combination of exact diagonalization and transfer matrix techniques and are the best numerical values available so far for hypercubic lattices; dimension $d = 6$ can be compared with the only one available result of Ref. [68], $W_c^{\rm ggc} = 74.5 \pm 0.7$, which, due to the choice of boundary conditions, is an underestimation of the transition point and is obtained from the analysis of spectral statistics. The values corresponding to higher dimensionalities have no source of comparison in the literature.

The data in Table 3.2 clearly show that the forward approximation gives an upper bound to the critical disorder, since the cancellation effects provided by the (modified) self-energy corrections are neglected, and the effects

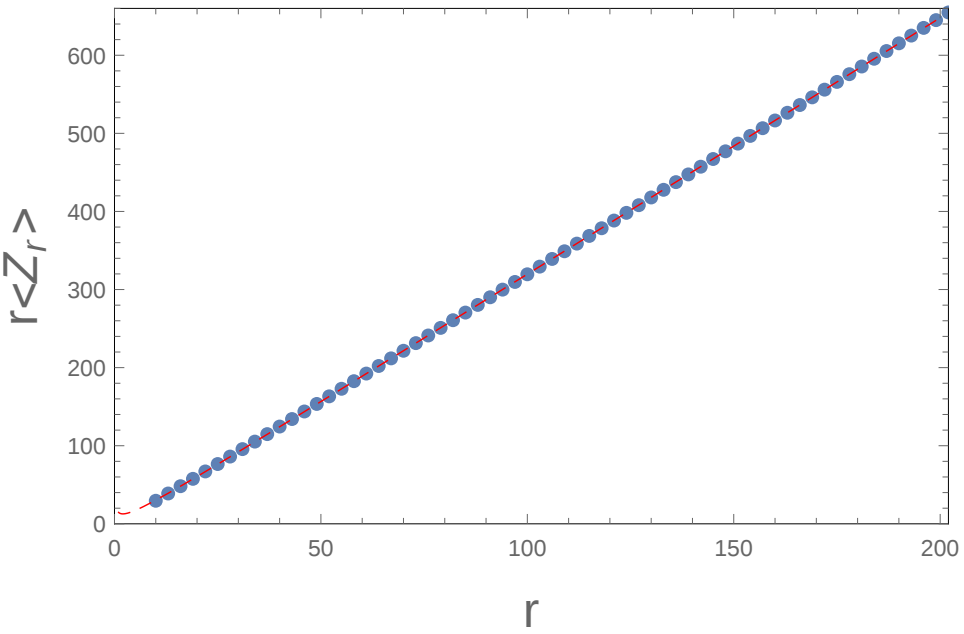

Figure 3.7: Scaling of the mean value of rZ_r with the distance r, for $d = 3$. The fit is linear with a correction $\propto r^{\omega_{FA}(3)}$. The results of the fit are, with reference to Eq. (3.50): $c_1 = -18.2 \pm 0.3$, $W_c = 27.03 \pm 0.02$, $c_2 = 29.6 \pm 0.8$. The same behavior holds for higher dimensionality and results in the estimates of the critical disorder values in Table 3.2.

of resonances are thus enhanced. However, increasing the dimensionality the discrepancy between the numerical estimates of W_c decreases; the enhanced precision of the forward approximation result is due to the fact that the loops giving rise to the self-energy corrections become less relevant in higher dimensional lattices, and thus the forward approximation becomes asymptotically exact in this limit.

Table 3.2: Comparison of the critical value for localization in the Anderson model in d dimensions predicted by the forward approximation with the numerical results of Ref. [66]. The relative error decreases faster than d^{-6}.

d	W_c^{FA}	W_c^{num}	Error
3	27.03 ± 0.03	16.536 ± 0.007	39%
4	41.4 ± 0.1	34.62 ± 0.03	16%
5	57.8 ± 0.2	57.30 ± 0.05	0.9%
6	77.0 ± 0.3	-	-
7	93.8 ± 0.3	-	-

3.3.4 Divergent length scales and critical exponents

For fixed non-critical values of the parameters t and W and for finite r, the probability of resonances (3.46) is determined by the tails of the distribution of Z_r. We are interested in looking at its behavior with r, which allows to identify a length scale which diverges at the transition point, as the asymptotic limit for the probability switches from 0 to 1.

Indeed, for an increasing r, the asymptotic limit is approached in a different way at the two sides of the transition: for $W > W_c$, the probability of resonances goes to zero exponentially with r. Below the transition, the probability converges to one much faster, with corrections that are only double exponential in r. We perform a linear fit of the quantities

$$\log\left[P\left(\log|\psi_r|^2 > 0\right)\right] \tag{3.51}$$

and

$$\log\left|\log\left[1 - P\left(\log|\psi_r|^2 > 0\right)\right]\right| \tag{3.52}$$

as functions of r for $W > W_c$ and $W < W_c$, respectively. Examples of the fits of the probability of resonances are shown in Fig. 3.8.

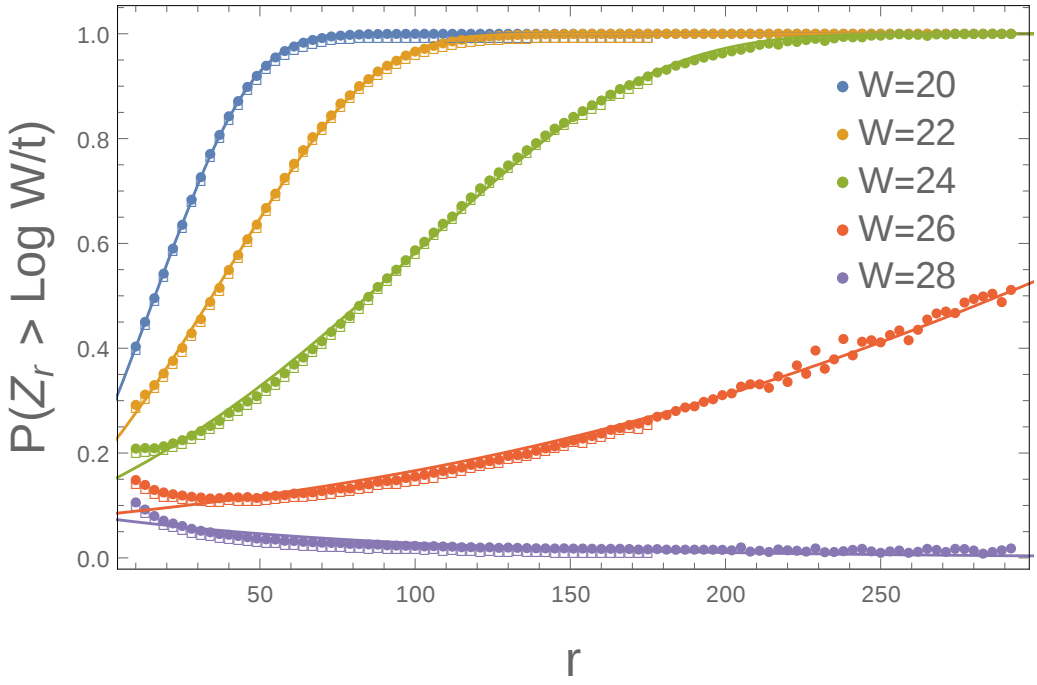

Figure 3.8: Probability of resonances $P\left(Z_r > \log \frac{W}{t}\right)$ as a function of the distance r from the origin, for $d = 3$. Asymptotically in r, the probability reaches 0 exponentially fast in the localized phase, and 1 double exponentially fast in the delocalized phase. The squares are the results of the transfer matrix calculation, the points of the dominating path (see Sec. 3.4.2) while the continuous lines are the exponential or double exponential fit. Very similar results are obtained for higher dimensionality.

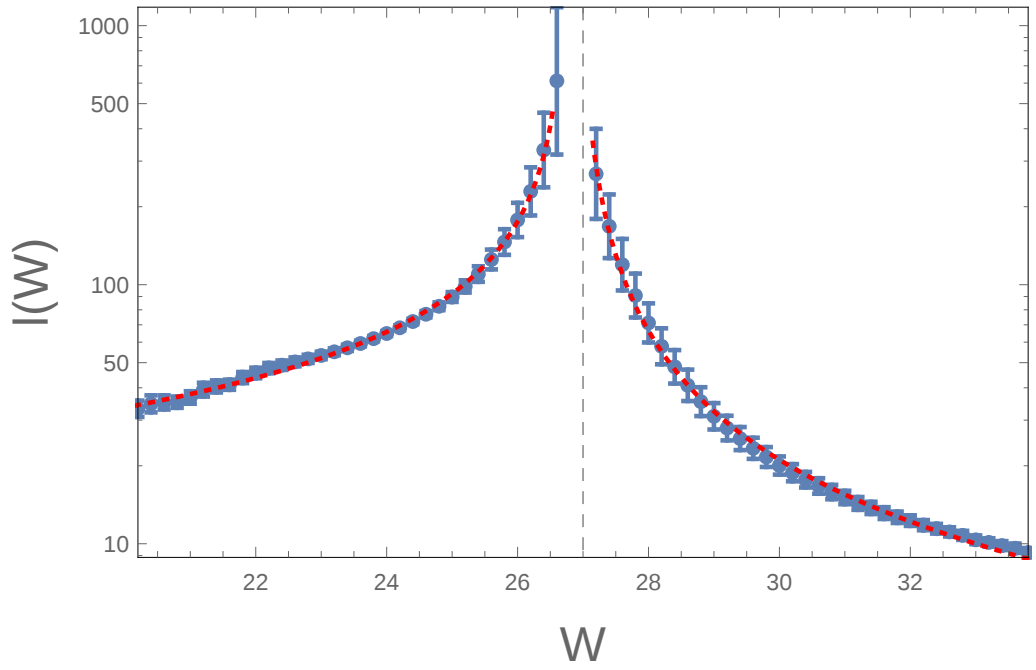

Figure 3.9: Power law divergence of $l(W)$. The values of $l(W)$ for fixed W are determined from fits such as the ones in Fig. 3.8. The power law fit produces a critical exponent $\simeq 1$ and a critical value W_c compatible with the ones listed in Table 3.2. The results shown here are for $d = 3$; very similar results are obtained for higher dimensionality. Note how in the delocalized phase the distance to observe a resonance is typically larger (for the same $|W - W_c|$) than the localization length in the localized phase.

The fitting procedure allows to extract a W-dependent length scale $l(W)$, which diverges at the critical disorder W_c^{FA}. In particular, we expect this length scale to diverge in the same way as the localization length/correlation length does in the localized/delocalized phase, respectively. The length scale $l(W)$ is plotted in Fig. 3.9 for $d = 3$, and it is found to diverge with a power-law exponent $\simeq 1$ for all the dimensionalities.

Indeed, in the appendix of Ref. [3], this numerical result for the different decays of the probability of resonances at the two sides of the transition is confirmed by computing an approximate expression for the density of the variable Z_r. The approximation consists in considering the different paths contributions as independent variables. Moreover, an expression for $l(W)$ valid within this approximation is given, and it is shown that it diverges as $\sim |W - W_c|^{-1}$ for $W \to W_c$, consistently with the numerical results.

Connections with the problem of directed polymers in random medium

In the single particle case, the energy denominators associated to different sites along the paths are independent variables. Thus, the expression for the wavefunction amplitude in the forward approximation, Eq. (3.11), resembles the expression for the partition function of a directed polymer in a random potential, with the thermal weights for the polymer configurations given by the amplitudes of the different paths. This analogy is not straightforward, due to the occurrence of negative contributions in (3.11). Nevertheless, it has been fruitfully exploited both for the single particle problem [58, 69–71], and for problems of interacting spins on the Bethe lattice [72–75].

Motivated by this analogy the authors of Ref. [58] have proposed a scaling form analogous to (3.48) for the logarithm $\log g$ of the conductance of an Anderson model. There, the conductance in $d = 2$ is obtained from the Green functions, which are computed numerically in the strong disordered regime. It is shown that the fluctuations of $\log g$ scale with an exponent $\omega(d = 2) = 1/3$, and that the distribution of the variable u is compatible with a Tracy-Widom distribution. The authors argue that the same results are obtained if the Green functions are computed within a modified forward approximation, the modification consisting in taking energy denominators that are not arbitrarily small but are bounded from below, with a cutoff which mimics the effect of the self energy corrections. Note that if this constraint is relaxed and the energy denominators are allowed to be arbitrarily small, $\log g$ is found to be proportional to the quantity rZ_r that we are considering.

The results of Ref. [58] are consistent with the conjecture [59, 76] that in the strongly localized phase, where the expansion in non-repeating paths is best controlled, the Anderson model in dimension d belongs to the same universality class of the directed polymer in dimension $1 + D$, with $D = d - 1$. In particular, the conjecture implies that in the limit of large r the distribution of $\log g$ has the scaling form (3.48), with $\omega(d)$ coinciding with the droplet exponent [77] in $1 + (d - 1)$ dimensions (which is exactly known [78] to be equal to $1/3$ for $D = 1$), and u having the same distribution of the fluctuations of the free energy in the disordered phase of the polymer, which are distributed according to the Tracy-Widom distribution [79–82] in $D = 1$.

The values of the scaling exponents extracted from our data (see Table 3.1) do not compare well with the droplet exponents $\omega(D = d - 1)$ of the directed polymer, which we read from Ref. [83] and references therein. Curiously, they compare within errors with $\omega(D + 1)$. We do not have an explanation for this curious behavior, and we leave its analysis for future work.

Broadly speaking, the discrepancies with respect to the directed polymer results might be generated by the fat-tail of the distribution of the paths' amplitudes in (3.43), produced by the arbitrarily small energy denominators. It might be that the finite size effect are more pronounced in the case of unbounded denominators. On the other hand, it is quite natural to expect that the models of non-repeating paths with bounded amplitude considered in Ref. [58] exhibit a stronger dependence on the dimensionality, due to the fact that the domination by one single path is less pronounced in that case. Additional comments on this point are in Sec. 3.4.2.

Summarizing these result on the strong similarities with the problem of directed polymers in a random medium, from this statistical analysis it emerges that the scaling exponents describing the fluctuations of the wavefunctions are non-mean field, but also not equal to those of the directed polymer. Moreover, the limiting distribution of the appropriately rescaled wavefunctions seems to depend more weakly on dimensionality with respect to the directed polymer case.

3.4 Further approximation: the optimal directed path

Up to now we have discussed the full expression for the forward approximation, Eq. (3.11); this sum has been numerically computed through transfer matrix multiplications. However, it is possible to consider an additional approximation, which performs very well for the single particle model with uncorrelated energies. It consists of taking only one of the exponentially many paths between the origin and the site where we are computing the wavefunction amplitude, i.e. the dominant one; since a lot of less important information is disregarded, this method is much faster and efficient in terms of required memory space, allowing to inspect much bigger system sizes. Some of the data already presented in this chapter, in particular those relative to higher dimensions and/or system sizes, has been computed making use of this approximation.

3.4.1 Numerical method for computing the dominating path

We start by noting that, if the terms are independent from one another, the sum in Eq. (3.11) is dominated by the maximum term, being a sum of terms

which, in the localized phase, have a power law distribution[3]. Therefore we could approximate it by taking only the path to which the greatest weight corresponds. We can select this path by viewing the lattice as a directed graph; indeed, we use the Dijkstra algorithm to find the best path in the weighted directed graph generated by weighting the edges of the lattice with

$$\chi_p \equiv \log|\epsilon_p| - \min_k \left(\log|\epsilon_k|\right), \tag{3.53}$$

where p is the site which the edge connects to, i.e. the next site to be visited; we subtract the minimum in order to use the Dijkstra algorithm (a greedy algorithm which requires positive weights), which, denoting with e and $v = N$ the number of edges and vertices respectively, has computational complexity[4] $O(e + v \log v)$. Then the absolute value of the path weight is:

$$|w_p| = \mathrm{e}^{-\tilde{w}_p}, \quad \text{where } \tilde{w}_p = \sum_e x_e, \tag{3.54}$$

which, for the optimal path, corresponds to the maximum weight.

This result is to be compared with the full sum given by Eq. (3.11) with the transfer matrix result. As it will be shown in Sec. 3.4.2, this will turn out to be a very good approximation, which enables to numerically access much bigger system sizes; indeed, computing the wavefunction with this method has lower time complexity (recall that matrix multiplication has complexity $O(v^{3-\epsilon})$ if dense, $O(v + e)$ if sparse, and the number of multiplications to perform is equal to the path length r). In terms of required memory, the complexity is $O(e^2)$ for the Dijkstra algorithm[5] and $O(v^2)$ or $O(v + e)$ respectively for the dense and sparse transfer matrix multiplication.

Second best directed path

Note that we can also calculate the successive best paths in a similar way. The algorithm used for finding the second best path is based on finding the best path from the initial to the final site which is different from the shortest path at least by one site; this is obtained by considering the sub-graph in which each of the sites belonging to the shortest path is removed, one at a time; it was devised originally by Yen in Ref. [84]. In more detail, one does the following:

[3] In Sec. 1.2 we saw that, in the localized phase, the wavefunction amplitudes have a Porter Thomas distribution, $P(x) = \frac{\mathrm{e}^{-x/2}}{\sqrt{2\pi x}}$.

[4] For the $d-$dimensional hypercube, the time complexity for the dominating path using Dijkstra's algorithm is equal to $O(d\,N + N \log N)$

[5] For the $d-$dimensional hypercube, the memory space complexity translates in $O(dN)$

- calculate the shortest path between two sites, a and b, and its weight as in Sec. 3.4;
- for each node l in the shortest path, excluding the initial and final nodes a and b:
  - consider the graph which is generated by deleting the node l from the original graph;
  - in this subgraph, calculate the shortest path between a and b and its weight and store it;
- find the path with minimum weight between the ones which have been computed in the previous step.

Excluding both the best and second best paths we can calculate the third best path and so on. The computational complexity of computing all the subsequent paths in this way is $O(Kv(e + v \log v))$, where K is the order of the successive best path to compute.

3.4.2 The structure of the dominating path

Connection with the directed polymer

A relevant difference between the expression in Eq. (3.11) and the partition function of directed polymers is that while the weight associated to the polymer has an upper bound [64], the single factors in (3.11) are unbounded, with diverging average. As a consequence, the strongly localized phase in the Anderson model (where the forward approximation is better controlled) always corresponds to a "frozen" phase of the directed polymer, in which most of the weight in the total sum (3.11) is given by one single path.

Comparison with the forward approximation

Let us now proceed to compare the statistics of the wavefunction amplitudes in the forward approximation with that of the optimal path, i.e. the path with maximal amplitude; we will see that the full sum is strongly dominated by the extremal path amplitude.

Let us first consider the Anderson model on the hypercube. The amplitude ω_r^* of the optimal path p^* is computed by means of the Dijkstra algorithm [85]; to apply the algorithm, as explained in Sec. 3.4.1, we assign an orientation to each edge $\langle i, j \rangle$ of the d-dimensional cube (since the paths in $\text{path}^*(a, b)$ are non-repeating, the orientation of the paths from the starting site a to the final one b induces a natural orientation of the edges) together

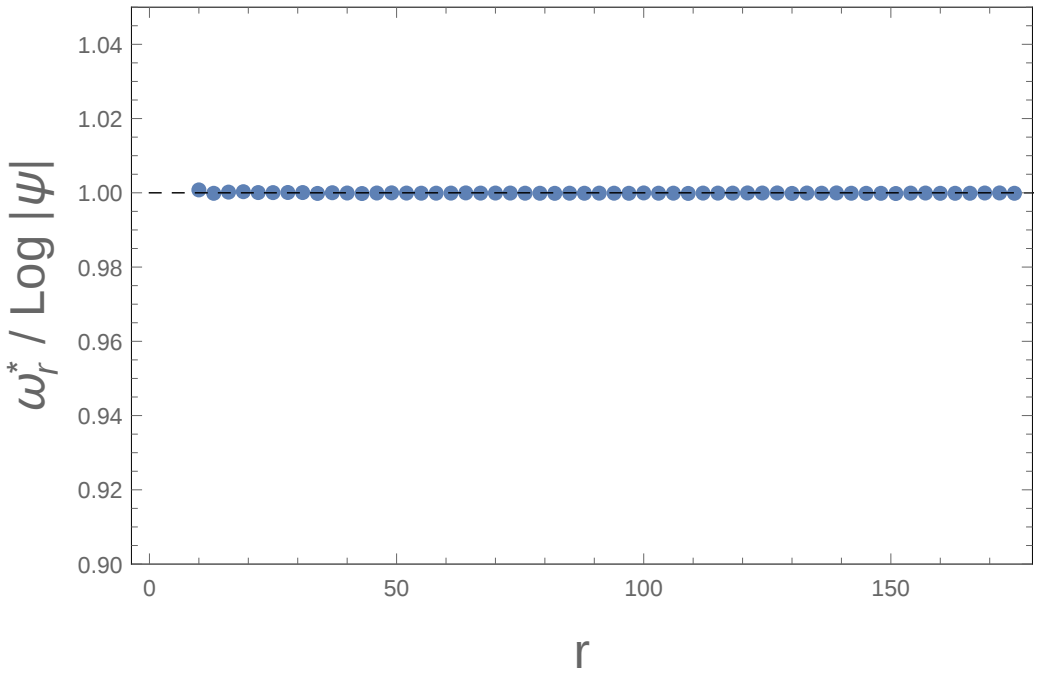

Figure 3.10: Average ratio of the dominating path weight ω_r^* and the sum in Eq. (3.43) computed using a transfer matrix technique, for the same disorder realization. The plot corresponds to $d = 3$, and each point is averaged over $3 \cdot 10^4$ disorder realizations. Similar results are obtained for higher dimensionality, for those r accessible with the transfer matrix technique. The standard deviation error bars are within the point size.

with the cost (3.53), i.e. $\chi_p \equiv \log|\epsilon_p| - \min_k \log|\epsilon_k|$. The edge cost is chosen in such a way that it is positive, as required by the algorithm. The total cost of a path p is the sum of the costs of the edges belonging to it, and the path p^* with maximal amplitude is the one minimizing the total cost function. In order to make a comparison with the transfer matrix results, one can compute the ratio between ω_r^* and the full sum (3.43) computed via the transfer matrix technique, for the same given disorder realization. The distribution of the ratios turns out to be very narrowly peaked around one. Fig. 3.10 displays its average as a function of the length of the paths r for $d = 3$, which is extremely close to one, uniformly in the path length.

As a further check of the agreement between the values computed with the two methods, in Fig. 3.8 we plot, together with the result from the full sum (3.43), the r-dependence of the probability (3.14) determined with the substitution $|\psi_r| \to \omega_r^*$. The data are plotted as points, which are almost

indistinguishable from the transfer matrix results (squares). This indicates that the statistics of distant resonances is fully captured by the optimal path. Therefore, we have shown that in the single particle case the correlation between different paths does not play a relevant role, since the sum is dominated by the extremum, as it would happen for independent random variables with fat-tailed distribution. Based on this observation, the numerical analysis outlined in the previous sections can be (and indeed has been) carried out for much bigger system sizes with respect to the ones accessible with the transfer matrix technique.

In order to check with the results in the literature [58], one can also take a modified forward approximation in which the small denominators are bounded, which is sufficient to break the picture presented here. Indeed, we take the energy denominators uniformly distributed in $[-1, -W^{-1}] \cup [W^{-1}, 1]$ in $d = 3$ for two values of the cutoff, $W = 25$ and $W = 35$. In this case, the ratio between the maximal path and the transfer matrix result departs from one for increasing r, suggesting that more than one path dominates the transfer matrix result. It is natural to expect that in this case the number of dominating paths depends on the geometry of the system, thus introducing a stronger dependence on the dimensionality. For the following analysis we go back to the case of unbounded denominators.

Structure of the dominating path

One could ask what is the quality of the dominating path, i.e. whether it has the dominating weight due to the fact that includes a single, very favourable site, or instead all the sites belonging to it contribute to make it the path with the biggest weight.

To characterize the optimal path one can compute the inverse participation ratio (IPR) of the edge weights contributing to ω_r^*; for this calculation, let us consider $\epsilon_i \in [-1, 1]$ (i.e. $W = 2$) and define

$$\mathrm{IPR} = \frac{\left(\sum_i \log|\epsilon_i|\right)^2}{\sum_i (\log|\epsilon_i|)^2}, \tag{3.55}$$

where i labels the sites belonging to the optimal path p^*. The disorder-averaged IPR scales linearly with the length of the path r, indicating that an extensive (in r) number of edges contributes to the total path weight, and cooperate to produce the atypically big path weights dominating (3.43) (see Fig. 3.11).

Let us also look more closely at the distribution of the variables that make up the dominating path. Indeed, Fig. 3.12 shows the distribution of the absolute value of the energies along the optimal path for $W = 2$, $d = 3$,

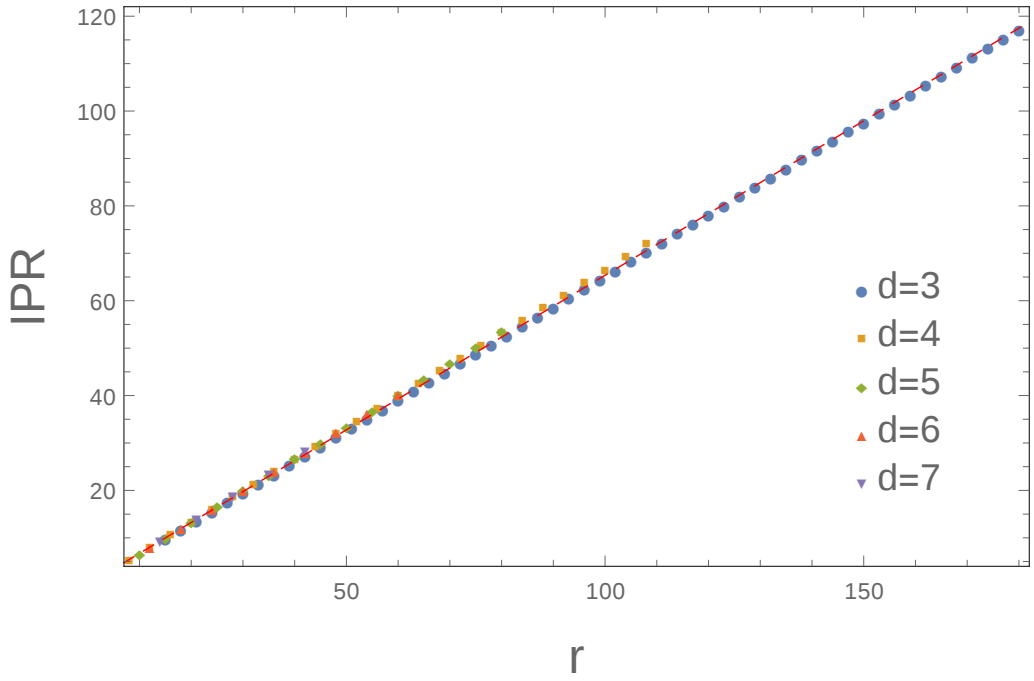

Figure 3.11: Inverse participation ratio (3.55) of the energies corresponding to the sites belonging to the dominating path. The linear behavior with the path length, i.e. the number of these sites, implies that all the sites contribute to the atypically big weight of the dominating path. The dashed line is a linear fit of the form $\mathrm{IPR} = ar + b$ corresponding to $d = 3$; its parameters are $a = 0.6516 \pm 0.0002$ and $b = 0.20 \pm 0.02$.

$r = 210$ and $\epsilon_a = 0$, showing a power law. The fitting function, shown in a dashed line, has the form $\rho_r(\epsilon) = c_r + b_r|\epsilon|^{a_r}$. The power-law behavior is consistent with the considerations in Ref. [75]. There, the authors' arguments for the distribution of the energies along the paths included in the forward approximation sum starts from the fact that, on typical paths, the energies in the denominators are uniformly distributed; the optimal path will be an extreme event, and performing a constrained maximization calculation one can recover a power law behavior. Adapting their reasoning to the finite dimensional case, one can argue that asymptotically in r (and under the hypothesis of independent paths) the biased energy distribution along the optimal path has the form

$$\rho(\epsilon) = \frac{1-2x}{|\epsilon|^{2x}}, \tag{3.56}$$

with x solving the d-dependent equation

$$\log\left(\frac{d}{1-2x}\right) - \frac{2x}{1-2x} = 0. \tag{3.57}$$

Fitting the r-dependence of the coefficients c_r, b_r, a_r one finds that the asymptotic limits are in agreement with (3.56), once one performs a careful extrapolation to $r \to \infty$ (see the inset of Fig. 3.12).

3.5 Corrections to the forward approximation

So far we have established that the forward approximation is very good in higher dimensions, giving reasonably precise results already in $d = 5$ for the localization/delocalization transition values. One can think to improve on this result by partially restoring the self energy contribution in the denominators of Eq. (3.11).

Indeed, one could reintroduce the self energy in a perturbative way by accounting for just the smallest self avoiding loops around a give site l: assuming that $l_1, \ldots, l_n$ are its nearest neighbors, such loops are of the kind $l \to l_i \to l$, and there are n of them. Thus, we consider:

$$\Sigma_l(E) = \sum_{i=1}^{n} \frac{1}{E - \epsilon_{l_i}}. \tag{3.58}$$

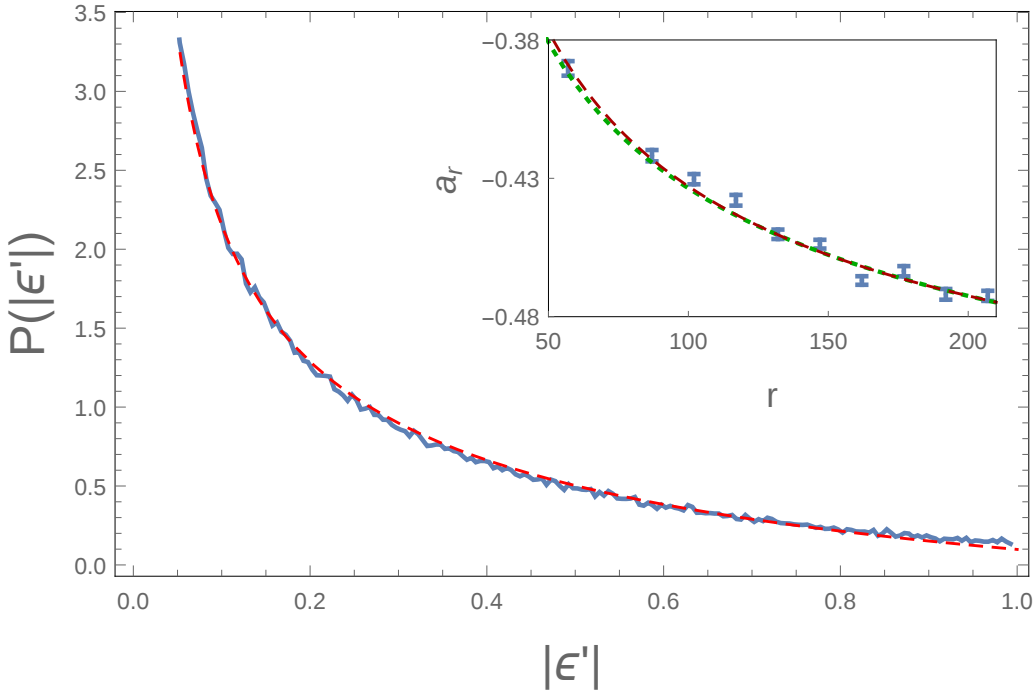

Figure 3.12: Probability distribution of the energy denominators along the optimal path, for $d = 3$ and $r = 210$. The dashed red line is the fitting function of the form $c_r + b_r|\epsilon|^{a_r}$, with fitting parameters $c_r = -0.95 \pm 0.04$, $b_r = 1.04 \pm 0.03$ and $a_r = 0.472 \pm 0.005$. Very similar results are obtained for higher dimensionality. *Inset.* Plot of the exponents a_r of the distribution of the energy denominators along the optimal path as a function of r. Due to the absence of a theoretical reasoning for the finite size scaling, there are two fit forms: one with logarithmic and one with $1/\sqrt{r}$ corrections. The green curve is a fitting function of the form $a + c/\log(r)$, with fit parameters $a = -0.73 \pm 0.05$ and $c = -1.4 \pm 0.3$; the red curve is a fitting function of the form $a + c/\sqrt{r}$, with fit parameters $a = -0.57 \pm 0.02$ and $c = -1.4 \pm 0.3$. The asymptotic value a obtained with the logarithmic fitting function is compatible with the solution of the Eq. (3.57) for $d = 3$.

This is different than the second order term of the self energy (Eq. (2.24)), which would be

$$\Sigma_l^{\neq l_{i^*}}(E) = \sum_{i \neq i^*}^{n} \frac{1}{E - \epsilon_{l_i}} \tag{3.59}$$

where l_{i^*}, in a given path, is the previously visited site; that is, $\Sigma_l^{\neq l_{i^*}}$ is a path-dependent value. In the estimation (3.58), instead, we do not exclude the previously visited site; this is wrong, but allows to compute the on-site energy corrections without adding dependence to the specific path. One can argue that in high dimensionality, where the number n of nearest neighbors is high, this estimation is increasingly good.

In order to implement this correction in our numerical scheme of transfer matrix multiplication, we first compute the shifted on-site energies. Using the notation of Sec. 3.2.2, we build a transfer matrix which allows travel in all directions, not only the forward one; indeed, we consider the one dimensional full adjacency matrix

$$T_a = (\{l+1, l\} \to 1)_{l,m=1..L} + (\{l, l+1\} \to 1)_{l,m=1..L} \tag{3.60}$$

and then construct the $d-$dimensional full adjacency matrix as before:

$$A_a = \left(\underbrace{T_a \otimes \mathbb{1} \otimes \cdots \otimes \mathbb{1}}_{d} + \cdots + \mathbb{1} \otimes \cdots \otimes \mathbb{1} \otimes T_a \right). \tag{3.61}$$

The transfer matrix is then

$$\mathcal{T}_a = W A_a, \tag{3.62}$$

where W is the diagonal matrix of the inverse energy differences, as in Eq. 3.22. The first order of the self energy correction of the site $|l\rangle$ will thus be given by:

$$\Sigma_l(\epsilon_a) = \mathcal{T}_a |l\rangle \cdot \mathbb{1}_{N\times 1} = \frac{1}{\epsilon_a - \epsilon_{l_1}} + \frac{1}{\epsilon_a - \epsilon_{l_2}} + \cdots + \frac{1}{\epsilon_a - \epsilon_{l_n}}. \tag{3.63}$$

The 'corrected locators' are then $(\epsilon_a - \epsilon_l - \Sigma_l(\epsilon_a))^{-1}$, which are elements of the 'corrected weights' matrix

$$W' = \mathrm{diag}\left[\frac{1}{\epsilon_a - \epsilon_k - \Sigma_k(\epsilon_a)} \right]_{k=1..N}, \tag{3.64}$$

with which we now build the forward transfer matrix $\mathcal{T}' = M A_f$ and proceed as in Sec. 3.2.2 for the calculation of the forward approximation sum (3.11).

Numerical estimations of the transition values in a $d = 3$ cube using this modified forward approximation show results that approach the true transition value after one iteration step of this resummation procedure. Indeed, the transition point goes from $W_c^{FA} = 27.03 \pm 0.03$ in the (uncorrected) forward approximation (see Table 3.2) to $W_c' = 24.0 \pm 0.5$ (to be compared with the most precise numerical result available $W_c^{\text{num}} = 16.536 \pm 0.007$). However, applying this self energy resummation repeatedly, one converges to the self energy correction of a Bethe lattice superimposed on the cube; controlling this convergence is still an open problem and a natural follow-up to the work presented in this thesis. Moreover, one can indeed take into account the path-dependent self energies; this requires to enlarge the transfer matrix, doubling its size to store the information about the visited sites.

3.6 Final remarks on the forward approximation

In this chapter we have discussed advantages and the limitations of the forward approximation, showing that it is a powerful tool in exploring the properties of disordered systems. The additional approximation of considering only the dominating path opens numerical opportunities for an extended study of single particle systems, while the possibility of restoring the self energies as a perturbation is a worthwile follow-up question.

As a final comment, it is worth highlighting the nature of the forward approximation as a mean-field approximation. The mean field attribute should be intended in the sense that, as the dimensionality (or local coordination) of the system increases, the approximation becomes increasingly exact. Using the forward approximation in order to find the value of the critical disorder W_c for the localization transition in the Anderson model, we noticed that it grows indefinitely with d with an error with respect to the exact value rapidly approaching zero, meaning that the hopping t is becoming an almost negligible perturbation at the transition. This feature is quite peculiar, since in ordinary, second order phase transitions the critical exponents above the upper critical dimension are correctly reproduced by a mean field approximation, while the location of the transition (e.g. a critical temperature) is never exactly given by the mean field value. The locator expansion and the forward approximation can be therefore considered better suited candidates for a mean field model, e.g. with respect to the $2 + \epsilon$ expansion of the nonlinear supersymmetric sigma model [86].

Chapter 4

Using the forward approximation: A localized system coupled to a *small* bath

In this chapter it will be shown how the forward approximation can be usefully employed to study nontrivial systems, for which an exact solution is not available. Nontrivial localization properties emerge if one considers a single particle system interacting with a mesoscopic quantum bath [4]. These results are both interesting on their own, and an additional example of the fruitfulness of the forward approximation.

4.1 Introduction

In chapter 3 we have built a picture of the forward approximation and its features. Let us now make use of it as a tool to inspect a specific system showing peculiar localization properties. Indeed, we consider a system composed by a particle in a disordered system coupled to a localized bath and analyze its localization properties using the forward approximation [4]. Exploring the properties of this kind of systems is interesting in its own because in experiments we rarely have absence of interactions with the environment, and the effect of the bath may influence the localization properties of the system. In addition to that, this will prove as a productive playground to work in the forward approximation.

This investigation is justified by the fact that much work on quantum localization considers only the idealized (and experimentally unrealizable) limit of a completely closed quantum system, perfectly isolated from any environment; works that have studied what happens when a localized system

is coupled to a thermodynamically large bath exist [87–90] and show that when a localized system is weakly coupled to a large bath the exact eigenstates of the combined system and bath immediately become thermal (while signatures of localization remain in local operators). More complex phenomenology can however appear if a localized system is exposed to a *small* bath, containing very few degrees of freedom, and if there are no restrictions on the coupling to be weak.

The result obtained by analyzing this system is that localization is stable in presence of a coupling to a bath, on the condition that the bath is mesoscopic; the transition boundary is modified in a nontrivial way due to the interplay between the opposite mechanisms of 'borrowing' energy from the bath, which favors delocalization, and of the quantum Zeno effect, which for strong couplings forbids the evolution of the state. Overall, localization is present for any value of the coupling to the bath for sufficiently strong disorder, and there is a crossover between the two localization mechanism of Anderson and Zeno localization.

In this chapter we will follow a qualitative discussion of the model which will give the correct intuition on its localization properties. This qualitative intuition can be confirmed by accurate analytic calculations in the forward approximation, of which we will discuss the setup of the procedure and the results, and by numerical exact diagonalization.

4.2 The model

We consider a system composed of a single particle in a random on-site potential coupled to a delocalized bath. Let us start by considering the particle, whose Hamiltonian is

$$H_0 = -t \sum_{\langle ij \rangle} c_i^\dagger c_j + \sum_i \epsilon_i c_i^\dagger c_i, \tag{4.1}$$

where ϵ_i is a random on-site energy taken from a uniform distribution in the interval $[-W, W]$. The lattice dimensionality is d, arbitrary and, for finite size systems, we take L^d lattice sites.

Then, we consider a bath. There are two key conditions that we require of the bath, that is it has to be of finite size (a *small bath*, with a discrete spectrum) and it has to be protected against localization. Indeed, previous works on this kind of systems which considered a delocalized thermodynamically large bath found that the delocalized bath forces the total system to be in a delocalized state too (the reason for this will be explained in the

following, since it will become clear once the mechanism for which the particle can borrow energy from the bath is understood); on the other hand, if we consider a small bath that is not protected against localization, then the additional degrees of freedom would localize as soon as it is coupled to a localized system [87–90]. Note that such kind of delocalized bath is not unphysical; examples include the longest wavelength Goldstone modes associated with the spontaneous breaking of a continuous symmetry [91] and the extended states in systems where there is a topological obstruction to the construction of localized Wannier orbitals [92].

We model the bath as a quantum dot or a zero-dimensional system. This is done in order to couple the particle uniformly to the bath, avoiding to add any spatial disorder. We take the Hamiltonian of the bath to be

$$H_{\text{bath}} = \omega \sum_{\alpha',\beta'} M_{\alpha',\beta'} |\alpha'\rangle\langle\beta'|, \tag{4.2}$$

where we take M to be a $N \times N$ GOE random matrix, distributed according to

$$P(M) \propto \exp\left(-\frac{1}{2}\,\text{tr}\left[M^2\right]\right), \tag{4.3}$$

with

$$\langle M_{\alpha,\beta}\rangle = 0, \quad \langle M^2_{\alpha,\beta}\rangle = \frac{1}{2} \text{ for } \alpha \neq \beta, \quad \langle M^2_{\alpha,\alpha}\rangle = 1, \tag{4.4}$$

in order to obtain a bath protected against localization. This is thus a system which can be in any of N possible states with energy in a bandwidth $2\omega\sqrt{2N}$. Note that the density of states is given by the well-known semicircle law

$$\rho(E) = \frac{4N}{\pi\omega\sqrt{2N}} \tag{4.5}$$

and therefore the level spacing, in the middle of the spectrum, is

$$\delta = \frac{1}{\rho(0)} = \frac{\pi\omega}{\sqrt{2N}}. \tag{4.6}$$

Finally, we choose a coupling that does not change the localization properties of the bath but is still able to transfer energy to the particle in the d-dimensional lattice. The simplest one which has this effect is a coupling of strength λ which can scatter the bath from any eigenstate to any eigenstate with a random amplitude $M^{(i)}_{\alpha,\beta}$:

$$H_{\text{couple}} = \lambda \sum_{i,\alpha,\beta} M^{(i)}_{\alpha,\beta} c_i^\dagger c_i \otimes |\alpha\rangle\langle\beta|. \tag{4.7}$$

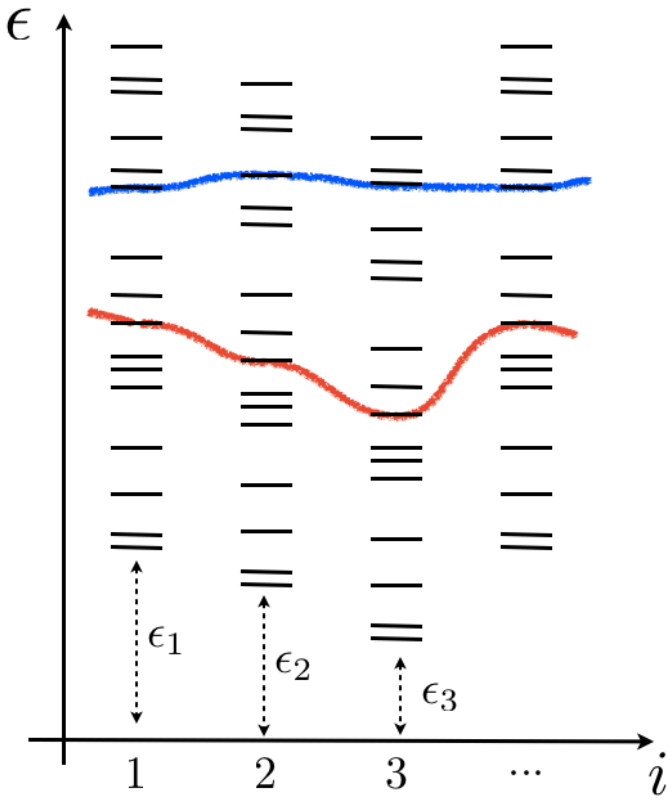

Figure 4.1: Figure illustrating the basic setup. There is a tower of states for every site i, which differ only in the state of the bath. The states in the tower have energies spanning a bandwidth $\omega\sqrt{N}$ and level spacing $\omega/\sqrt{N}$. The red line is the one the hopping follows in the weak coupling regime (i.e. there is no change in the state of the bath); the blue line represents an on-shell hopping, which can happen if the states in the bath get hybridized as the coupling grows.

We choose the amplitudes to form L^d random matrices, one for each lattice site.

The Hamiltonian of the full system is then:

$$H = H_0 \otimes \mathbb{1}_{N\times N} + \mathbb{1}_{L^d\times L^d} \otimes H_{\text{bath}} + H_{\text{couple}}. \tag{4.8}$$

4.3 Analysis of the system

Let us start by understanding what happens in the system with the hopping t and the interaction with the bath λ switched off. For each position of the particle, there is a 'tower' of N bath states, with bandwidth $\omega\sqrt{N}$ and level

spacing $\omega/\sqrt{N}$. For each different site, this tower is shifted in energy by the on-site disorder corresponding to that site, which is of order W. In the following we will consider overlapping towers, that is $\omega/\sqrt{N} < W < \omega\sqrt{N}$, and, in particular, that the overlapping happens away from the Lifshits tails. This setup is represented schematically in Fig. 4.1.

In the case $t = \lambda = 0$ the eigenstates of the total system are clearly the product states of particle and bath where the states of the particle are exactly localized in site i:

$$|\psi\rangle = |i\rangle \otimes |\alpha\rangle. \tag{4.9}$$

Keeping the coupling $\lambda = 0$ and turning on the hopping, the particle will clearly be in the strong Anderson localization regime for $W \ll t$ (meaning that the localization length will be less than or of the order of the lattice spacing) and in a weak localization (for $d = 1, 2$) or delocalization (for $d \geq 3$) regime for $W \gg t$. Note that the dependence on dimensionality in the presence of the bath can be understood once one views even the "strong hopping" problem as a (multi band) problem of a fermion moving in a random potential; this problem always exhibits localization in one and two dimensions. The presence of localization can be seen by applying the locator expansion, which will converge in the former case and diverge in the latter.

Let us now turn on the coupling with the bath. The system will go through three regimes, which differ according to the hybridization of the bath states with the tower corresponding to neighboring sites. Indeed, at weak λ the bath states do not hybridize and remain the same as the eigenstates of M. The hoppings of the particle can happen with an energy cost equal to the disorder strength, properly rescaled by the presence of the coupling to the bath. In Fig. 4.1 this is showed by the trajectory in red. At intermediate λ the states of the bath start to hybridize over an energy window of width Δ, which, eventually, for strong λ involves all the states of the bath. This results in the possibility of on-shell hopping trajectories, as pictured with a blue line in Fig. 4.1. This, at least in the case of intermediate λ, makes it so that the hopping requires less energy for the particle, since the particle is effectively borrowing energy from the bath. Note that this clarifies why a coupling with an infinite bath results always in a delocalized particle, as mentioned in Sec. 4.2: in that case, hybridization always occurs, for infinitesimal λ.

Let us now discuss in more details these three cases by looking at the convergence of the locator expansion.

4.3.1 Weak λ: Anderson localized regime

In this regime the effect of the coupling to the bath is limited to a rescaling of the hopping and disorder strength. Indeed, supposing that the particle is at position i, the effective Hamiltonian for the bath is $\omega M + \lambda M^{(i)}$. The bath eigenstates will start to mix with each other when λ becomes comparable to the level spacing associated with the bare bath Hamiltonian, that is[1] $\sim \omega/\sqrt{N}$. This absence of hybridization means that there are no mechanisms which enhances the hopping of the particle for $\lambda < \omega/\sqrt{N}$. We can easily check this by considering the $O(t)$ correction to the localized eigenstate:

$$|\Psi\rangle \simeq |i\rangle \otimes |\alpha\rangle + \sum_{\beta} A_{i+1,\beta} |i+1\rangle \otimes |\beta\rangle + \dots \,. \tag{4.10}$$

If $\lambda < \delta$, for a hopping leaving the bath untouched, perturbation theory gives

$$A_{i+1,\alpha} = \frac{t}{\epsilon_{i+1} - \epsilon_i} \sim \frac{t}{W}, \tag{4.11}$$

while for a hopping that changes the state of the bath to $\beta \neq \alpha$ the same ratio is at most

$$\begin{aligned} \max_{\beta} A_{i+1,\beta} &= \frac{t}{\epsilon_{i+1} - \epsilon_i} \max_{\beta} \frac{\lambda}{\epsilon_i - \epsilon_{i+1} + E_\alpha - E_\beta} \\ &\sim \frac{t}{\epsilon_i - \epsilon_{i+1}} \frac{\lambda}{\delta} \sim \frac{t\lambda}{W\delta} < A_{i+1,\alpha}. \end{aligned} \tag{4.12}$$

So in this regime, the bath is typically not excited by the traveling particle, meaning that the bath state does not change. The contribution given by the presence of the bath is, instead, a rescaled disorder and hopping. Indeed, since the coupling between the particle and the bath is different for each site (by means of the matrices $M^{(i)}$), there is an additional source of static disorder; therefore the particle is hopping in an effective on-site potential, which has strength $W_{\text{eff}} \approx \sqrt{W^2 + \lambda^2} \approx W\left(1 + \frac{\lambda^2}{2W^2}\right)$. At the same time, the bath opens up additional hopping channels, increasing the effective hopping to $t_{\text{eff}} \approx t\left(1 + \frac{\lambda^2}{2\delta^2}\right)$.

[1] Indeed, a more precise criterion is:

$$\lambda \lesssim \frac{\omega}{\sqrt{N}\log N}.$$

This comes from interpreting the effective Hamiltonian as a fully connected graph [49,93].

The criterion for the breakdown of the locator expansion for $\lambda = 0$, that is $W < t$, is then modified in $W_{\text{eff}} < t_{\text{eff}}$. We note that, since $\delta < W$, the opening of new channels is the dominant effect. The net result, therefore, is making localization less stable, changing the critical hopping to[2] $t_c = W\left(1 - \frac{\lambda^2}{2\delta^2} + \frac{\lambda^2}{2W^2}\right)$. For $t < t_c$, we have strong localization, and for $t > t_c$ we have either weak localization (in one or two dimensions) or delocalization (in three dimensions).

It should also be noted that in the weakly coupled strong localization regime the exact eigenstates are effectively product states of particle and bath states, and the entropy of entanglement of the system with the bath is near zero.

4.3.2 Intermediate λ

As mentioned before, the key property of this regime is that the eigenstates of $M^{(0)}$ start to hybridize within an energy window Δ. For simplicity, let us first consider the system with the hopping turned off, $h = 0$. Then, the window of hybridization that opens as $\lambda > \frac{\omega}{\sqrt{N}}$ can be determined by calculating the decay rate of an eigenstate of $\omega M^{(0)}$ due to the perturbation $\lambda M^{(i)}$ using Fermi's golden rule. Indeed,

$$\Delta \simeq 2\pi\lambda^2\delta^{-1} = 2\pi\lambda^2\frac{\sqrt{2N}}{\pi\omega}; \tag{4.13}$$

moreover, this indicates that the broadened spectral line is a Lorentzian with width Δ, meaning that the eigenstates $|\alpha_{(i)}\rangle$ of $\omega M + \lambda M^{(i)}$ should be wavepackets of eigenstates $|\alpha_{(0)}\rangle$ of ωM, with overlap

$$|\langle\alpha_{(i)}|\alpha_{(0)}\rangle| = \sqrt{\frac{\delta\Delta/\pi}{(E_{\alpha_{(i)}} - E_{\alpha_{(0)}})^2 + \Delta^2}}. \tag{4.14}$$

The weak and strong λ limits are matched by the Fermi golden rule interpolation: as $\lambda \to \omega$, the hybridization window widens so that it covers all the bath states, that is $\Delta \to 2\omega\sqrt{2N} = \Omega$; on the other hand, as $\lambda \to \delta$, we

[2] In high dimensions the result for t_c is modified as an extra factor is needed [51], obtaining

$$t_c = \frac{W}{d\log d}\left(1 - \frac{\lambda^2}{2\delta^2} + \frac{\lambda^2}{2W^2}\right)$$

fall in the limit of no hybridization, that is $\Delta \to 2\pi\delta$. Moreover, the window becomes comparable to the disorder strength W for the value

$$\lambda_c = \sqrt{\frac{W\omega}{2\sqrt{2N}}}. \tag{4.15}$$

As we turn on a small t, it should be noted that now the hopping is perturbative in t but non-perturbative in λ; the eigenstates will be of the form:

$$\begin{aligned} |\Psi\rangle \quad &= \quad |i\rangle|\alpha_i\rangle \\ + \quad &\sum_{\alpha_{i+1}} \quad \frac{t\langle\alpha_{i+1}|\alpha_i\rangle}{\epsilon_{i+1} + E_{\alpha_{i+1}} - \epsilon_i - E_{\alpha_i}} |i+1\rangle|\alpha_{i+1}\rangle \\ + \quad &\quad \ldots \, . \end{aligned} \tag{4.16}$$

On-shell hopping is now possible, i.e. the hopping involves staying on an energy shell up to a precision $\delta \sim \frac{\omega}{\sqrt{N}}$ (see the blue line path in Fig. 4.1), due to the non-zero overlap between the two states $|\alpha_{i+1}\rangle$ and $|\alpha_i\rangle$ at the same energy; since there is a difference of on-site energy $|\epsilon_i - \epsilon_{i+1}| \sim W$ in the lattice, this means that the process must involve transitions between bath states with $\left|E_{\alpha_i} - E_{\alpha_{i+1}}\right| \sim W$. Indeed, inserting $E_{\alpha_i} - E_{\alpha_0} \sim W$ into Eq. (4.14) we are able to compute the correction to the wavefunction due to this "direct hopping" process, which is equal, at the leading order in t, to

$$\sim \left(\frac{t}{\delta} \frac{\sqrt{\Delta\delta}}{\sqrt{W^2 + \Delta^2}} \right). \tag{4.17}$$

For $\lambda > \lambda_c$, these processes become "easy", in the sense that the hybridization window Δ becomes larger than the typical gap W, and Eq. (4.17) can be approximated with $\frac{t}{\lambda}$ (recall that $\Delta \simeq \frac{\lambda^2}{\delta}$). Instead, for $\lambda < \lambda_c$, Eq. (4.17) can be approximated with $\frac{t\lambda}{W\delta}$; indeed, in this case, a direct on-shell hopping is forbidden since the overlap between the states is small, but a two-step transition in which the particle hops without changing the bath state and going off-shell by an energy W, followed by a relaxation of the bath will be the main mechanism for the hopping.

4.3.3 Strong λ: Zeno localization

Finally, let us consider the limit of strong λ. In this regime, as mentioned, the particle becomes localized again due to the strong coupling to the bath, a phenomenology that we dubbed "Zeno localization". Indeed, it resembles

the quantum Zeno effect of the non-evolution, or evolution in a subspace only, of the dynamics of a small system coupled to a mesoscopic quantum system (such as a measurement apparatus) [94–96].

In order to explain this effect, let us again start from the system with the hopping t turned off, and recall that we are in the fully hybridized region (so that the eigenenergies of the bath E_{α_i} acquire a lattice position index i). In the limit of very strong λ, that is $\lambda \gg \omega$, the Hamiltonian of the bath is dominated by the coupling to the particle, i.e. $M^{(i)}$; moreover, note that the hybridization is different for each site i. Therefore the overlap between two states (involving a change in the state of the bath $\alpha \to \beta$ and of the site $i \to j$) is:

$$\langle \alpha_i | \beta_j \rangle = \delta_{\alpha,\beta}\delta_{i,j} + \frac{(1-\delta_{i,j})x_{ij}}{\sqrt{N}}, \tag{4.18}$$

where the $\delta_{i,j}$ is a Kronecker delta function and x_{ij} is a Gaussian random variable $\langle x_{ij} \rangle = 0$ and $\langle x_{ij}^2 \rangle = 1$.

Turning on the hopping t, when the particle hops to another site the state of the bath will change, and it will be chosen among the bath states with accessible energy, i.e., in this regime, all of them. Indeed, we can map the problem to a Bethe lattice problem with connectivity $\kappa = N$, effective hopping

$$\tau = t\frac{1}{\sqrt{N}}, \tag{4.19}$$

and effective disorder

$$\mathcal{W} = \lambda\sqrt{N}. \tag{4.20}$$

The effective disorder $\mathcal{W}$ is determined from the bandwidth of the local bath Hamiltonians $\omega M + \lambda M^{(i)}$, that is $\sqrt{2N\omega^2\left(1+\frac{\lambda^2}{\omega^2}\right)} \sim \lambda\sqrt{N}$ for $\lambda > \omega$. The localization criterion is well known in the Bethe lattice (see Sec. 2.3), that is, we have localized states if

$$t \lesssim \frac{\lambda}{\log N}, \tag{4.21}$$

while in the opposite case the locator expansion does not converge and there is either weak localization or delocalization, depending on the system dimensionality.

Another way to see this behavior is as a consequence of the orthogonality catastrophe, i.e. the contribution of the bath to the full wavefunction is

very different depending on the site on which the particle is, which in turn strongly suppresses the overlap between states corresponding to the particle being in adjacent sites, and therefore the matrix element corresponding to the effective hopping between sites. Indeed, in the limit $\lambda \to \infty$ the states are exact eigenstates of the system-bath coupling, the hopping being completely ineffective; they are the product states $|\Psi\rangle = |i\rangle|\alpha_i\rangle$. Note that the entropy of entanglement of particle and bath, in an eigenstate, is zero, and the particle is localized on a single site.

4.4 Numerical and analytic results

So far we have presented a qualitative argument, which is enough to have a detailed intuition about the behavior of the system. Still, the analysis sketched in Sec. 4.3 has been performed in the forward approximation in a more quantitatively accurate way in the appendix of Ref. [4]. In this chapter we will not go into the details of this analytic calculation, opting instead to sum up their result: the convergence region of the forward approximation, schematically shown in Fig. 4.2, corresponds to

$$t \lesssim \begin{cases} W(1 - \lambda^2/2\delta^2 + \lambda^2/2W^2) & \text{if } \lambda < \delta \\ W\delta/\lambda & \text{if } \delta/\sqrt{2\pi} < \lambda < \lambda_c \\ \lambda/\log N & \text{if } \lambda > \lambda_c. \end{cases} \tag{4.22}$$

The important feature of this analysis is that the behavior in λ is non-monotonic. Comparing with the intuition gained in Sec. 4.3, at the smallest $\lambda < \omega/\sqrt{N}$, the coupling to the bath destabilizes localization by opening up new hopping channels. For $\omega/\sqrt{2\pi N} < \lambda < \lambda_c = \sqrt{\frac{\omega W}{2\sqrt{2N}}}$, the coupling to the bath assists the particle in hopping, by allowing it to 'borrow' the energy required to get on shell. For $\lambda > \lambda_c = \sqrt{\frac{\omega W}{2\sqrt{2N}}}$, the coupling to the bath enhances the stability of localization, because of a 'quantum Zeno effect.' It is worth highlighting the agreement between the qualitative argument and the results (4.22).

The more precise analytical calculation of the stability of the locator expansion starts by considering the wavefunction amplitude $A_{j,\beta}$ for the particle to be in the site j of the lattice and with the bath being in the state $|\beta\rangle$. For a state localized in the vicinity of a site i, the amplitude to find a particle at a site j at distance n from i is exponentially small in the distance, implying that, for some $z < 1$,

$$P\left(\max_{\beta} |A_{j,\beta}| < z^n\right) \to 1 \tag{4.23}$$

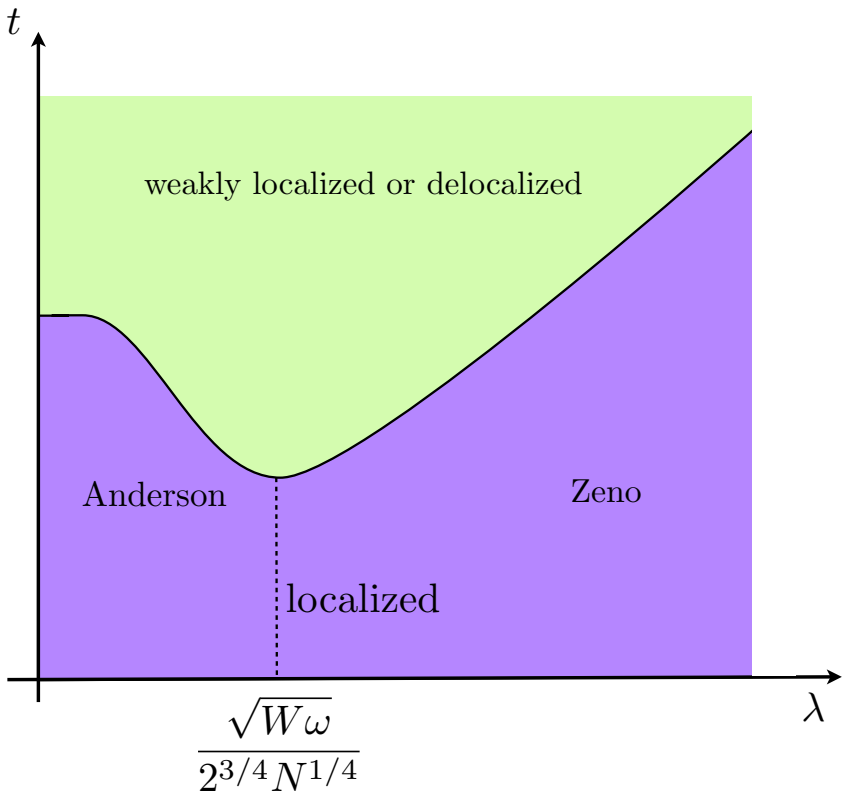

Figure 4.2: Schematic phase diagram which indicates the boundary of stability of the locator expansion. On the small t side of the phase boundary, the system is strongly localized. Within the strong localization regime there is a crossover from Anderson localization at small λ to quantum Zeno localization at large λ. The locator expansion is maximally unstable around $\lambda_c = \sqrt{\frac{\omega W}{2\sqrt{2N}}}$. The large t side of the phase boundary is the regime of crossover to weak localization (in one or two dimensions) or transition to a delocalized phase (in three dimensions).

as $n \to \infty$, where P is the probability measure over the realizations of the disorder. The minimum z for which this condition is still true gives the localization length as $z = e^{-a/\xi}$ where a is the lattice constant.

The result of the calculation is shown in Fig. 4.3. There, in the bottom panel, the localization length extracted in the forward approximation is plotted as a function of the coupling λ, having kept the other parameters, namely W/t, fixed, for a one dimensional system; this corresponds to taking an horizontal slice in the phase diagram 4.2. The increase in the localization length signals the crossover to weak localization (it would diverge in the case of a dimensionality equal or higher than 3, indicating true delocalization). This information can be used to construct the phase diagram in the top panel, which ideally corresponds to the schematic plot of Fig. 4.2; in the very weak λ regime the Fermi golden rule (4.13), which is used in the forward approximation calculation, is no longer valid. This results in the absence of the weak λ plateau, which can instead be recovered by directly performing a perturbation theory in λ, as in Sec. 4.3.1.

4.4.1 Overview of the numerical method

In order to support this analytic result in the forward approximation, we can estimate the localization properties of this system in a way unrelated to this approximation. The most careful numerical check that can be done makes use of exact diagonalization of the total Hamiltonian, which implies that no approximations are made. However, in general, when using exact diagonalization, one should be careful in taking into account the finite size effects and if possible extrapolate in the infinite size limit the quantity that one is computing; this is because the system sizes usually accessible through exact diagonalization are very small.

One is able to easily build H_0, the "system" part of the Hamiltonian, in the position basis composed of the eigenstates of the number operator $n = c^\dagger c$ for a particle in any one of the lattice sites[3]. The on-site energies are diagonal in this basis, while the hopping term of the Hamiltonian is nonzero where it corresponds to connected lattice sites, i.e. is proportional to the adjacency matrix of the lattice. The bath Hamiltonian H_{bath} and the coupling H_{couple} are given as (properly arranged) random matrices; therefore the full

[3]For the one-dimensional system the adjacency matrix is simply:

$$\{A\}_{ij}, \quad A_{ij} = \begin{cases} 1 & j = i \pm 1 \\ 0 & \text{else.} \end{cases}$$

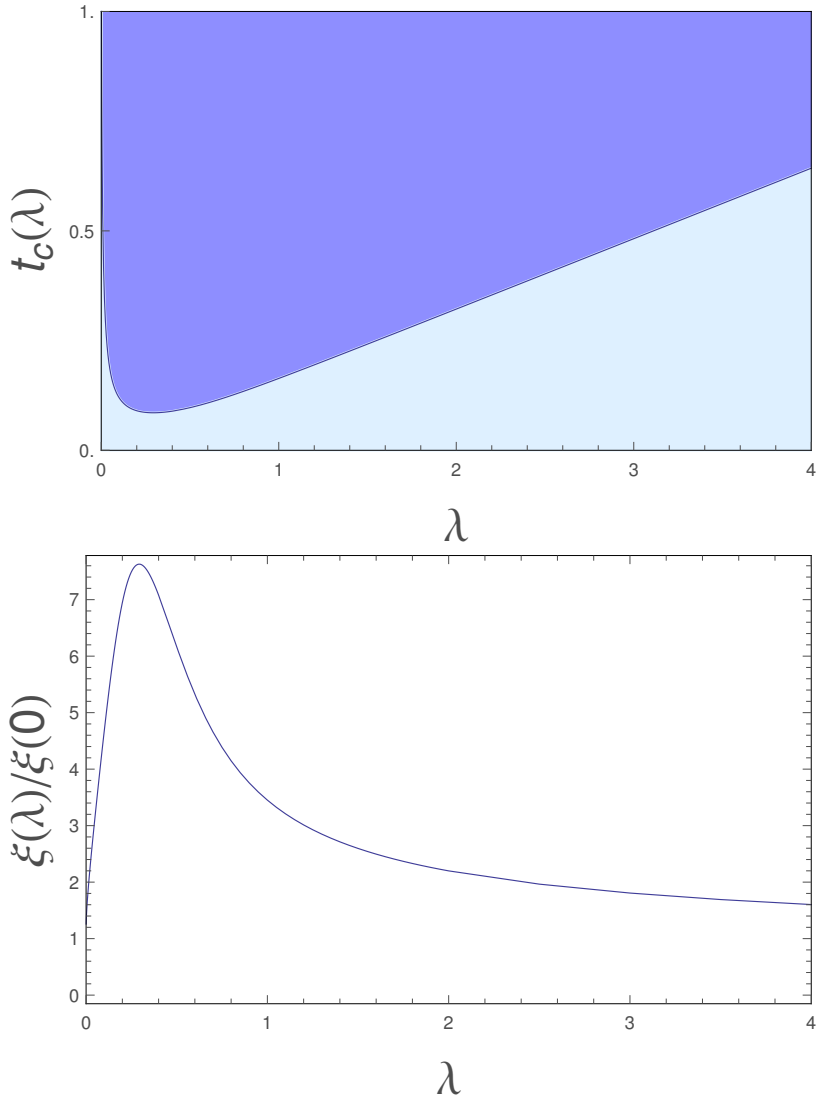

Figure 4.3: Results of analytic calculations in the forward approximation for fixed $W = 3$, $N = 300$, $\omega = 4$. With these parameters $\lambda_c = 0.5$. *Top.* $t - \lambda$ phase diagram; the dark region is the weakly localized/delocalized region, the light region is localized. Note that very small λ are excluded: the calculation assumes that states in the bath are hybridized according to Eq. (4.14), and is thus not applicable at $\lambda < \delta/\sqrt{2\pi}$. *Bottom.* Localization length as a function of λ, along a horizontal slice through the top diagram that always stays on the 'strongly localized' side of the phase boundary. The maximum in the localization length is close to $\lambda \approx 0.3$ and it indicates that the system is least localized at this intermediate value of λ; this is reasonably similar to $\lambda_c = 0.5$ obtained by the simple argument detailed in Sec. 4.3.

Hamiltonian (4.8) can be easily constructed through Kronecker products. Note that the Hamiltonian matrix is fairly sparse. We are interested in the states in the middle of the band; in the presence of mobility edges, these are the last states to localize and are therefore the ones that characterize the system at infinite temperature.

The best algorithmic way to compute the eigenstates of this given matrix which we are interest in is to make use of the Lanczos iterative method (for Hermitian matrices); with this technique, the eigenvalues and eigenvectors are approximated iteratively by constructing a sequence of powers of the matrix, i.e. taking a starting random vector b and building the sequence

$$[b,\, Hb,\, H^2b,\, \ldots,\, H^nb], \tag{4.24}$$

and then forming a orthogonal basis from them, known as Krylov basis. The eigenvector corresponding to the largest eigenvalue will be approximated by H^nb and, after orthogonalization, a subset of the vectors in the Krylov subspace will approximate the eigenvectors corresponding to the successive largest eigenvalues, with a very fast convergence for the more extreme eigenvalues.

The states at the center of the spectrum are the numerically harder to compute; one can however apply spectral transformations to the Hamiltonian in order to make the desired window of energies the dominant eigenvalues of the transformed Hamiltonian. Indeed, let us consider an eigenvalue λ_k of the matrix H; then one can consider the matrix

$$\frac{1}{H-\alpha\mathbb{1}}, \tag{4.25}$$

which has $(\lambda_k-\alpha)^{-1}$ as the dominant eigenvalue. However, inverting the matrix is costly and not convenient; we can instead proceed iteratively by selecting an initial guess vector x_0 (of unit norm), solving the linear system

$$(H-\alpha\mathbb{1})y_n = x_n, \tag{4.26}$$

and normalizing $x_{n+1} = \frac{y_n}{||y_n||}$ for the next iteration. x_∞ will converge to the dominant eigenvector, while

$$\frac{1}{c_\infty}+\alpha, \text{ where } c_n = y_n^T x_n, \tag{4.27}$$

will converge to its eigenvalue.

4.4.2 Exact diagonalization check of the forward approximation result

We now proceed to check the forward approximation analytic result with the numerical, exact one obtained through the diagonalization of the system Hamiltonian. Indeed, we can compute quantities which are proportional to the localization length; thus, we can discriminate between a strongly localized phase and a weakly localized or delocalized phase. Note that, since in this work only one dimensional systems are numerically accessible, the aim is to spot the crossover to weak localization, which is an arbitrary task in the absence of information about the convergence of the locator expansion. Thus, instead of trying to numerically reproduce the phase diagram in Fig. 4.2 or in the top panel of Fig. 4.3, we will be satisfied by detecting in the localization length a behavior which matches the analytic result of the bottom panel of Fig. 4.3 (and, specifically, the position of its peak).

One way to numerically estimate the localization properties of the system of Eq. (4.8) is by looking at the probability distribution of the position of the particle in the eigenstate $|\Psi\rangle$ of the coupled particle and bath:

$$p_i = \sum_{\alpha_i=1}^{N} |\langle i, \alpha_i|\Psi\rangle|^2. \tag{4.28}$$

One can then define the inverse participation ratios of order q of p as:

$$I_q = \left(\sum_i p_i^q\right)^{-1}. \tag{4.29}$$

For example the localization length can be estimated from the first non trivial I_q, i.e.

$$I_2 \sim \xi^d. \tag{4.30}$$

Additional information is contained in the entropy of the entanglement of the system with the bath, which can be extracted from the reduced density matrix $\rho = \mathrm{Tr}_{\mathrm{bath}}|\Psi\rangle\langle\Psi|$, where $|\Psi\rangle$ is an exact eigenstate of the full system. The entanglement entropy is

$$S = -\mathrm{Tr}(\rho \log \rho). \tag{4.31}$$

For the present problem the entanglement entropy and the inverse participation ratios are correlated, since the less the particle is localized, the more it is entangled with the bath.

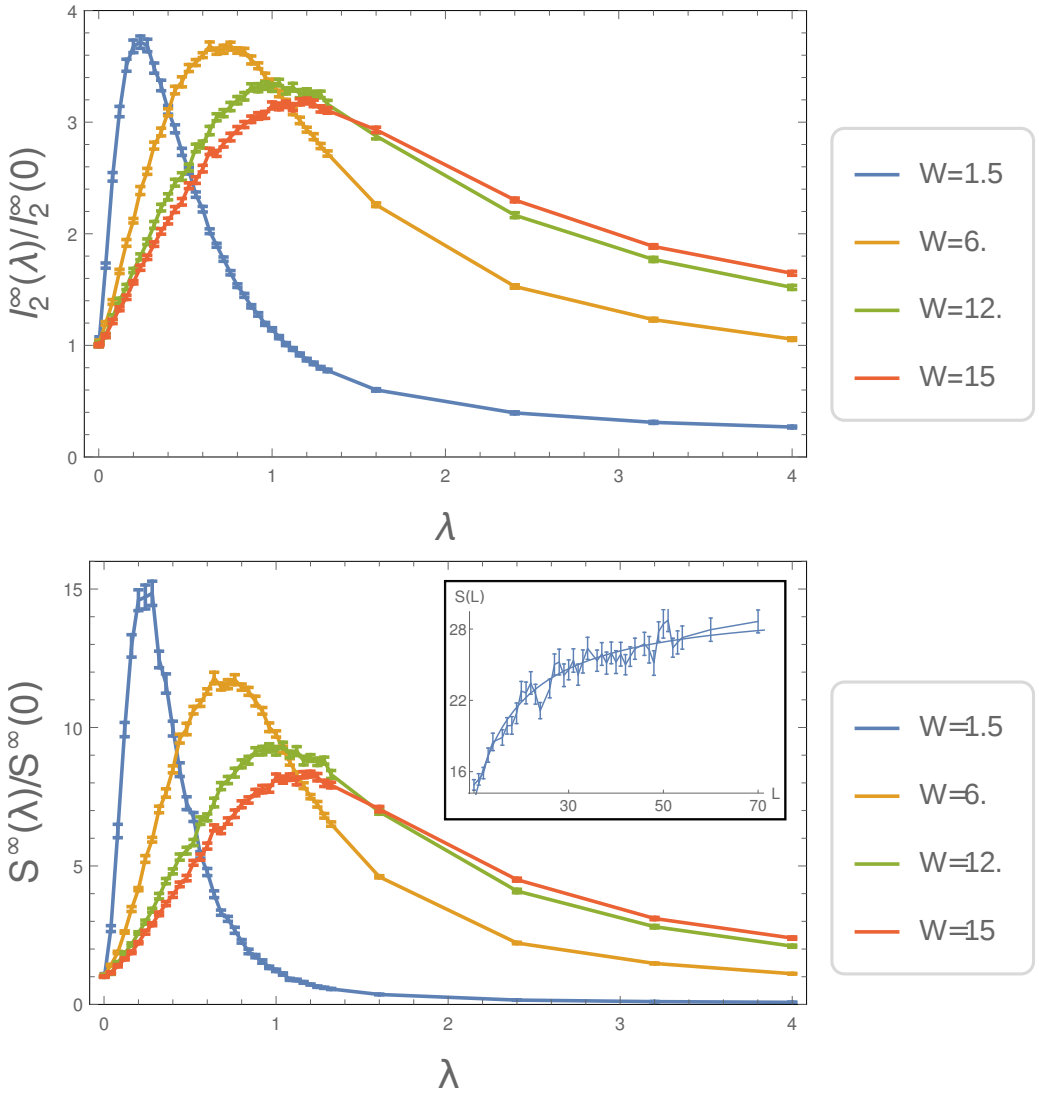

Figure 4.4: Numerical results relative to a one dimensional system coupled to a small bath. The plots are for parameters $t = 1$, $\omega = 4$, $N = 300$, and varying W, spanning the phase diagram in Fig. 4.2. The entanglement entropy and the participation ratios have a pronounced maximum close to the (same) hybridization threshold λ_c, with a sharper peak when going through the weak localization regime. *Inset.* Example of the finite size scaling of S^L for a given value of $\lambda = 0.8$ and $W = 6$. To extrapolate the infinite size S^∞ Eq. (4.33) is used, with L ranging from 10 through 70.

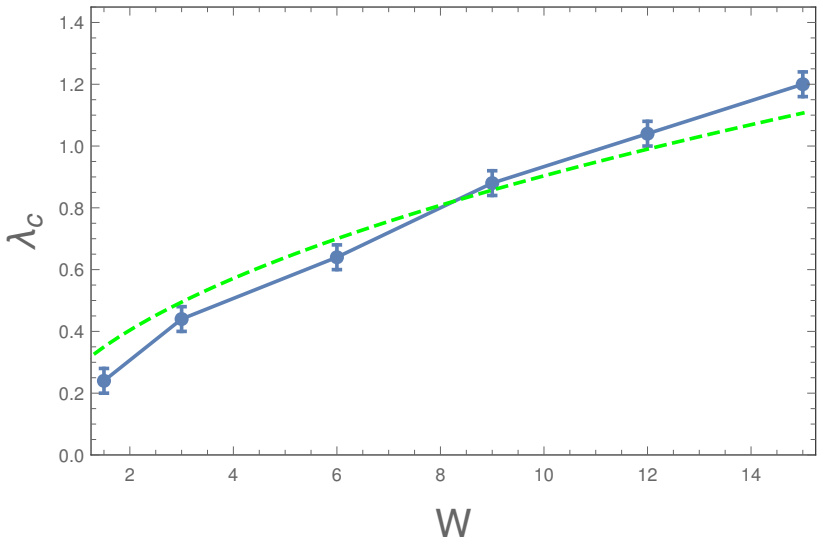

Figure 4.5: Value of λ_c for $t = 1$ and the different disorders W. The numerical data are plotted in blue, with the corresponding errors coming from the resolution in λ at which the plots in Fig. 4.4 are computed. The analytic estimate of Eq. (4.15) is plotted in dashed green . The exact diagonalization data agree well with the analytic prediction.

The results of calculating I_2 and S from the exact wavefunction obtained by diagonalizing the Hamiltonian (4.8) are non-monotonic as the coupling with the bath λ increases, keeping the disorder and hopping strengths W and t constant. This implies that the localization length follows the same behavior. Let us take for example a one-dimensional system, which is well accessible by numerical methods; the results in Fig. 4.4 are obtained performing exact diagonalization for about 50 states in the center of the band for the parameters $t = 1$, $\omega = 4$, $N = 300$, and varying W. The values of W are chosen so that the phase diagram of Fig. 4.2 is spanned, slicing through the 'weak localization' region for $W \lesssim \frac{2\sqrt{2N}}{\omega} \approx 12$, whereas for $W > 12$ we stay always in the strong localization regime. The figure shows that, as a function of λ, the entanglement entropy and the participation ratios have a pronounced maximum close to the (same) hybridization threshold λ_c, the peak being sharper if we go through the weak localization regime. In particular for the entanglement entropy, at weak λ, the particle becomes more entangled with the bath as λ is increased, but for larger λ the entanglement entropy becomes a decreasing function of the coupling, and in the extreme $\lambda \to \infty$ limit one recovers an unentangled product state.

The values that are computed through exact diagonalization in systems

of finite size (with L ranging from 10 to 70, with 50 disorder realizations each) are extrapolated to infinite size by using a fit of the form

$$I_q(L) = I_q(\infty) + a_I/L \tag{4.32}$$

for the inverse participation ratio and

$$S(L) = S(\infty) + a_S/L \tag{4.33}$$

for the entanglement entropy. They turn out to fit very well the numerical data (see the inset of Fig. 4.4 for an example of the finite-size extrapolation).

The value of λ_c, i.e. the value of the bath coupling which maximizes both the participation ratio and the entanglement entropy, can be extracted from the numerical result and compared with our analytic estimate of Eq. (4.15), obtaining a good agreement (see Fig. 4.5, in which the value λ_c is plotted as a function of the disorder strength W).

Strong localization is least stable when $\lambda \approx \lambda_c$, and becomes more stable both for weak λ (the Anderson localization limit), and for strong λ (the quantum Zeno limit). The minimum value of t that can cause the breakdown of the locator expansion is $t_c(\lambda_c) = \sqrt{\frac{\omega W}{2\sqrt{2N}}}$. Thus, for any t, the localization length should peak at this value of λ. We can conclude that this is observed both in the numerics (Fig. 4.4) and in the forward approximation analytic calculations (Fig. 4.3).

4.5 Conclusions on small bath

In this chapter we examined the behavior of a single particle localized system coupled to a finite sized bath that is protected against localization. It is a relevant result, especially for experimental works, that the localization of the particle is stable in presence of this kind of coupling; moreover, the stability is modified in a non-monotonic way, highlighting the effects of Anderson localization and of the quantum Zeno effect.

Chapter 5

Adding interactions: Many Body Localization

5.1 Introduction

In 2006 the topic of localization in disordered systems was revived by the influx of the new ideas by Basko, Aleiner and Altshuler [2], who introduced a new treatment of interactions and showed that a 'many-body localized' phase is possible. This has solved a crucial question that resisted an answer for almost fifty years, that is the stability of localization in presence of interactions, and has since sparked a renewed interest in the topic, making many-body localization the paradigmatic mechanism for ergodicity breaking in interacting systems.

In this chapter a contribution to this topic will be provided by showing that applying the forward approximation framework presented in Chapter 3 to the interacting many-body case is possible and results in a powerful tool. Moreover, we will inspect the ergodicity properties using a properly defined inverse participation ratio and extract a phase diagram for the many-body localization transition.

5.2 Many body localization and ergodicity

In Sec. 1.5 we discussed some known properties of the many-body localized and delocalized states. Indeed, a delocalized state can be thought as a state that extends over the whole many-body configurations space, while a localized state is very similar to a Slater determinant of single particle states. Note that the many-body configurations space in the infinite size limit is hierarchical and highly branching and is thus similar to a Bethe lattice, which

can be used as its approximation [49]. A property of the Bethe lattice is that two given sites are connected only by one path and, as a consequence, resonant sites may be much sparser than ordinary lattices of given dimension d, raising questions about ergodicity in many-body systems. It is a known result that at criticality in the wavefunctions of the single particle Anderson model on a finite dimensional lattice there are indeed such non-ergodic states [40, 97–99]. Moreover, it has been shown [100] that in the Bethe lattice, even away from criticality, the extended states are indeed multifractal; thus they are ergodic on a subset of the full lattice which has a (spectrum of) fractal dimension.

A way to inspect the ergodicity of the wavefunctions is by means of the participation ratio (1.33), or, equivalently, through the moments of the distribution of the wavefunction amplitudes (more specifically, the first non-trivial one, i.e. the second moment). Intuitively, the participation ratio measures the *participation* of each basis element to the wavefunction support. Following the reasoning of Sec. 1.5 one can understand how the participation ratio can be used to determine whether a state is many-body localized. Additionally, information on the (multi-) fractal behavior is also encoded in its scaling with system size.

In this section some results coming from the exact diagonalization of many-body models with two kinds of disorders are reported; from the analysis of the wavefunction participation ratio and the eigenvalue statistics we can construct a phase diagram and identify the many-body localization transition.

5.2.1 Participation ratio and ergodicity

Let us specifically consider the Hamiltonian (1.27) of fermionic particles in a one dimensional lattice of N sites, i.e.

$$H = -t \sum_{i=0}^{N-1} (c_i^\dagger c_{i+1} + c_{i+1}^\dagger c_i) + \sum_{i=0}^{N} h_i c_i^\dagger c_i - \Delta \sum_{i=0}^{N-1} c_i^\dagger c_{i+1}^\dagger c_i c_{i+1}, \tag{5.1}$$

where the $c_i^\dagger, c_j$ satisfy $\{c_i^\dagger, c_j\} = \delta_{ij}$, with periodic boundary conditions. The on-site disorder h_i can be either truly random and uniformly distributed in $[-W, W]$ (interacting Anderson model) or a quasidisorder, i.e. $h_i = W\cos(2\pi\phi^{-1}i + \delta)$, where $\phi = (1+\sqrt{5})/2$ and δ is a phase chosen randomly in $[0, 2\pi)$ (interacting Aubry–André model). Let us also consider the usual configurations basis $\{|\vec{n}\rangle\}$ in the half filling sector, so that the Fock space has dimension $\mathcal{N} = \binom{N}{N/2}$. Finally, let us denote the normalized many-

body eigenfunction coefficients in the configurations basis with $\Psi_n = \langle \vec{n}|E\rangle$, and define $x = \mathcal{N}\Psi_n^2$.

Let us consider the moments of the wavefunction distribution

$$I_q = \langle \sum_{\vec{n}} |\langle \vec{n}|E\rangle|^{2q} \rangle = \mathcal{N}^{1-q}\langle x^q \rangle; \tag{5.2}$$

note that I_2 is clearly related to the inverse participation ratio following the definition (1.33). With a reasoning analogous to the one used for the normalized participation ratio, one can see that, for infinite temperature, ergodicity of the wavefunction means that $I_q \propto \mathcal{N}^{1-q}$, which implies that the mean $\langle x^q \rangle$ is well behaved and therefore the distribution $P(x)$ has a well behaved thermodynamic limit. A subleading scaling with the size of the configurations basis instead signals the breaking of ergodicity, including localization (which can be detected upon suitably normalizing).

We can define the fractal dimension by means of the moments I_q. Taking into account that the embedding space has volume $\mathcal{N}$, the fractal dimension is the exponent τ of

$$I_q = \mathcal{N}^{-\tau(q)}. \tag{5.3}$$

In principle, one can have a continuum of fractal dimensions, which results in a multifractal.

5.2.2 Participation ratio for localized and delocalized wavefunctions

In order to gain insight about the transition between ergodic and non-ergodic states in the interacting many-body system, let us now proceed to extract the wavefunction participation ratio of eigenstates in the middle of the spectrum and analyze their behavior with respect to the system size.

Let us consider the model (5.1) with the random Anderson and the Aubry–André quasidisordered on-site potentials. One can obtain eigenfunctions corresponding to the center of the energy spectrum by exactly diagonalizing the model Hamiltonian; in the following, 50 states in the center of the spectrum are considered and are averaged over. The parameters for both models are set to $t = 1/2$ and Δ ranging from 1 to 4, with the disorder strengths W for the random and quasirandom potentials both ranging from 1 to 6. Note that for this choice of parameters the fermionic system with random potential can be mapped to an XXZ spin chain, whose transition point W_c for $\Delta = 1$ is estimated in the literature as in between 3 and 4

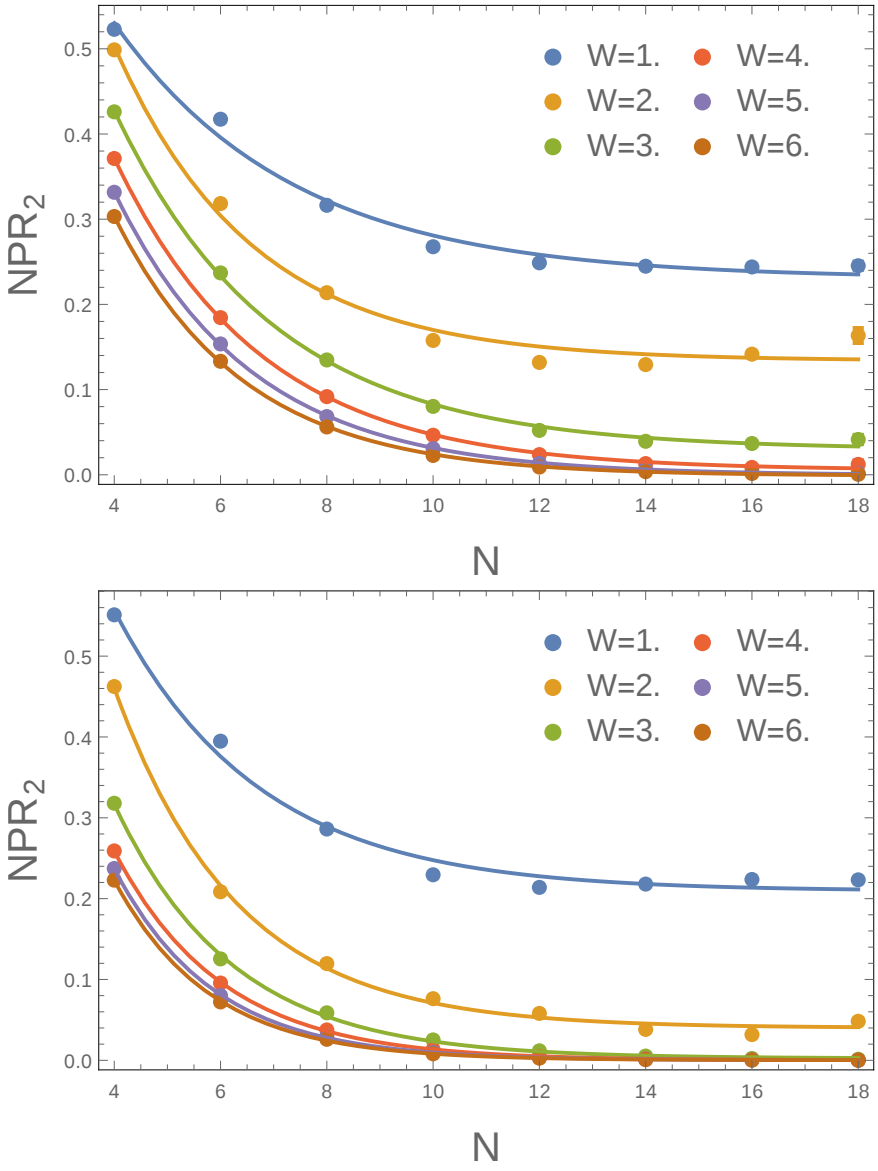

Figure 5.1: Scaling of the wavefunction normalized participation ratio NPR_2 with the system size for the interacting model (5.1) with the random Anderson (top panel) and the Aubry–André quasidisordered (bottom panel) on-site potentials, with parameters $t = 1/2$, $\Delta = 1$ and varying disorder strength. NPR_2 is of $O(1)$ in the ergodic phase and decays exponentially to zero in the localized phase. Each value is computed as an average over 50 states in the middle of the energy spectrum and at least 10^4 disorder realizations (except for $N = 18$, for which at least 100 disorder realizations are considered). The continuous lines are the exponential fits of Eq. (5.4).

($W_c = 3.72(6)$ in Ref. [21]); for the quasirandom potential the transition point for the noninteracting system is instead exactly known to be $W_c = 2$.

The normalized participation ratio $\mathrm{NPR}_2 \equiv \langle x^2 \rangle^{-1}$ (recall its definition in Eq. (1.33)) is shown in Fig. 5.1 as a function of the system size for both models; for weak disorder NPR_2 is of $O(1)$, as expected for extended states. Both in the disordered and in the quasidisordered model the participation ratio decays exponentially to zero (in the localized phase) or to a finite asyptotic value (in the delocalized phase), corresponding to the infinite size NPR_2.

The ergodicity detected through the scaling of the participation ratio can be used to construct a phase diagram and to find the transition between the localized, nonergodic phase and the ergodic one. In Fig. 5.2 a phase diagram for varying interaction and disorder strength is shown for the random disorder model. A finite size scaling has been performed in order to obtain the reported values: an exponential form

$$\mathrm{NPR}_2(N) = c\, \mathrm{e}^{aN} + \mathrm{NPR}_2(\infty) \tag{5.4}$$

is a good fit (see the continuous lines in Fig. 5.1), which allows to extrapolate the infinite size value of the participation ratio $\mathrm{NPR}_2(\infty)$. This result can be compared with the one of Ref. [101], in which a phase diagram is constructed for a system of $N = 12$ spins using a quantity related to the spin autocorrelator. The effect of the interaction is non-monotonic. At low interactions, delocalization is favored, that is, the interaction between the particles induces inelastic hopping; this can be seen also as the consequence of an effective reduction of the disorder caused by the increasing correlations in the denominators of the locators. For big values of the interaction localization is again favored because of a 'glue effect' and the dynamics is dominated at most by collective motions. Indeed, the localization in the area at low disorder and high interaction is due to the configurational disorder of the initial state; this is a genuine many-body effect which exists in this class of systems in addition to Anderson localization [102].

Since the participation ratio goes to zero continuously, the Anderson localization transition point can be more easily identified through the eigenvalue statistics; the r parameter introduced in Eq. (1.14) is especially useful in allowing to discriminate between the Poissonian ($r \approx 0.39$) and the Wigner Dyson ($r \approx 0.53$) statistics of the gaps in the localized and delocalized regimes respectively. In Fig. 5.2 the transition values obtained from the finite size scaling of the r parameter are superimposed to the color code of the participation ratio. Indeed, the value of the r parameter approaches the Poissonian or the Wigner Dyson value as the system size increases; thus, the crossover of r as a function of the disorder becomes increasingly sharp and

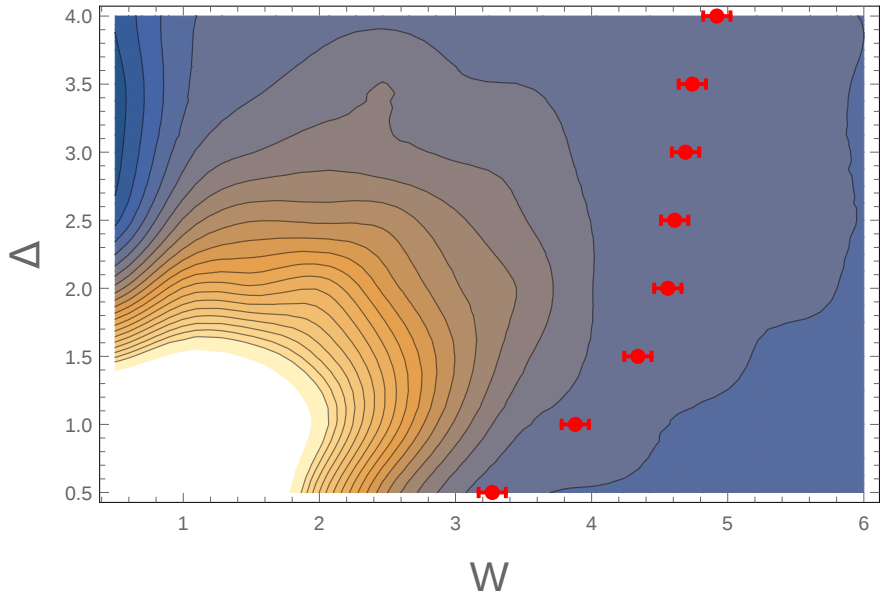

Figure 5.2: Contour plot of the participation ratio NPR_2; this is used to construct a phase diagram highlighting the ergodic and localized phases for the interacting model (5.1) with the random Anderson on-site potentials, with $t = 1/2$ and varying interaction and disorder strengths. The values used in the diagram come from the infinite system size scaling of participation ratios like the ones plotted in Fig. 5.1. Lighter colours correspond to higher values of the NPR_2. The red points are the Anderson transition points obtained through a finite size scaling analysis of the r parameter.

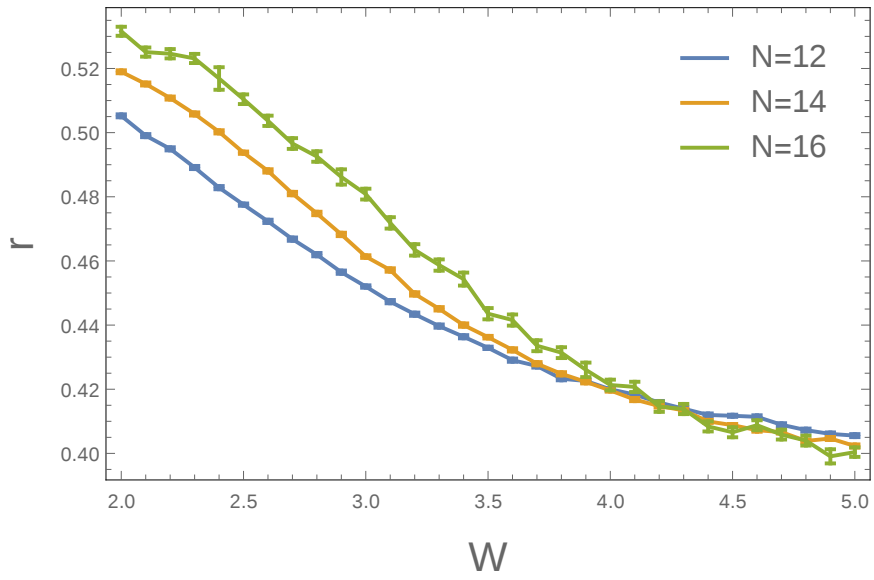

Figure 5.3: r parameter for the interacting Anderson model as a function of disorder for fixed interaction $\Delta = 1$ and for different finite system sizes. As the system size increases, r approaches the Poisson or the Wigner Dyson value on the two sides of the transition; the point where the curves cross corresponds to the transition value W_c. Each data point has been computed as the average over 50 states in the middle of the spectrum and over at least 10^4 disorder realizations, except for $L = 16$ for which at least 10^3 realizations have been used.

the crossing of the curves corresponding to different finite system sizes signals the transition. An example of this finite size scaling is given in Fig. 5.3 for $\Delta = 1$.

5.3 The forward approximation in Many Body systems

In Chapter 3 we have focused on the single particle Anderson model, for which a clear formulation of the perturbative series for the wavefunction is the locator expansion. An extension of the forward approximation analysis to many-body systems is indeed possible, bearing the same advantages as in the single partcle case.

The starting point is the analysis done by Basko, Aleiner and Altshuler [2], who took into account perturbatively the interactions at finite temperature and particle density for the imaginary part of the propagator of an excitation on top of an eigenstate. This perturbative series almost surely converges for weak interactions; along the lines of the reasoning for the single particle, this implies the localization of the excitation and the absence of transport, as mentioned in Sec. 5.1.

The many-body localization problem however can be also interpreted alternatively as a single particle tight binding problem in the space of many-body configurations [49], with the interactions playing the role of an effective hopping. Indeed, in this case localization is intended as happening on the occupation number basis vectors of the configurations space. When performing this mapping, we must take into account a few non-trivial differences with respect to the single particle case. First, the on-site energies in the resulting effective lattice are no longer independent and identically distributed random variables, but their values are strongly correlated and result from both how the on-site disorders interplay with a given basis vector and from the particle interactions on that same state. Secondly, the effective lattice is generated by the non-diagonal part of the Hamiltonian, i.e. the spin flipping (or hopping, in case of particles) part. Therefore the connectivity of a configuration in the many-body problem depends on the system size, as it scales as a power of it, and thus it diverges in the thermodynamic limit, making it impossible to define a limiting graph. Moreover, different sites have different connectivity. Finally, taking two many-body configurations in a reasonably isotropic region, as their distance grows when the system size is increased, the number of paths connecting them grows factorially, and many cancellations occur among them; since the distance between two such configurations

is of the order of the system size, the number of paths grows factorially in the system size; in contrast, for the single particle problem, one would have only an exponential growth.

Summarizing, the mapping of an N interacting spin problem to a single particle problem results into a complicated correlated disorder problem on a section of an N-dimensional hypercube. Taking advantage of the study conducted so far of the forward approximation in hypercubes for single particle systems, let us now approach an interacting XXZ spin problem, as many analogous results can be obtained also in this kind of systems.

5.3.1 The Heisenberg model with random fields

Let us consider an XXZ spin-1/2 chain in random magnetic field,

$$H(t) = -\sum_{i=1}^{L} h_i s_i^z - \Delta \sum_{i=1}^{L} s_i^z s_{i+1}^z - t \sum_{i=1}^{L} (s_i^x s_{i+1}^x + s_i^y s_{i+1}^y), \tag{5.5}$$

where periodic boundary conditions are assumed ($s_1^\alpha = s_{L+1}^\alpha$), and the random fields h_i are uniformly distributed in $[-h, h]$. This spin Hamiltonian (5.5) has been studied in a large number of works [15, 18, 19, 50, 100, 103–106], in which numerical evidence of the existence of a localization/delocalization transition is provided, mainly based on exact diagonalization results. The critical disorder is estimated [21] to be $h_c \simeq 3.72(6)$ for states in the middle of the energy band and parameters $t = 1$ and $\Delta = 1$.

As mentioned in Sec. 5.3, the many-body problem can be seen as a single particle hopping problem in the configuration space, which is composed of the 2^L product states in the basis of s_i^z, which span the full Hilbert space and diagonalize $H(0)$. We denote these basis states with $|n\rangle$, and refer to them as the "configurations basis". The mapping to an hopping problem is obtained by interpreting each state $|n\rangle$ as a vertex n of a graph, with associated random energy E_n defined by $H(0)|n\rangle = E_n|n\rangle$. The third term in (5.5) provides the hopping between different sites, thus defining the topology of the graph, as shown in Fig. 5.4 for a small system of six spins. Note that due to spin conservation, the full configurations space, and consequently the graph, is partitioned into disjoint sectors corresponding to different total spin; we restrict to the sector of total spin equal to zero, corresponding to a connected graph with $\binom{L}{L/2}$ vertices.

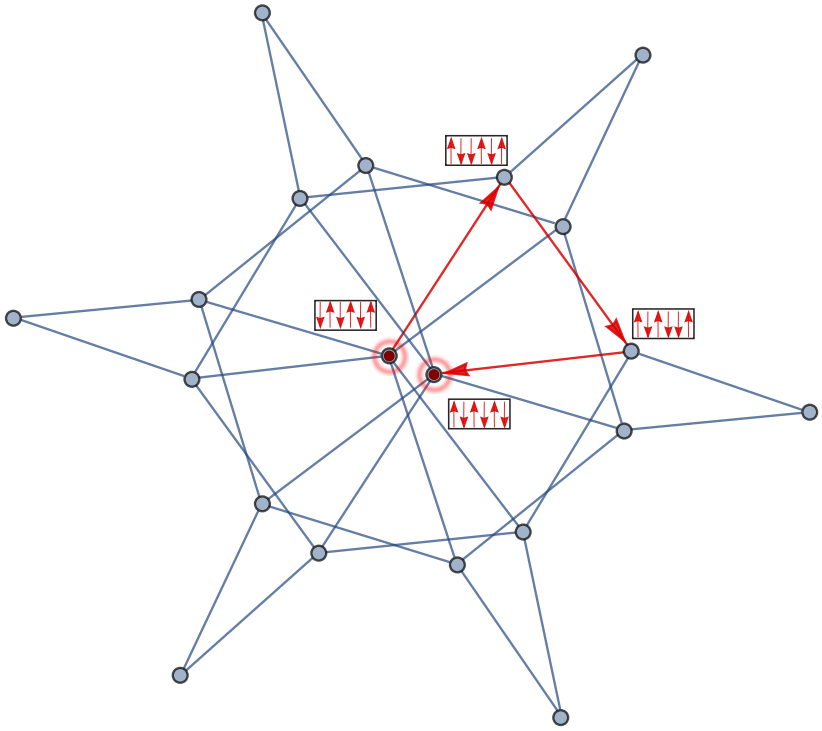

Figure 5.4: Lattice interpretation of the many-body Hamiltonian (5.5) for $L = 6$ spins. Each site represents a spin configuration and is associated to a product state in the basis of s_i^z; only sites corresponding to states with zero total spin are represented. Starting from the Neel state $|\downarrow\uparrow\ldots\rangle$, one of the $(L/2)!$ paths connecting it to the fully flippled Neel state $|\uparrow\downarrow\ldots\rangle$ is highlighted in red, along with the visited configurations. The path has length $L/2 = 3$.

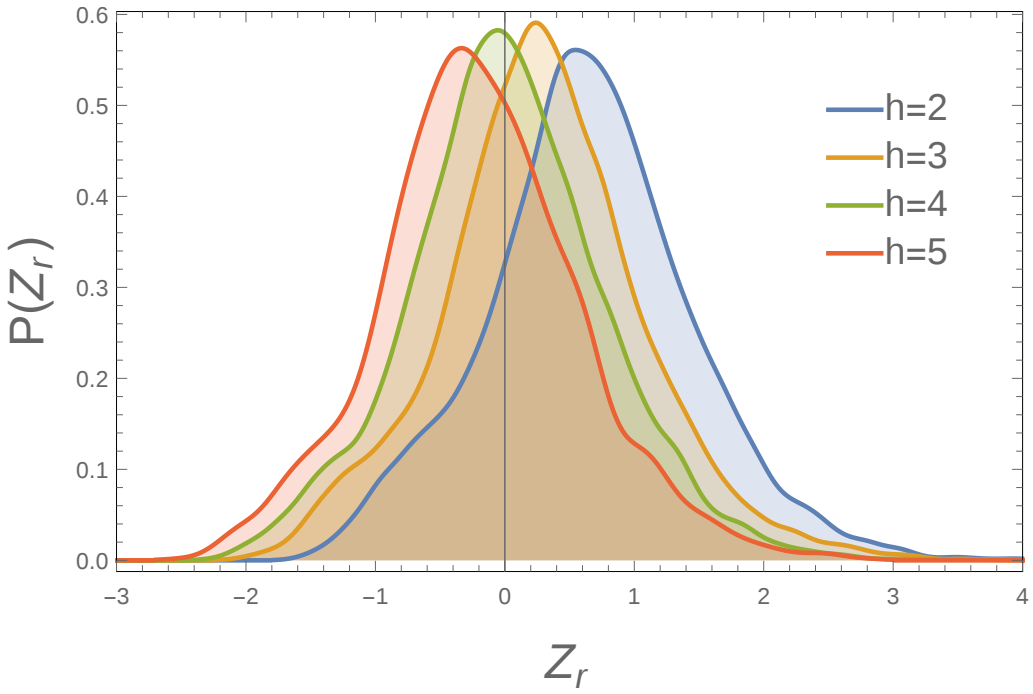

Figure 5.5: Probability density of the random variable $Z_r(h)$ defined in Eq. (5.7), for a spin chain of length $L = 20$ and different values of disorder h. Each curve is obtained with $3 \cdot 10^3$ realizations.

5.3.2 The forward approximation in the Heisenberg model

The effective hopping problem can be analyzed using the procedure set up for the single particle case, this time on the lattice generated by the many-body Hamiltonian such as the one in Fig. 5.4: the amplitude Ψ_α of an eigenstate of the effective single particle problem is given in the lowest order forward approximation by

$$\Psi_\alpha(n_2) = \sum_{p \in \text{spaths}(n_1,n_2)} \prod_{n \in p} \frac{t}{E_{n_1} - E_n}, \tag{5.6}$$

where it is assumed that the eigenstate satisfies $\Psi_\alpha(n) \to \delta_{n,n_1}$ for $t \to 0$. A sample path between two states in the "bulk" of the lattice is highlighted in red in the figure.

The results of Eq. (5.6) are the coefficients of the eigenstates of (5.5) in the configurations basis at the lowest order in the coupling t. The exponential decay of the coefficients implies localization in the configurations space;

this means that the many-body eigenstates are a superposition of few configuration states which are all at a short distance from the initial configuration. The two main consequences of this structure of the wavefunction is that they have significantly less entanglement than ergodic states [50, 100, 107] and that, using Kubo's formula for linear response [51], one can prove that they cannot support transport on macroscopic distances.

Similarly to the Anderson case, we fix an initial configuration of spins, taking care to select it in the bulk of the effective lattice, and we look at the amplitude in perturbation theory corresponding to the configuration in which all the spins have been flipped, which is the most distant configuration. In particular, we fix the localization center to be the site correspondent to the Neel state $|n_1\rangle = |\uparrow\downarrow \dots\rangle$, and consider the wavefunction amplitude on the site corresponding to the fully flipped Neel state $|n_2\rangle = |\downarrow\uparrow \dots\rangle$. These two sites, n_1 and n_2, are connected by $2(L/2)!$ paths on the graph, of length $r = L/2$ each.

By means of the transfer matrix we compute the rescaled amplitude

$$Z_r(h) \equiv \frac{\log |\Psi_r|^2}{2r} \tag{5.7}$$

for different disorder strength h, with Ψ_r given by (5.6). We consider spin chains of size $6 \div 20$ with hopping and interaction constants respectively $t = 1$ and $\Delta = 1$, and $h = 1 \div 6$. As it was mentioned in Sec. 5.3, recall that, even though the general framework is the same as in the Anderson problem, the transfer matrix calculation is by no means identical; indeed, in the many-body case the energies associated to the different graph vertices are a linear combination of the independent random variables, and are therefore correlated. Moreover, the number of paths connecting two sites proliferates with the size of the chain L, with a scaling that is faster than exponential. These paths present correlations that are much stronger with respect to the Anderson problem; the consequences of this will be discussed in more detail in Sec. 3.4.2.

As for the Anderson model, the probability density of $Z_r(h)$ can be plotted, revealing a peaked distribution; in Fig. 5.5 various curves for a spin chain of length $L = 20$ and different values of h are shown. Additionally, Fig. 5.6 shows the behavior of the probability of resonances as function of the distance between the Neel states. As expected, the r-dependence of the probability of resonances changes with the disorder: the probability decays to zero at large h, and increases towards one for the smaller h. To detect the transition point, we again make use of the position of the extrapolated peak of the probability distribution function of Z_r or, equivalently, the extrapolated value $\langle Z_\infty(h)\rangle$. Since in the many-body case it is not possible

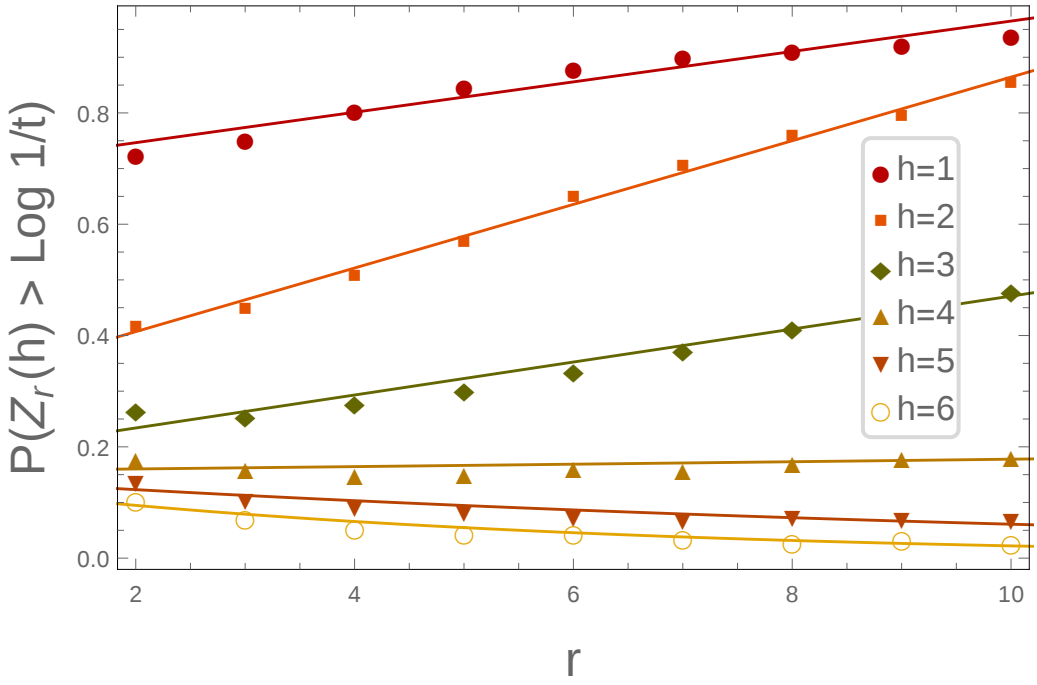

Figure 5.6: Probability of resonances $P(Z_r(h) > -\log t)$ as a function of the distance r between the two Neel states n_1 and n_2, for $t = 1$. Asymptotically the probability reaches zero exponentially in the localized phase and one in the delocalized phase. Here we show the result of the forward approximation for values of the disorder strength h which span the delocalized, localized and critical regimes. We average over 10^4, $5 \cdot 10^3$ and $3 \cdot 10^3$ realizations for $r \leq 8$, $r = 9$ and $r = 10$, respectively. Linear and exponential fits in the delocalized and localized regions respectively are plotted as continuous lines.

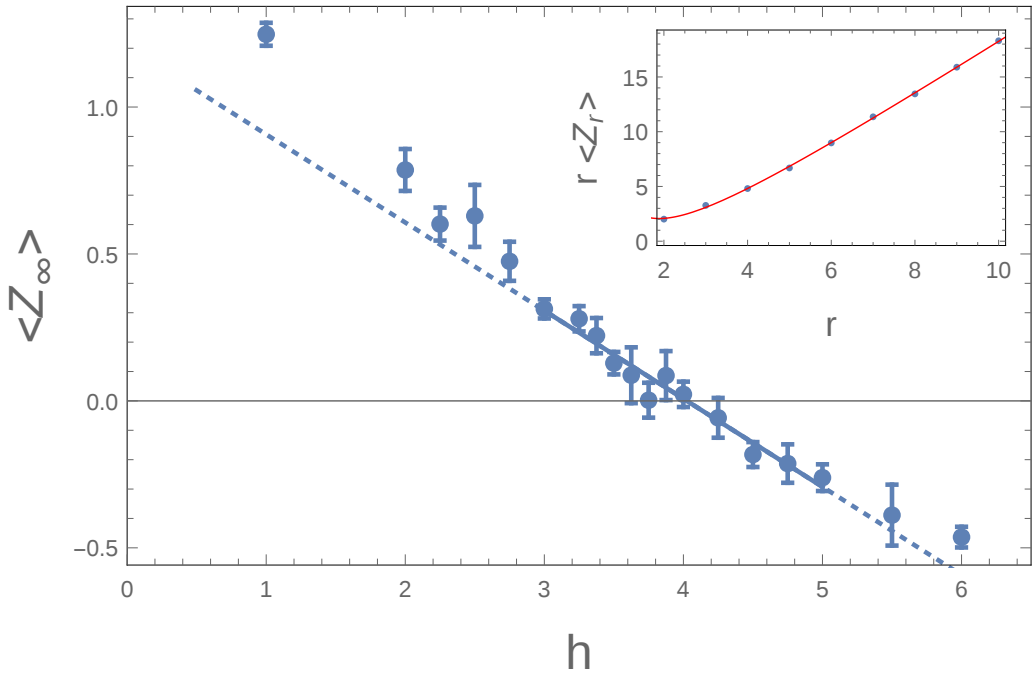

Figure 5.7: Extrapolated value of the mean $\langle Z_\infty \rangle$. The crossing of the x-axis signals the many-body localization/delocalization transition (see Eq. (5.8)), obtaining a transition value $h_c = 4.0 \pm 0.3$. The errors are obtained from the fitting procedure (see Inset). *Inset.* Finite size scaling of $r \langle Z_r \rangle$ with the distance r between the Neel states n_1 and n_2. A linear form with an r^{-1} correction, i.e. Eq. (5.9), is a very good fit. Here we show a fit of $r \langle Z_r(h) \rangle$ with $h = 1$ with parameters (with reference to Eq. (5.9)) $c_1 = -7.2 \pm 0.4$, $\langle Z_\infty(2) \rangle = 1.23 \pm 0.02$ and $c_2 = 8.8 \pm 0.7$. The finite-r values for the mean are obtained over at least 10^4 realizations for $r < 7$ and at least $2 \cdot 10^3$ realizations for $r \geq 7$.

to extract the dependence on the disorder strength h from the extrapolated $\langle Z_\infty(h)\rangle$, the criterion for the transition reads

$$\langle Z_\infty(h_c)\rangle = -\log t. \tag{5.8}$$

From the numerical data obtained in this model, let us then look at the distributions $P(Z_r(h))$. In Fig. 5.7 the values of $\langle Z_\infty(h)\rangle$, extrapolated from the finite size values using the fitting function

$$r\,\langle Z_r(h)\rangle = c_1 + \langle Z_\infty(h)\rangle\, r + c_2\, r^{-1}, \tag{5.9}$$

are plotted as a function of the disorder strength h. Since $t = 1$, the critical point h_c is estimated from the condition $\langle Z_\infty(h_c)\rangle = 0$. The resulting value is $h_c = 4.0 \pm 0.3$, which is, as expected, larger than the result obtained from exact diagonalization.

The probability of resonances in Fig. 5.6 is expected to converge to zero or one at least exponentially in r (for large r); however, the exponential behavior is not clearly detectable in the delocalized phase, due to the few accessible system sizes. For $h < h_c$ one can define and extract a length scale $l(h)$ by taking the inverse of the derivative of the curves in Fig. 5.6, while in the localized phase we can more reasonably fit with an exponential form. The length scale $l(h)$ extracted with this procedure is plotted in Fig. 5.8, together with a power law fit diverging as $\sim |h - h_c|^{-1}$ at the transition. Note the asymmetry of the curve with respect to h_c, which indicates that at fixed $|h - h_c|$ the typical distance to find a resonance in the delocalized phase is larger than the localization length at the corresponding value of disorder in the localized phase. A possible consequence of this phenomenon, which occurs also in the Anderson model (see Fig. 3.9), could be a large "critical region" in the dynamics in the delocalized phase.

As we discuss in Sec. 3.4.2, in the many-body case the sum (5.6) is no longer dominated by a single path; therefore, the algorithm for the best path is not applicable in this context, and the limited system sizes accessible with the transfer matrix do not allow to investigate whether a scaling form exists for the distribution $P(Z_r(h))$ also for (5.7) in the limit of large r, as it was found in the Anderson model. For the available system sizes, the distributions of the rescaled variables

$$\tilde{Z}_r(h) = \frac{(Z_r(h) - \langle Z_r(h)\rangle)}{\sigma_{Z_r(h)}} \tag{5.10}$$

do not seem to collapse into a unique curve, and the scaling of the variances $\sigma^2_{Z_r(h)}$ with r appears to be compatible with a power-law, but with an exponent dependent on the disorder strength h. Having access to bigger system

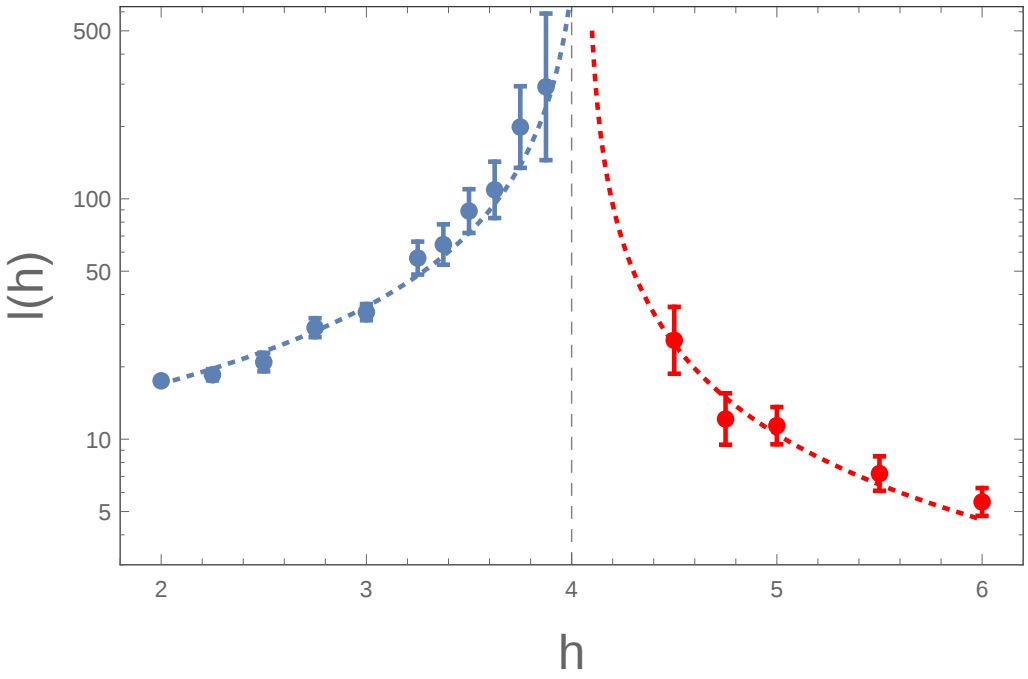

Figure 5.8: Divergence of the length scales $l(h)$ extracted from the fits of the probability of resonances as a function of r. The dotted curve is a power law fit, resulting in a critical exponent $\simeq 1$. The vertical dashed line indicates the critical value h_c found in Fig. 5.7.

sizes would be necessary to give a conclusive statement on the asymptotic behavior; unfortunately this proves to be a challenging numerical problem due to the algorithmic complexity in space and time of the transfer matrix method.

5.3.3 Absence of a dominating path in many body systems

In Sec. 3.4 we compared the forward approximation of the wavefuction to the result obtained by considering only the optimal path, showing that the forward approximation sum is indeed dominated by only one term. In the many-body case, however, most of the paths have comparable amplitude and the much stronger correlations between them give rise to non-negligible interference effects, resulting in many cancellations.

Indeed, when performing the same analysis of Sec. 3.4 for the Heisenberg chain, one finds that the statistics of the sum (5.6) is not well reproduced by the optimal path alone: the distribution of the ratios between the full sum and the optimal path is very wide and peaked at values that are far from one. In this case, despite also in many-body systems the amplitude of the single paths are fat-tailed distributed, there is not a single one dominating. Indeed, one can look at the composition of the sum (5.6) by looking at the average IPR* of the paths amplitudes (which we denote with ω_p)

$$\mathrm{IPR}^* = \frac{\left(\sum_p \omega_p\right)^2}{\sum_p \omega_p^2} \tag{5.11}$$

over all the paths connecting the two Neel states, which we take as starting and ending point as in Sec. 5.3.2. One finds that it scales linearly with the total number of paths $N^* = 2(L/2)!$ (see Fig. 5.9), indicating that there are factorially many (in the length of the chain L) paths having amplitudes that are comparable in absolute value. This is a signature of the strong correlations between the paths, which is not surprising in view of the many-body nature of the model. Following Ref. [51], one can argue that the strongest correlations are among those paths associated to processes in which the same spin flips occur, but in different order: the different orderings of the flips produce different energy denominators in (5.6), and thus different path amplitudes; however, the resulting terms are trivially correlated, and one can expect that for those realizations of the random fields producing one particularly large path weight, the other ones (related to it by permutation of the order of the number of spin flips) will also have a large amplitude in absolute value. However, in the sum (5.6) the paths contribute with well defined

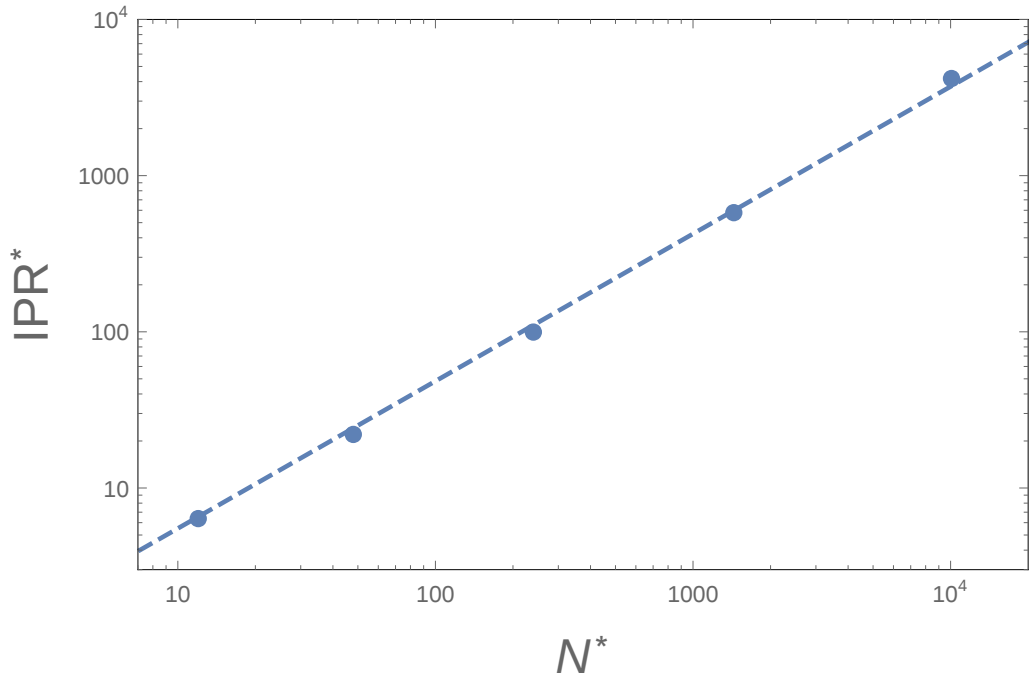

Figure 5.9: Average IPR* of the paths, as in Eq. (5.11), as a function of the number of paths $N^* = 2(L/2)!$ for random spin chains of different lengths L. The IPR* is linear in the total number of paths.

relative signs, leading to cancellations between these factorially many terms, which are fully taken into account only with the transfer matrix method.

5.4 Pushing the limits on many body localization

The many-body localization transition is at the cutting edge of research in disordered and localized systems. The investigation of this class of systems is however hard, both with numerical and with analytical calculations. Between these two options, indeed, a common choice is to advance our knowledge in this matter using numerical evidence; in this case one is able to study only systems of small size by exactly diagonalizing the Hamiltonian matrix or using methods of equivalent complexity. By scaling the information obtained from the exact diagonalization of finite size systems to the thermodynamic limit we can gain insight about the localization transition (see for example

Ref. [21] or the results of Sec. 5.2).

In this chapter it has been shown that an alternative way is given by methods based on the forward approximation of the correlated-disorder locator expansion for the many-body wavefunctions. The proof-of-principle numerical computations presented in Sec. 5.3 hold under comparison with the current state-of-the-art results obtained using exact diagonalization, suggesting the usefulness of this technique.

Conclusion

This Ph.D. thesis mainly focused on the analysis of the forward approximation of the locator expansion of the resolvent of disordered Hamiltonians. Disorder in quantum systems being an analytically and numerically difficult problem, the understanding we have so far allows to simplify in a controlled way the calculations of many quantities which involve the wavefunction overlaps. This includes an improved insight into the mechanisms that give rise to resonances in many-body delocalized systems and the differences that occur between the single particle and the many-body systems.

Moreover, the emphasis that has been put on the forward approximation method should not overshadow the result obtained when analyzing a non-isolated system; the coupling of an Anderson system with a mesoscopic bath has a strong relevance in experimental works. Varying the coupling strength has the result, besides of modifying non-monotonically the stability of the localized phase, of changing the mechanism behind localization from an Anderson-like localization to a 'Zeno localization'.

The hope is that this thesis has been successful in communicating the value, the potential for new findings and the fundamental importance of the topic of localization in disordered systems. There is still much to do in order to understand this lively topic; one may expect that a few potential directions have been suggested from the results obtained in this thesis.

Bibliography

[1] P. W. Anderson. Absence of Diffusion in Certain Random Lattices. *Phys. Rev.*, 109:1492–1505, Mar 1958.

[2] DM Basko, IL Aleiner, and BL Altshuler. Metal–insulator transition in a weakly interacting many-electron system with localized single-particle states. *Annals of physics*, 321(5):1126–1205, 2006.

[3] Francesca Pietracaprina, Valentina Ros, and Antonello Scardicchio. The forward approximation as a mean field approximation for the Anderson and Many Body Localization transitions. *arXiv:1508.05097*.

[4] David A. Huse, Rahul Nandkishore, Francesca Pietracaprina, Valentina Ros, and Antonello Scardicchio. Localized systems coupled to small baths: From Anderson to Zeno. *Phys. Rev. B*, 92:014203, Jul 2015.

[5] Andrea De Luca, Francesca Pietracaprina, and Antonello Scardicchio. *(unpublished)*.

[6] L. P. Pitaevskii and E. M. Lifshits. *Theoretical Physics X: Physical Kinetics*. Butterworth-Heinemann, 1981.

[7] Y. Imry. *Introduction to mesoscopic physics*. Oxford University Press, 1997.

[8] G. Giuliani and G. Vignale. *Quantum Theory of the Elecron Liquid*. Vambridge University Press, 2005.

[9] E. Akkermans and G. Montambaux. *Mesoscopic Physics of Electrons and Photons*. Cambridge University Press, 2007.

[10] G. Feher. Electron Spin Resonance Experiments on Donors in Silicon. I. Electronic Structure of Donors by the Electron Nuclear Double Resonance Technique. *Phys. Rev.*, 114:1219–1244, Jun 1959.

[11] D. J. Thouless. Electrons in disordered systems and the theory of localization. *Physics Reports*, 13(3):93–142, 1974.

[12] Bernhard Kramer and Angus MacKinnon. Localization: theory and experiment. *Reports on Progress in Physics*, 56(12):1469, 1993.

[13] M. L. Mehta. *Random Matrices*. Academic Press, 2004.

[14] M. V. Berry and M. Tabor. Level Clustering in the Regular Spectrum. *Proceedings of the Royal Society of London A: Mathematical, Physical and Engineering Sciences*, 356(1686):375–394, 1977.

[15] Arijeet Pal and David A. Huse. Many-body localization phase transition. *Phys. Rev. B*, 82(17):174411, November 2010.

[16] Jonas A. Kjäll, Jens H. Bardarson, and Frank Pollmann. Many-Body Localization in a Disordered Quantum Ising Chain. *Phys. Rev. Lett.*, 113:107204, Sep 2014.

[17] Ronen Vosk and Ehud Altman. Dynamical Quantum Phase Transitions in Random Spin Chains. *Phys. Rev. Lett.*, 112:217204, May 2014.

[18] M. Žnidarič, T. Prosen, and P. Prelovšek. Many-body localization in the Heisenberg XXZ magnet in a random field. *Physical Review B*, 77(6):064426, Feb 2008.

[19] Jens H. Bardarson, Frank Pollmann, and Joel E. Moore. Unbounded Growth of Entanglement in Models of Many-Body Localization. *Phys. Rev. Lett.*, 109:017202, July 2012.

[20] James M Hickey, Sam Genway, and Juan P Garrahan. Signatures of many-body localisation in a system without disorder and the relation to a glass transition. *arXiv preprint arXiv:1405.5780*, 2014.

[21] David J Luitz, Nicolas Laflorencie, and Fabien Alet. Many-body localization edge in the random-field Heisenberg chain. *Physical Review B*, 91(8):081103, 2015.

[22] S. Kullback and R. A. Leibler. On Information and Sufficiency. *Ann. Math. Statist.*, 22(1):79–86, 03 1951.

[23] O. Agam, B. L. Altshuler, and A. V. Andreev. Spectral Statistics: From Disordered to Chaotic Systems. *Phys. Rev. Lett.*, 75:4389–4392, Dec 1995.

[24] Steven W. McDonald and Allan N. Kaufman. Spectrum and Eigenfunctions for a Hamiltonian with Stochastic Trajectories. *Phys. Rev. Lett.*, 42:1189–1191, Apr 1979.

[25] M Robnik. Quantising a generic family of billiards with analytic boundaries. *Journal of Physics A: Mathematical and General*, 17(5):1049, 1984.

[26] M. V. Berry. Quantizing a classically ergodic system: Sinai's billiard and the {KKR} method. *Annals of Physics*, 131(1):163–216, 1981.

[27] G. Casati, B. V. Chirikov, and I. Guarneri. Energy-Level Statistics of Integrable Quantum Systems. *Phys. Rev. Lett.*, 54:1350–1353, Apr 1985.

[28] Oriol Bohigas. Random matrix theories and chaotic dynamics. Technical report, Paris-11 Univ., 91-Orsay (France). Inst. de Physique Nucleaire, 1991.

[29] O. Bohigas, M. J. Giannoni, and C. Schmit. Characterization of Chaotic Quantum Spectra and Universality of Level Fluctuation Laws. *Phys. Rev. Lett.*, 52:1–4, Jan 1984.

[30] M. Berry. Quantum Chaology: The Bakerian Lectures. *Proceedings of the Royal Society A*, 413:237–271, 1977.

[31] Mark Srednicki. Chaos and quantum thermalization. *Phys. Rev. E*, 50:888–901, Aug 1994.

[32] J. M. Deutsch. Quantum statistical mechanics in a closed system. *Phys. Rev. A*, 43:2046–2049, Feb 1991.

[33] L. D'Alessio, Y. Kafri, A. Polkovnikov, and M. Rigol. From Quantum Chaos and Eigenstate Thermalization to Statistical Mechanics and Thermodynamics. *ArXiv e-prints*, September 2015.

[34] Mark Srednicki. The approach to thermal equilibrium in quantized chaotic systems. *Journal of Physics A: Mathematical and General*, 32(7):1163, 1999.

[35] Mark Srednicki. Thermal fluctuations in quantized chaotic systems. *Journal of Physics A: Mathematical and General*, 29(4):L75, 1996.

[36] A. V. Andreev, O. Agam, B. D. Simons, and B. L. Altshuler. Quantum Chaos, Irreversible Classical Dynamics, and Random Matrix Theory. *Phys. Rev. Lett.*, 76:3947–3950, May 1996.

[37] A. V. Andreev, B. D. Simons, O. Agam, and B. L. Altshuler. Semiclassical field theory approach to quantum chaos. *Nuclear Physics B*, 482(3):536–566, 1996.

[38] Fausto Borgonovi, Giulio Casati, and Baowen Li. Diffusion and Localization in Chaotic Billiards. *Phys. Rev. Lett.*, 77:4744–4747, Dec 1996.

[39] NF Mott. Conduction in non-crystalline materials. *Philosophical Magazine*, 19(160):835–852, 1969.

[40] Ferdinand Evers and Alexander D Mirlin. Anderson transitions. *Reviews of Modern Physics*, 80(4):1355, 2008.

[41] Anatoli Polkovnikov, Krishnendu Sengupta, Alessandro Silva, and Mukund Vengalattore. *Colloquium* : Nonequilibrium dynamics of closed interacting quantum systems. *Rev. Mod. Phys.*, 83:863–883, Aug 2011.

[42] R. Nandkishore and D. A. Huse. Many-Body Localization and Thermalization in Quantum Statistical Mechanics. *Annual Review of Condensed Matter Physics*, 6:15–38, March 2015.

[43] V. Oganesyan and D.A. Huse. Localization of interacting fermions at high temperature. *Physical Review B*, 75(15):155111, 2007.

[44] I. V. Gornyi, A. D. Mirlin, and D. G. Polyakov. Interacting electrons in disordered wires: Anderson localization and low-t transport. *Phys. Rev. Lett.*, 95:206603, Nov 2005.

[45] Giacomo Roati, Chiara D'Errico, Leonardo Fallani, Marco Fattori, Chiara Fort, Matteo Zaccanti, Giovanni Modugno, Michele Modugno, and Massimo Inguscio. Anderson localization of a non-interacting Bose–Einstein condensate. *Nature*, 453(7197):895–898, 2008.

[46] Chiara D'Errico, Eleonora Lucioni, Luca Tanzi, Lorenzo Gori, Guillaume Roux, Ian P. McCulloch, Thierry Giamarchi, Massimo Inguscio, and Giovanni Modugno. Observation of a Disordered Bosonic Insulator from Weak to Strong Interactions. *Phys. Rev. Lett.*, 113:095301, Aug 2014.

[47] Michael Schreiber, Sean S. Hodgman, Pranjal Bordia, Henrik P. Lüschen, Mark H. Fischer, Ronen Vosk, Ehud Altman, Ulrich Schneider, and Immanuel Bloch. Observation of many-body localization of interacting fermions in a quasirandom optical lattice. *Science*, 349(6250):842–845, 2015.

[48] Juliette Billy, Vincent Josse, Zhanchun Zuo, Alain Bernard, Ben Hambrecht, Pierre Lugan, David Clément, Laurent Sanchez-Palencia, Philippe Bouyer, and Alain Aspect. Direct observation of Anderson localization of matter waves in a controlled disorder. *Nature*, 453(7197):891–894, 2008.

[49] B.L. Altshuler, Y. Gefen, A. Kamenev, and L.S. Levitov. Quasiparticle lifetime in a finite system: A nonperturbative approach. *Phys. Rev. Lett.*, 78(14):2803–2806, 1997.

[50] Bela Bauer and Chetan Nayak. Area laws in a many-body localized state and its implications for topological order. *J. Stat. Mech*, 2013:P09005, 2013.

[51] V Ros, M Müller, and A Scardicchio. Integrals of motion in the many-body localized phase. *Nuclear Physics B*, 891:420–465, 2015.

[52] John Z Imbrie. On many-body localization for quantum spin chains. *arXiv:*, 1403.7837, 2014.

[53] I. H. Kim, A. Chandran, and Dmitry A. Abanin. Local integrals of motion and the logarithmic lightcone in many-body localized systems. *arXiv:*, 1412.3073.

[54] R. Abou-Chacra, D. J. Thouless, and P. W. Anderson. A selfconsistent theory of localization. *Journal of Physics C: Solid State Physics*, 6(10):1734, 1973.

[55] Elihu Abrahams, P. W. Anderson, D. C. Licciardello, and T. V. Ramakrishnan. Scaling Theory of Localization: Absence of Quantum Diffusion in Two Dimensions. *Phys. Rev. Lett.*, 42:673–676, Mar 1979.

[56] P. W. Anderson. The size of localized states near the mobility edge. *Proceedings of the National Academy of Sciences*, 69(5):1097–1099, 1972.

[57] R. Abou-Chacra and D. J. Thouless. Self-consistent theory of localization. II. Localization near the band edges. *Journal of Physics C: Solid State Physics*, 7(1):65, 1974.

[58] J. Prior, A. M. Somoza, and M. Ortuño. Conductance distribution in two-dimensional localized systems with and without magnetic fields. *The European Physical Journal B*, 70(4):513–521, 2009.

[59] Ernesto Medina and Mehran Kardar. Quantum interference effects for strongly localized electrons. *Physical Review B*, 46(16):9984, 1992.

[60] VL Nguyen, BZ Spivak, and BI Shklovskii. Pis' ma Zh. Eksp. Teor. Fiz. 41, 35 (1985)[Sov. Phys. *JETP Lett*, 41, 1985. [Pis'ma Zh. Eksp. Teor. Fiz. **41**, 35 (1985)].

[61] VL Nguyen, BZ Spivak, and BI Shklovskii. JETP Lett. 41 42 Nguyen VL, Spivak BZ and Shklovskii BI 1985. *Sov. Phys.—JETP*, 62:1021, 1985. [Zh. Eksp. Teor. Fiz. **89**, 11 (1985).

[62] VL Nguyen, BZ Spivak, and BI Shklovskii. Hopping-conductivity fluctuations in small samples. *JETP Lett*, 43(1), 1986. [Pis'ma Zh. Eksp. Teor. Fiz. **43**, 35 (1986)].

[63] B. Derrida. Directed polymers in a random medium. *Physica A Statistical Mechanics and its Applications*, 163:71–84, February 1990.

[64] B. Derrida and H. Spohn. Polymers on disordered trees, spin glasses, and traveling waves. *Journal of Statistical Physics*, 51(5-6):817–840, 1988.

[65] Timothy Halpin-Healy and Yi-Cheng Zhang. Kinetic roughening phenomena, stochastic growth, directed polymers and all that. Aspects of multidisciplinary statistical mechanics. *Physics reports*, 254(4):215–414, 1995.

[66] Keith Slevin and Tomi Ohtsuki. Critical exponent for the Anderson transition in the three-dimensional orthogonal universality class. *New Journal of Physics*, 16(1):015012, 2014.

[67] Yoshiki Ueoka and Keith Slevin. Dimensional Dependence of Critical Exponent of the Anderson Transition in the Orthogonal Universality Class. *Journal of the Physical Society of Japan*, 83(8):084711, 2014.

[68] Antonio M. García-García and Emilio Cuevas. Dimensional dependence of the metal-insulator transition. *Phys. Rev. B*, 75:174203, May 2007.

[69] A. M. Somoza, M. Ortuño, and J. Prior. Universal Distribution Functions in Two-Dimensional Localized Systems. *Phys. Rev. Lett.*, 99:116602, Sep 2007.

[70] A. M. Somoza, P. Le Doussal, and M. Ortuño. Unbinding transition in semi-infinite two-dimensional localized systems. *Phys. Rev. B*, 91:155413, Apr 2015.

[71] Cécile Monthus and Thomas Garel. Statistics of renormalized on-site energies and renormalized hoppings for Anderson localization in two and three dimensions. *Phys. Rev. B*, 80:024203, Jul 2009.

[72] M. V. Feigel'man, L. B. Ioffe, and M. Mézard. Superconductor-insulator transition and energy localization. *Phys. Rev. B*, 82:184534, Nov 2010.

[73] L. B. Ioffe and Marc Mézard. Disorder-Driven Quantum Phase Transitions in Superconductors and Magnets. *Phys. Rev. Lett.*, 105:037001, Jul 2010.

[74] Markus Müller. Magnetoresistance and localization in bosonic insulators. *EPL (Europhysics Letters)*, 102(6):67008, 2013.

[75] Xiaoquan Yu and Markus Müller. Localization of disordered bosons and magnets in random fields. *Annals of Physics*, 337:55–93, 2013.

[76] Ernesto Medina, Mehran Kardar, Yonathan Shapir, and Xiang Rong Wang. Interference of Directed Paths in Disordered Systems. *Phys. Rev. Lett.*, 62:941–944, Feb 1989.

[77] Daniel S. Fisher and David A. Huse. Directed paths in a random potential. *Phys. Rev. B*, 43:10728–10742, May 1991.

[78] David A. Huse, Christopher L. Henley, and Daniel S. Fisher. Huse, Henley, and Fisher respond. *Phys. Rev. Lett.*, 55:2924–2924, Dec 1985.

[79] Kurt Johansson. Shape Fluctuations and Random Matrices. *Communications in Mathematical Physics*, 209(2):437–476, 2000.

[80] Michael Prähofer and Herbert Spohn. Universal Distributions for Growth Processes in $1 + 1$ Dimensions and Random Matrices. *Phys. Rev. Lett.*, 84:4882–4885, May 2000.

[81] Michael Prähofer and Herbert Spohn. Scale invariance of the PNG droplet and the Airy process. *Journal of statistical physics*, 108(5-6):1071–1106, 2002.

[82] Michael Prähofer and Herbert Spohn. Exact scaling functions for one-dimensional stationary KPZ growth. *Journal of statistical physics*, 115(1-2):255–279, 2004.

[83] Cécile Monthus and Thomas Garel. Random transverse field Ising model in dimension d¿ 1: scaling analysis in the disordered phase from the directed polymer model. *Journal of Physics A: Mathematical and Theoretical*, 45(9):095002, 2012.

[84] Jin Y. Yen. An algorithm for finding shortest routes from all source nodes to a given destination in general networks. *Quarterly of Applied Mathematics*, (27):526–530, 1970.

[85] E.W. Dijkstra. A note on two problems in connexion with graphs. *Numerische Mathematik*, 1(1):269–271, 1959.

[86] Konstantin Efetov. *Supersymmetry in disorder and chaos*. Cambridge University Press, 1999.

[87] Rahul Nandkishore, Sarang Gopalakrishnan, and David A. Huse. Spectral features of a many-body-localized system weakly coupled to a bath. *Phys. Rev. B*, 90:064203, Aug 2014.

[88] Sonika Johri, Rahul Nandkishore, and R. N. Bhatt. Many-Body Localization in Imperfectly Isolated Quantum Systems. *Phys. Rev. Lett.*, 114:117401, Mar 2015.

[89] Sarang Gopalakrishnan and Rahul Nandkishore. Mean-field theory of nearly many-body localized metals. *Phys. Rev. B*, 90:224203, Dec 2014.

[90] Rahul Nandkishore. Many-body localization and delocalization in the two-dimensional continuum. *Phys. Rev. B*, 90:184204, Nov 2014.

[91] V. Gurarie and J. T. Chalker. Bosonic excitations in random media. *Phys. Rev. B*, 68:134207, Oct 2003.

[92] D J Thouless. Wannier functions for magnetic sub-bands. *Journal of Physics C: Solid State Physics*, 17(12):L325, 1984.

[93] Andrea De Luca, BL Altshuler, VE Kravtsov, and A Scardicchio. Anderson localization on the Bethe lattice: nonergodicity of extended states. *Physical review letters*, 113(4):046806, 2014.

[94] A. Beskow and J. Nilsson. *Arkiv für Fysik*, 34(561), 1967.

[95] L. A. Khalfin. *Jetp Lett*, 8(65), 1968.

[96] B. Misra and E. C. G. Sudarshan. The Zeno's paradox in quantum theory . *Journal of Mathematical Physics*, 18(756), 1977.

[97] Franz Wegner. Bounds on the density of states in disordered systems. *Zeitschrift für Physik B Condensed Matter*, 44(1):9–15, 1981.

[98] BL Altshuler, VE Kravtsov, and IV Lerner. Statistical properties of mesoscopic fluctuations and similarity theory. *JETP Lett.*, 43(7), 1986.

[99] VE Kravtsov, IV Lerner, BL Altshuler, and AG Aronov. Universal spectral correlations at the mobility edge. *Phys. Rev. Lett.*, 72(6):888, 1994.

[100] Andrea De Luca and Antonello Scardicchio. Ergodicity breaking in a model showing many-body localization. *Europhys. Lett.*, 101(3):37003, 2013.

[101] Pablo R. Zangara, Axel D. Dente, Aníbal Iucci, Patricia R. Levstein, and Horacio M. Pastawski. Interaction-disorder competition in a spin system evaluated through the Loschmidt echo. *Phys. Rev. B*, 88:195106, Nov 2013.

[102] Mauro Schiulaz, Alessandro Silva, and Markus Müller. Dynamics in many-body localized quantum systems without disorder. *Phys. Rev. B*, 91:184202, May 2015.

[103] Arun Nanduri, Hyungwon Kim, and David A. Huse. Entanglement spreading in a many-body localized system. *Phys. Rev. B*, 90:064201, Aug 2014.

[104] Yevgeny Bar Lev, Guy Cohen, and David R. Reichman. Absence of Diffusion in an Interacting System of Spinless Fermions on a One-Dimensional Disordered Lattice. *Phys. Rev. Lett.*, 114:100601, Mar 2015.

[105] I. Mondragon-Shem, A. Pal, T. L. Hughes, and C. R. Laumann. Many-body mobility edge due to symmetry-constrained dynamics and strong interactions. *arXiv:1501.03824 [cond-mat.dis-nn]*.

[106] J. Goold, S. R. Clark, C. Gogolin, J. Eisert, A. Scardicchio, and A. Silva. Total correlations of the diagonal ensemble herald the many-body localization transition. *arXiv:1504.06872 [cond-mat.dis-nn]*, 2015.

[107] F. Buccheri, A. De Luca, and Antonello Scardicchio. Structure of typical states of a disordered Richardson model and many-body localization. *Physical Review B*, 84(9):094203, 2011.